Lund University, Faculty of Engineering LTH,
Department of Chemical engineering

Haldor Topsoe A/S

Simulation of a WSA process for SO_2 containing off gases from the metallurgical industry

KET050

Tutors:
Degerman M.
Nilsson B.
Odenbrand I.

Principal investigators:
Almqvist M.
Andersson N.
Holmqvist A.
Jönsson J.

2008-05-13

Abstract

The WSA process works satisfactory under relatively stationary conditions but has problem with processes suffering from heavy fluctuations. Such problems are common in the metallurgical industry with batch Pierce-Smith converters. The fluctuations are caused by periodical changes in the number of operating Pierce-Smith converters. In order to investigate how fluctuations in feed condition propagate through the WSA process, a mathematical model of the converter was derived from the continuity principle applied to a catalytic tubular reactor. The model derived reflects dispersion phenomena through the three adiabatic catalytic beds as well as the three interbed heat exchangers. The one dimensional discretization, according to the finite volume method, divided the converter (the catalytic beds respectively the heat exchangers) into elements with equal volumes, in which the solution of the continuous partial differential equations (PDEs) was computed. The implementation was carried out using MATLAB R2007a. Time derivates are integrated by the implemented MATLAB solver *ode15s* which can solve stiff initial value problems for ordinary differential equations. To be able to approach the given steady state values, several tuning parameters were introduced. Once the model was considered to have sufficient accuracy, the investigation of steady state case switching and transient behavior were carried out.

Haldor Topsoe A/S gave guarantee of a maximum of 2 kg SO_2 emission per ton 100 % sulfuric acid produced for this case study. When simulating the three cases, the steady state results indicated that the guarantees were hardly fulfilled during cases which correspond to the maximum and minimum of sulfur dioxide content. The model generated conversions for the cases above are 99.56 respectively 99.82 mole %, which can be compared with the reference steady state values 99.14 and 98.92 mole %. The steady state conversions correspond to exit sulfur dioxide content that does not fulfill the guarantee and the model generated content hardly fulfills the guarantee. This implied that extra tail gas treatment with H_2O_2 was necessary in order to achieve desired sulfur dioxide content in the stack gases. The transient behavior indicated in conformity with previous conclusion, according to the steady state behavior, that the tail gas treatment was of great importance.

The derived converter model is far from complete since many essential process characteristics are not included. The heat transfer between the gas bulk and the catalyst is of highest importance along with external mass transfer through the stagnant gas film around the catalyst particles. The model used in this report neglects both external mass and heat transfer but complete theoretical models are presented for further work.

The intention was to expand the derived model so more unit operations, e.g. the WSA condenser and the mist control unit, were included. This was not implemented because of lack of time.

Table of contents

1. Introduction

Current legislation demands a strict decrease in sulfur containing off-gases. Emission of sulfur containing compounds affects the environmental fauna and flora, due to its acidifying properties. To achieve a good environment, it is important to clean flue-gases from sulfur oxides properly. Haldor Topsoe A/S provides an efficient solution, the Wet Gas Sulfuric Acid (WSA) process, to this specific problem. It enables both high sulfur content reduction and supplies high qualitative concentrated sulfuric acid in an energy efficient way. The WSA technology has been industrially applied since 1980 with plants worldwide within a wide range of different industries.

1.1 Problem definition

The process works satisfactory under relatively stationary conditions but has problem with processes suffering from heavy fluctuations. Such problems are common in the metallurgical industry with batch Pierce-Smith converters.

The fundamental principles of the WSA plant are the catalytic SO_2 conversion to SO_3 and the WSA condenser where typically 98 wt % sulfuric acid is produced. The WSA process reduces these emissions by conversion to sulfuric acid. The conversion takes place in two steps; initially the SO_2 is oxidized to SO_3 in the SO_2 converter step, subsequently the SO_3 is condensed in the WSA condenser to form sulfuric acid. Refinery off-gases contain H_2S that has to be converted to SO_2 through burners, while the metallurgical off-gases already contain SO_2, which makes the process somewhat easier in that sense[1]. The process is schematically shown in figures 1 and 2.

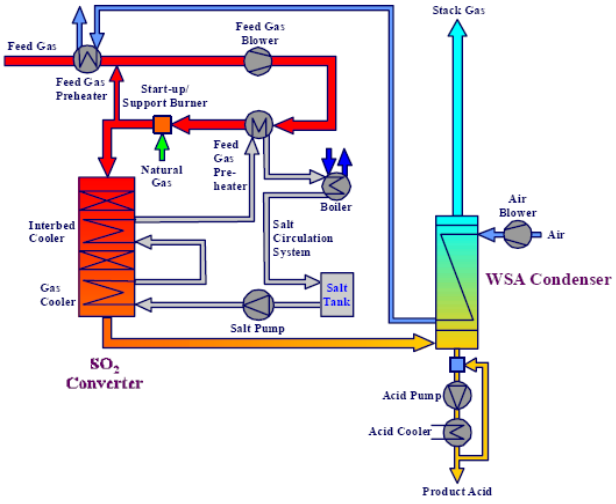

Figure 1. The WSA process shown schematically[1].

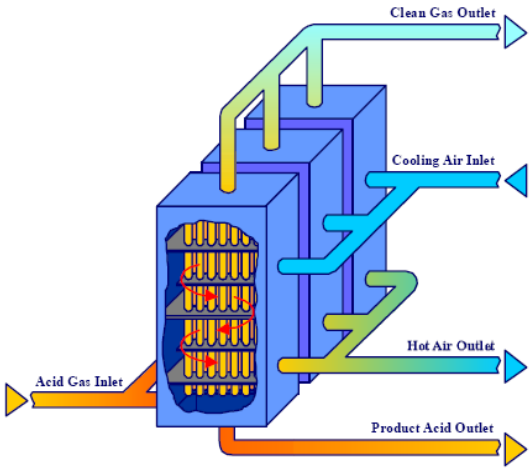

Figure 2. Patented condenser of Haldor Topsoe[1].

[1] Kristiansen A., 2005, *Topsoe Wet Gas Sulfuric Acid (WSA) Technology For Fixation Of SO_2 In Off-Gases In The Metallurgical Industry*

In the SO_2 converter the wet SO_2 is driven through Haldor Topsoe's VK-catalyst. The process is similar to an acid plant based on absorption except that the catalytic reaction takes place in a wet gas. To get high enough yields the conversion often takes place in multiple beds with internal cooling between the beds. This is required for optimal catalyst conditions, described in section 9.3 reaction thermodynamics. In the lower section of the SO_2 converter the gas stream is cooled below 290 °C, but well above the sulfuric acid dew point at approximately 260 °C.

In the WSA condenser, shown in figure 2, which is a glass tube falling film condenser, the sulfuric acid condenses on the acid resistant boron-silicate tubes. The acid is cooled by recirculated cold acid before it is stored and sold.

To achieve an energy efficient plant the heat is transferred by a salt circulation system consisting of a molten water free mixture of KNO_3, $NaNO_2$ and $NaNO_3$. The salt absorbs energy from the SO_2 converter while cooling it and is heat exchanged with the feed. Heat from the WSA condenser is heat exchanged with air, which subsequently warms up the feed.

A typical smelter complex consists of one continuous electric furnace and two Pierce-Smith converters running batch wise. Because of the batch wise converters, the SO_2 concentration and the gas flow varies heavily. There are three major operating points, the first containing only the continuous process, the second when one of the typical fluctuation characteristics shown in Figure 3. Before the off-gas reaches the sulfuric acid plant, the WSA plant, it is cleaned from catalyst poisons, like dust, metalloids and halogens through scrubbers, ESP's and WESP's[2].

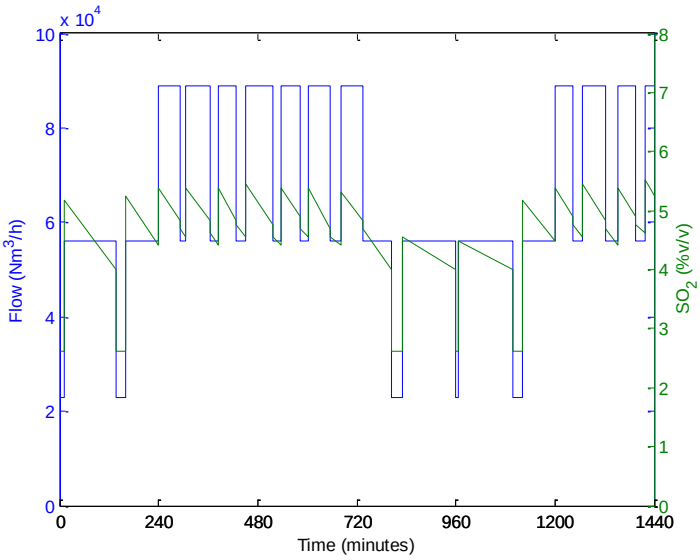

Figure 3. SO_2 concentration and flow variations over one day.

[2] G. Westcott et. al, 2007,*Impala Platinum Smelter, Rustenburg-an integrated smelter off-gas treatment solution*, The Journal of the Southern Africa institute of mining and metallurgy vol 107 May, pages 282-285

1.2 Project description

The aim of this project is to perform a case study on the application of the WSA process in a metallurgical application. The proposed parts that the report should include are:

1. Literature study of upstream processes with focus on qualitative assessment of which parameters may influence the operation of the WSA plant.
2. Identification of problems during fluctuations of feed gas flow and SO_2 concentration.
3. Suggestions for changes or additions in the design upstream WSA to minimize fluctuations of SO_2
4. Suggestions for control philosophy to enable handling of fluctuations of SO_2 (number of feed forward loops, placement of analysis equipment etc.)
5. Methods/tools for dynamic simulation of the process with fluctuations.
6. Cost estimation of the proposed process alterations.
7. Project evaluation including economic and technical analysis.

2. Background

2.1 Off gas treatment and environmental considerations

The off-gas from the WSA process can contain small quantities of sulfur dioxide, sulfur trioxide and sulfuric acid. All the substances are toxic and can damage the environment. Sulfur dioxide oxidizes slowly to sulfur trioxide without any catalyst and therefore can be transported far away from the source by air. After the sulfur dioxide has been oxidized, the solubility increases dramatically, and in contact with water it reacts fast to sulfuric acid which affects the environment[3].

Trace material and dust is removed upstream from the WSA process if the concentrations are significant. The cleaning process starts with a cyclone that removes big particles like dust. The majority of the dust left after the cyclone is then removed in a hot gas electrostatic precipitator and the remaining impurities are removed by scrubbing the gases. Some of the impurities are not removed by the scrubber, because they form minute solids or liquid particles. These are almost completely removed by a wet electrostatic precipitator which often is divided in two, connected in series, to ensure that no impurities reach the WSA plant [4, 5].

After the converter the amount of sulfur dioxide content in the process gas may still be high considering limiting values. The amount depends on the sulfur dioxide conversion and also the sulfur dioxide content of the converter feed gases. To attain maximum conversion, the gas conditions in the inlet should be as constant as possible. This is hard to achieve when fluctuations are normal in the upstream process. To minimize the sulfur dioxide emissions, a scrubber system is used, in which the sulfur dioxide is reacting with hydrogen peroxide into sulfuric acid. The hydrogen peroxide is introduced at a stoichiometric ratio proportional to the amount of sulfur dioxide to be removed according to reaction 1[4, 6].

Acid mist will be produced in connection with the sulfuric acid condensation and the amount of mist can increase if particles are introduced to the process gas. The acid mist particles are too small for separation from the process but the formation can be controlled.

[3] Warfvinge P., *Miljökemi*, 1997, pages 98-99
[4] Ullmann's *Encyclopedia of Industrial Chemistry*, 7th ed., 2007, a_25_635.pdf pages 36-43
[5] Ullmann's *Encyclopedia of Industrial Chemistry*, 7th ed., 2007, a_25_569.pdf pages 31-34
[6] Hansen F., 2007, *WSA Plant for Lead Smelter Process description Haldor Topsoe*, pages 2-7

By generating a small hot gas stream with small silicon particles, the mist can agglomerate to form larger droplets which are large enough to be separated. Before the gas leaves the process, it enters an acid mist filter where the remaining amount is reduced[6].

2.3 Existing WSA plants

The WSA technology has been developed and improved since it was introduced in the 1980's and the list of references exceeds 65 plants in a variety of industries. Out of this number, ten of the WSA plants are installed in the metallurgical industry[7]. The majority of the companies are listed in table 1[8].

Table 1. Existing metallurgical plants with Topsoe WSA technology. MTPD is metric tons per day

Client	Type of plant	Initial content of SO_2	Process gas Nm^3/h	H_2SO_4 prod. metric tons per day	Start-up
N.V. Sadaci S.A. Belgium	MoS_2 Roaster	0.6-2.8 %	35 000	106	1990
Molibdenos y Metales S.A. Chile	MoS_2 Roaster	2.0-2.4 %	40 000	104	1993
Metaleurop S.A. France	PbS Roaster	3.4 %	110 000	380	1993
Molymex S.A. de C.V. Mexico	MoS_2 Roaster	2.0-4.5 %	20 000	65	2001
Zhuzhou Smelter China	PbS Roaster	2.2-4.6 %	110 000	525	2001
ZAO Karabashmed Russia	CuS Smelter	6.5 %	170 000	1140	2003
OAO Kazzinc Kazakhstan	PbS Sinter ZnS Roaster	6.5 %	125 000	895	2004
Molibdenos y Metales S.A. Chile	MoS_2 Roaster	1.4-3.8 %	60 000	170	2007

2.3.1 Molybdenum roaster in Belgium

One of the first WSA plants constructed for the metallurgical industry, N.V. Sadaci's molybdenum sulfide roaster in Belgium, was constructed in 1990 and is still running. This plant uses gas/gas heat exchangers to achieve optimal temperature while modern plants uses a system of circulating molten salt.

2.3.2 Molybdenum roaster in Santiago de Chile

When the Chilean company Molibdenos y Metales S.A in the beginning of 2005 decided to construct their fourth WSA plant at their molybdenum sulfide roasting facility in Santiago de Chile the environmental authorities required that the SO_2 conversion was increased. This restriction was established because of the facilities location in a rather populated area close to the city of Santiago de Chile. Therefore the plant is equipped with an SO_2 converter with three catalysts bed with conventional catalyst in the two upper beds and a low temperature alkali promoted catalyst in the last bed. With this modification a conversion of 99.6 % is achieved[9].

[7] Christensen T, 2007, *An Economic and Flexible Process to Treat Streams with Varying Concentration of SO_2,* page 22

[8] Rosenberg, H., 2006, *Topsoe wet gas sulfuric acid (WSA) technology- an attracive alternative for reduction of sulfur emissions from furnaces and converters, International Platinum Conference " Platinum Surges Ahead",* The Southern African Institute of Mining and Metallurgy, page 197

[9] Rosenberg, H., 2006, *Topsoe wet gas sulfuric acid (WSA) technology- an attracive alternative for reduction of sulfur emissions from furnaces and converters, International Platinum Conference " Platinum Surges Ahead",* The Southern African Institute of Mining and Metallurgy, pages 195-196

2.4 Advantages of the WSA technology

There are many advantages why one should use the WSA process for flue-gas treatment. The process does not generate any waste products or waste water and does not use any absorbents. Firstly the process produces sulfuric acid, which is a more valuable compound in comparison to elemental sulfur. Secondly the process uses the water content in the process gas and therefore does not require large amount of water added, which enables production of high purity concentrated sulfuric acid. The technology thus offers a viable alternative to several of existing smelters entailing a considerably lower investment compared to rebuild or change to the smelter.

The overall process is exothermal and large amount of steam is produced in the heat exchangers, which is used for preheating of the feed gas and for addition of water if that is necessary. The excess heat can also be transformed into power in a turbine or used as a heating media in neighboring process units[10,11].

Many processes produce sulfuric off-gases, which can be hard to purify because of the elevated concentration of carbon dioxide, carbonyl sulfide and organic sulfur. In cases where the process gas has low sulfur content, other purification techniques than WSA, are hard to apply. In spite of the low sulfur content in the feed gas, it is possible to achieve a high concentrated sulfuric acid. In the 0.3 – 7mole% sulfur dioxide content, the WSA is the most economic alternative[12].

3. Flow sheet description

3.1 General

The wet-catalysis process contains aqueous vapour, contrary to other contact sulfuric acid processes. Sulfur dioxide is converted into sulfur trioxide by a vanadium pentoxide catalyst and sulfuric acid is produced instantly when sulfur trioxide react with the aqueous vapour. The temperature determines to which extent the acid is formed and the concentration of the product acid depends upon the H_2O/SO_3 ratio in the converted gases as well as on the condensation temperature[13].

The Topsoe WSA process is suitable for treating “cold” wet SO_2 gases from for instance smelter off-gas or “hot” gases from thermal incineration units.

The main parts of the process are the SO_2 converter, a heat exchanging system and a WSA condenser, see figure 1 and 4. The off gases are heated in two steps, first with hot air from the WSA condenser and second with heat (circa 200 ˚C) from the SO_2 converter. An in-line burner supplies whatever additional heat that is required to reach the appropriate inlet temperature for the SO_2 converter (circa 440 ˚C). If the incoming concentration of SO_2 exceeds circa 2.5 mole% then the WSA process will be auto thermal, and no supplement heat will be required. Surplus heat is for example used for steam production.

[10] Frank Hansen, 2008-02-06, Personal communication, Haldor Topsoe A/S, Lyngby Denmark
[11] Rud Bendixen O. Hansen H.K., *Topsoe WSA Technology Provides Efficient Desulfurization of Off-gases from Non-ferrous Roasters*, TMS Annual Meeting, EPD Congress 1996, 1996, pages 799-808
[12] O.Borre Jorgensen and P. Schoubye, 1982, *Advantages of the wet gas sulfuric acid process*, Chemical Engineering progress Feb, pages 44-47
[13] Ullmann’s *Encyclopedia of Industrial Chemistry*, 7th ed., 2007, a_25_635.pdf, pages 34-37

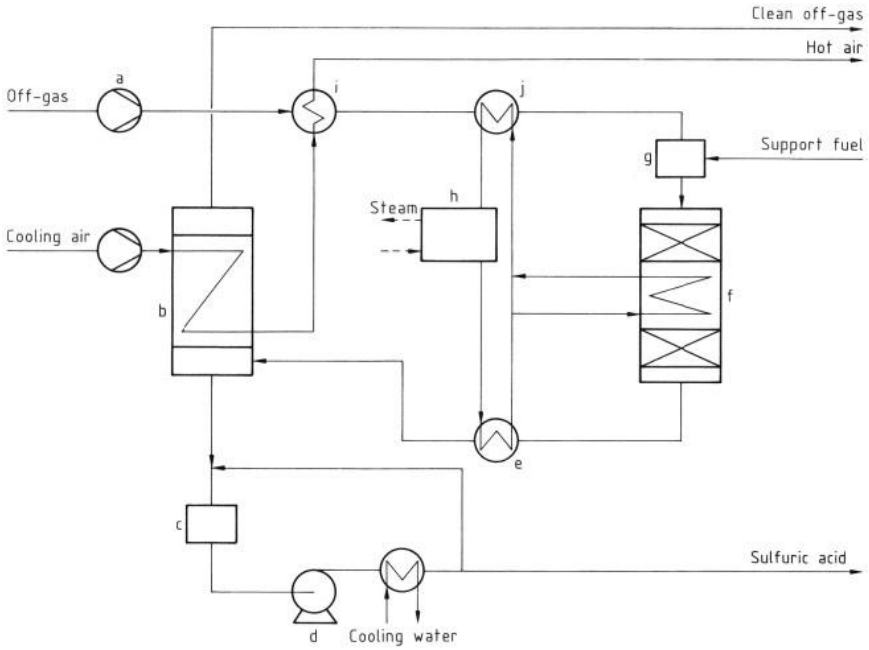

Figure 4. Haldor Topsoe WSA process a) Fan; b) WSA condenser; c) Acid tank; d) Pump; e) Gas cooler; f) SO2 converter; g) Burner; h) Salt system; i) Gas preheater; j) Gas heater[13]

Conversion of SO_2 to SO_3 is accomplished by oxidation over vanadium catalysts in a single-stage adiabatic converter or in a multi-stage converter with intermediate cooling, depending upon the SO_2 concentration or the required grade of SO_2 removal. When the gas leaves the converter, the temperature is lowered in another heat exchanger. The cooling causes the SO_3 to react with water in the off-gas to form sulfuric acid. Finally, the sulfuric acid vapour is condensed and concentrated in the WSA condenser, which is an air cooled glass tube device. The sulfuric acid is cooled to about 100 ˚C by ambient air passing on the shell side.

The acid is concentrated in the lower parts of the tubes by counter current contact with hot off-gas and thereafter collected at the bottom of the condenser. Hot acid is cooled in a water cooled plate cooler before being pumped to a storage tank. It is possible to keep the level of sulfuric acid in the cleaned off-gas low by careful control of the temperature and of the sulfuric acid droplets formation[14].

[14] Ullmann's *Encyclopedia of Industrial Chemistry*, 7th ed., 2007, a_25_635.pdf, pages 37 -38

3.2 Case study

3.2.1 Case study and guarantee

The smelting plant is running batch wise which gives three operational cases. Description of the periodical changes in flow rate and sulfur dioxide concentration is given in Table 2. Specific case data can be found in table I, II and III and a schematic presentation over a WSA converter in figure I in appendix D.

Table 2. Lead smelter cycle operation with feed gas flow and SO_2 concentration

Case	Flow rate (Nm^3/h)	Time (h)	SO_2 concentration (mole %)
Smelting period	17000	6	12.6
Reduction period	20000	1	0.5
Slag tapping period	7500	0.5	0

The following guarantee must be fulfilled at the end of the complete system:

- maximum 2 kg SO_2 per ton 100 % sulfuric acid
- maximum 0.075 kg SO_3 mist per ton 100 % sulfuric acid
- H_2SO_4 product minimum 98.0 wt%[10]

3.2.2 Feed gas heating

The feed gas from the metallurgical industry contains SO_2 gas saturated with water at 40 °C. The heating of the process gas is done in three steps. The first step in the WSA plant process is gas preheating to 150 °C in the feed gas preheater, by heat exchange with hot air from the WSA condenser. To raise temperature to 185 °C, hot air and hot recycled gas is added in a static mixer.

The hot air originates from the WSA condenser and is used for dilution of the process gas during the smelting period. This is important to keep the acid dew point inlet the WSA condenser below 260 °C. During the reduction period the dilution air is keeping a surplus of oxygen in the SO_2 converter. It is crucial to recycle the feed gas downstream the burner in order to maintain a minimum temperature of 185 °C. This temperature is chosen to eliminate the risk of corrosion in the process gas blower and to ensure that the temperature is above the melting point of the molten salt in the process gas heater. During slag tapping periods and reduction, the hot feed gas is mixed with evaporated SO_2 to avoid temperature decrease in the catalytic converter beds.

To gain the optimal temperature of 395 °C in to the SO_2 converter, the process feed is finally heat exchanged with the molten salt system. This optimal temperature corresponds to a conversion minimum of 99.2 % of SO_2 into SO_3 during smelting periods. In operating cases with low SO_2 concentration it is necessary to use the burner to supply the necessary heat to increase the process gas temperature to the inlet of the SO_2 converter. The burner is not expected to be in operating during the smelting periods.

The process gas is mixed with steam, produced in the salt cooler, before entering the SO_2 converter to ensure a water content of minimum 2 vol % in the process gas outlet of the WSA condenser. This is important in order to gain the wanted hydratisation of SO_3 to sulfuric acid in the WSA condenser [10, 15].

[15] Hansen F., 2007, *WSA Plant for Lead Smelter Process description Haldor Topsoe*, pages 4-5

3.2.3 SO_2 converter

In the SO_2 converter the SO_2 containing process gas is converted to SO_3 in three adiabatic catalytic beds loaded with catalyst from the VK-series. The oxidation of sulfur dioxide is limited by the equilibrium and in order to achieve high conversion rate, it is necessary to cool the process gas between the adiabatic catalytic beds in order to gain the optimal temperature, described in section 9.3 reaction thermodynamics.

As mentioned before molten salt is used as an interbed cooling media. After the first bed, the process gas is cooled to 430 °C, and after the second to 392 °C. During the final cooling a part of the SO_3 produced reacts with the water and transforms into sulfuric acid. The process gas leaves the converter at the temperature of 290 °C, which ensures a minimum temperature margin of 30 °C to the acid dew point.

3.2.4 WSA condenser

Right after leaving the converter, fine silicon particles are sprayed into the process gas in order to simplify the formation of droplets. These particles act as nuclei around which the acid mist can agglomerate to form larger droplets. The larger size will then enable proper separation of the acid in the condenser.

The WSA condenser is a falling film shell and tube type, where all the exposed area is made of glass. The condenser is built in modules with up to 1000 glass tubes per module. The condensed acid is collected in the acid resistant brick lined bottom of the WSA condenser. The condensed acid is mixed with cold circulating acid before entering the acid vessel. The mixture obtains a temperature of 70 °C, and is then further cooled to 40 °C.

The acid leaves the condenser with an average concentration of a minimum of 98 wt % and the process gas leaving the top of the condenser has a concentration of less than 20 ppm of acid mist. The temperature of the outlet process gas is 95 °C. The cooling of the process gas is achieved by blowing air through the shell side, passing tubes in cross flow direction where the shell side is divided into six passes is described in figure 2.

3.2.5 Tail gas treatment

Part of the sulfuric acid vapor will condense as a fine mist of liquid acid. These mist droplets are too small for separation from the process gas in the WSA condenser. A mist control unit, consisting of a quench tower followed by a H_2O_2 scrubber column, is installed in order to enable a conversion of 99.7 % and to minimize the mist content in the outlet gas.

The process gas from the WSA condenser is first treated in the quench tower where it is cooled with dilute sulfuric acid. In this way the temperature is reduced to about 50 °C. The concentration of the quench solution is maintained by adding water, which also compensates for the evaporated water loss in the scrubber.

The next unit operation is a scrubber column where the SO_2 concentration is reduced by reaction with hydrogen peroxide according to reaction 1.

$$SO_2(g) + H_2O_2(aq) \rightleftharpoons H_2SO_4(aq) \qquad \Delta H^o = -306\ kJ/mole \qquad \text{(reaction.1)}$$

The hydrogen peroxide is added to the circulating diluted acid as a 50 wt % solution. The diluted solution is passed through the packed bed of the scrubber column in counter flow with the process gas. The outlet gas from the scrubber column enters the mist filter, which is a low velocity mesh type filter, at 50 °C where the acid mist level is reduced to 2 vol. ppm. A fan is used to compensate for the

pressure drop from the tail gas treatment units. Finally, the process gas is mixed with hot surplus air from the feed gas preheater and sent to the stack at a temperature of about 80 °C.

3.2.6 Molten salt- and steam system

The molten salt mixture is first heat exchanged with the process feed gas and then with water to produce steam. The molten salt is recycled at 275-475 °C between the heat exchangers, according to figure I and table II in appendix D. The salt consists of a eutectic mixture of 53% KNO3, 40% $NaNO_2$ and 7% $NaNO_3$, which has appropriate thermal properties and therefore enables an efficient temperature control and a minimum space requirement.

As mentioned before the excess heat of the molten salt is used to produce saturated steam at the pressure of 15 bar g in the heat exchanger. It is crucial that the temperature of the cooling media is above the melting point of the salt, i.e. 142 – 160 °C.

The steam is then used for different applications such as addition of water to the process gas to ensure surplus of water for the hydration reaction and evaporation of liquid SO_2 in the SO_2 evaporator [10,16].

4. Operating conditions – case study

The WSA plant operates in three cyclical modes with gases from the lead smelter. First there is a six hour period with high concentration of sulfur dioxide (12.6%), smelting period, followed by one hour period of reduction with very low sulfur dioxide content (0.5%). Finally there is a thirty minutes period with no sulfur dioxide in the process gas, the slag tapping period.

4.1 Smelting period control parameters

The feed gas flow rate and SO_2 concentration is high and in order to reach the desired concentration in the inlet to the SO_2 converter, hot air is added. The size of this dilution air flow is based on the desired SO_2 concentration and feed flow rate, in order to achieve a dew point less than 260 °C. Further steam is added to the process gas in order to obtain 2 vol % of water in the outlet of the WSA condenser. To gain a stable outlet process gas temperature, it is crucial to control the cooling air in the WSA condenser. This control of the outlet gas temperature is an important parameter for minimizing the acid mist leaving the condenser. To ensure the minimization of the acid mist, 20 ppm, a controlled number of silicone particles are added.

The WSA condenser is followed by the H_2O_2 scrubber, where the addition of hydrogen peroxide is controlled to achieve less than 2 kg SO_2/ton produced 100 % H_2SO_4. After the H_2O_2 scrubber the remaining acid mist is reduced to 99.3% in the mist filter.

4.2 Reduction period control parameters

After the smelting period the feed gas flow is increased but the SO_2 and O_2 concentrations are low. Because of the low SO_2 concentration in the feed gas just a small amount of reaction heat is produced and therefore a natural gas supported burner is required for feed gas preheating. Liquid SO_2 is evaporated and added to the process gas to enhance the reaction.

Dilution of the feed gas is still necessary due to the low O_2 content and is based on calculation in order to achieve more than 3 % oxygen in the outlet of the converter. In contrast to the smelting period, it is not necessary to add steam since the water content is sufficient. Similarly to the smelting period, the unit operation conditions and the restrictions are similar.

[16] Hansen F., 2007, *WSA Plant for Lead Smelter Process description Haldor Topsoe*, pages 6-8

4.3 Slag tapping period control parameters

After the reduction period the feed gas flow decreases and no SO_2 is present in the process gas. To be able to operate the converter continuously, liquid SO_2 is evaporated. The maximum capacity available is 4167 kg/h, but the plant is designed for a minimum of 572 kg/h of sulfur dioxide. Similar to the reduction period it is not necessary to add steam but dilution air is still required. Because of the low SO_2 content the support of the burner is needed [10, 17].

5. Catalyst

With present-day catalysts, a temperature of 400 °C is necessary to initiate the reaction. The reaction mechanism varies depending on the catalyst used. According to present understanding, oxidation over a vanadium catalyst is a homogenous reaction that takes place in a liquid melt of active compounds on both the external and internal surfaces of an inert solid catalyst carrier. The reaction mechanism and the chemical structure of the active compounds have not yet been fully clarified.

The upper temperature limit of the catalyst is set by the thermal stability. Above 600-650 °C catalyst activity is lost permanently due to damage to the carrier structure and reduction of its internal surface[18].

5.1 Proposed reaction mechanism

The oxidation reaction may, depending on the reaction conditions, follow either an associative or a redox mechanism. Since the mechanism has not yet been defined, it has been suggested that for high temperatures the reaction mechanism is of the redox type[19].

$$V_2O_5 + SO_2 \rightleftharpoons V_2O_4 + SO_3 \qquad \text{(reaction.2a)}$$

$$V_2O_4 + \frac{1}{2}O_2 \rightarrow V_2O_5 \qquad \text{(reaction.2b)}$$

Reaction 2a is fast and causes the deviation of the catalyst composition, that can be described by the equation

$$\Delta[V^{5+}] = [V^{5+}] - [V^{5+}]_s \qquad \text{(eq.1)}$$

where $[V^{5+}]$ and $[V^{5+}]_s$ are the current and the steady state relative concentrations of the pentavalent vanadium. In non steady state conditions SO_2 can be converted either due to variations in the catalyst composition according to reaction 2a, or the catalytic reaction, which rate can be taken equal to that of reaction 2b. However, the rate of the catalytic oxidation depends on mass and heat transfer at the gas-liquid interface of the catalyst. Other parameters, such as gas velocity, gas distribution, and residence time in the catalyst bed, must be considered to determine how closely sulfuric dioxide conversion in practice will approach the theoretical equilibrium.

[17] Hansen F., 2007, *WSA Plant for Lead Smelter Process description Haldor Topsoe*, pages 10-11
[18] Ullmann's *Encyclopedia of Industrial Chemistry*, 7th ed., 2007, a_25_635.pdf, page 13
[19] Ponomarev V.E et. al., 1981, *Kinetics of SO_2 oxidation on $K_2S_2O_7$-V_2O_5 catalyst in non-steady conditions*, React. Kinet. Catal. Lett., Vol 18 No. 3-4 421-425, pages 421-423

5.2 Haldor Topsoe VK-series

Commercial catalysts contain 4-9 wt % vanadium pentoxide, V_2O_5, which is the active component together with alkali-metal sulfate promoters. During operating conditions these form a liquid melt in which the oxidation of sulfur dioxide takes place. Potassium sulfate promoter is often used in a K/V molar ratio of 2.5-3.5. To generate large specific surface areas, calcinated kieselguhr is used as carrier material in the form of silica gel or zeolites. The shape of the carrier material is of great importance to minimize the pressure drop and sensitivity to dust blockage[20].

During the activation process, the catalyst absorbs a large amount of sulfur trioxide through which molten alkali sulfates and pyrosulfates, $S_2O_7^{2-}$, are formed. The sulfates and pyrosulfates dissolve the vanadium salts and it has been recognized that the active part of the catalyst is a molten salt mixture. It has been shown that the stability of high catalytic activity is related to the ability of maintaining the vanadium in the pentavalent oxidation state and the $V^{5+} \rightleftharpoons V^{4+}$ equilibrium shifted to the left. Precipitation of $V^{3+}$and V^{4+}compounds occur at temperatures below circa 420 ˚C in water free environment and at even lower temperatures in humid surroundings.

Table 3. Composition and temperatures of deactivation, and precipitation for industrial SO_2 oxidation catalysts.

Catalyst	Chemical Composition	Mole% V2O5 of active phase	Average pore size	Tb (˚C)[a]	Apparent activation energy T > Tb (kcal/mol)	Apparent activation energy T < Tb (kcal/mol)
VK38[b]	K/Na/V = 3/0.8/1	20.8	Normal	421	20.9	60.1
VK38[c]	K/Na/V = 3/0.8/1	20.8	Normal	419	16.6	55.5
VK58[c]	K/Cs/Na/V = 3/1/0.25	19.0	Normal	382	16.6	56.0
VK58[b]	K/Cs/Na/V = 3/1/0.25	19.0	Normal	379	15.0	55.6
VK-WSA[b]	K/Na/V = 3/0.8/1	20.8	Small	421	11.7	28.5
VK-WSA[c]	K/Na/V = 3/0.8/1	20.8	Small	383	16.9	41.2

a) Tb is the temperature at which the compound precipitation (V^{IV} and/or V^{III}) occur simultaneously.
b) Feed gas: 0.2 % SO_2, 4.5 % O_2, 15 % CO_2 and 80 % N_2
c) Feed gas: 0.2 % SO_2, 4.0 % O_2, 14 % CO2, 74.8 % $N_2$and 7 % H_2O.

VK38 is a typical industrial SO_2 oxidation catalyst containing sodium and potassium salts as promoters. VK58 is an improved low-temperature activity catalyst and is typically placed as a last bed. The mixing of alkali promoters and Cs is very advantageous for the stability of V^{5+} compounds at lower temperature.

VK-WSA has the same chemical composition as VK38 but the difference is that VK-WSA has a modified porous kieselguhr support for use in humid feed gases. The composition of the catalysts is shown in table 3. It has been shown that the presence of water vapor in sulfuric acid has a beneficial effect for high catalytic activity at lower temperatures. The advantage of lower operating temperature is that the equilibrium, $SO_2 + ½O_2 \rightleftharpoons SO_3$ reaction, is shifted to the right and allows lower SO_2 emissions in the stack gas[21].

[20] Ullmann's *Encyclopedia of Industrial Chemistry*, 7th ed., 2007, a_25_635.pdf, pages 12-13
[21] A. Christodoulakis S. Boghoisan, *Molecular structure of supported molten salt catalysts for SO_2 oxidation*, Journal of Catalysis 215, 2003, pages 139-149

5.3 Service life

The dust load of the process gas entering the converter will eventually increase the pressure drop over the catalyst bed and reduce both gas throughput and sulfur dioxide conversion. This is the reason why the catalyst must be screened from time to time to remove dust. When catalyst is withdrawn, a certain amount is bound to be lost as a result of abrasion. The loss must be compensated by addition of more catalyst material. The properties of the catalyst are shown in table 4.

Vanadium catalysts are largely insensitive to catalyst poisons, in contrast to platinum. For example fluorine compounds in elevated concentrations will attack the carrier material, leading to increased abrasion loss, and volatilization of the vanadium and consequently decrease the activity.

Also water vapor can be harmful to the vanadium catalyst if the temperature is not sufficiently high to prevent condensation of sulfuric acid. At low temperatures there is also a danger that water will be absorbed by hygroscopic active parts, and this can decrease the mechanical strength of the catalyst[22].

Table 4. Typical properties of the VK-WSA series[23]

Catalyst	VK-WSA	
Description		
Diameter(outer/inner), (mm)	25/9	12/4
Length, (mm)	22-28	10-14
Chemical composition		
V_2O_5, (wt%)	6-8	
K, (wt%)	7-12	
Na, (wt%)	1-2	
Physical properties		
Approx. bulk density, (kg/m^3)	420-440	350-370
Attrition loss, (%)	4-6	2-4
Operating conditions		
Gas concentration, SO_2 (mole%)	0-10	
Minimum O_2/SO_2, (mole/mole)	0.6	

6. Process Control

7.1 General Control philosophy

Due to the heavy fluctuations in the process a proper control system has to be introduced to the process. There are several methods to control processes, depending on the purpose of the control and what can be measured. The main purpose of a control system is to make the output signal track the reference signal.

6.1.1 Feedback and feed forward

In feedback systems the output signal is sent back and compared with the reference signal to form an error signal that can be minimized through the controller. A drawback with pure feedback is that a deviation has to be registered in the error before any corrective action is taken by the controller. The idea of feed forward is to measure the disturbance and compensate before it enters the process. A drawback with feed forward is that it requires good process models. Feed forward is often combined with feedback, to give very effective controllers.

[22] Ullmann's *Encyclopedia of Industrial Chemistry*, 7th ed., 2007, a_25_635.pdf, pages 13-14
[23] LH/MSHJ, 2007, *Haldor Topsoe A/S Product Sheet, Sulfuric Acid Catalyst VK-WSA*

6.1.2 PID control

The most frequently used control system is PID control. In its basic form it consists of three terms:

$$u(t) = K_d \left(e(t) + \frac{1}{T_i} \int^t e(s)ds + T_d \frac{de(t)}{dt} \right) \quad \text{(eq.2)}$$

and can be expanded and rewritten on Laplace form:

$$u(t) = K_d \left(bU_c(s) - Y(s) + \frac{1}{sT_i}\left(U_c(s) - Y(s)\right) - \frac{sT_d}{1+\frac{sT_d}{N}} \right) \quad \text{(eq.3)}$$

where U, U_c and Y denotes the Laplace transforms of the input , reference and output signal. If only the proportional part is used a stationary error will occur. This is eliminated if integral action is introduced. When integral action is used there is a risk of saturation, integral part becomes greater than the actuator can be set. The integrator then integrates the value to a very large value and the controller becomes unstable. This is avoided by implementing an anti-windup scheme, for example tracking. If the output signal is very noisy, the derivative part is omitted.

There are a lot of methods to tune the controller parameters K_d, T_i, and T_d. A common way to do this is Ziegler-Nichols method, where a step response is made and the parameters are estimated from constants read from a diagram of the output signal versus the time.

6.1.3 Cascade control

Sometimes it can be difficult to reach an optimal controller performance with a simple feedback controller, for example if the process has large delays relative to the time constant. Sometimes measuring secondary process variables gives information about the disturbances before the effect is shown in the controlled variable. By introducing a cascade controller with two (or more) loops a primary (outer) loop can be used to give a reference signal to a secondary (inner) loop. The disturbance is then taken care of earlier with a result in improved performance[24].

6.1.4 State spaced Controllers

The controlled variable is not always measurable and has to be estimated by a model. The estimation is done in observers and can be done in different ways. This requires a good knowledge of the process dynamics and can be easily calculated if the system is known on state space form. The process is then controlled from the estimated controlled variable through state feedback[25].

7. Detection of sulfur dioxide

It is important to use accurate and reliable methods, since laws regulate the amount of sulfur compounds that's allowed in outgoing process gas to the surrounding environment. The quantitative chemical methods used to detect sulfur dioxide are iodometry, titrimetry, gravimetry or colorimetry. Continuous measuring methods, i.e. continuous in plant monitoring, of the sulfur dioxide content in roaster gases or tail gases in sulfuric acid plants are based on physical properties such as spectroscopic absorption in the infrared, or ultraviolet or electrical conductivity. It is essential to set sampling procedures for accuracy and reliability when using continuous monitoring[26].

---

[24] Wittenmark B., Åström, K. J., Bay Jørgensen S., 2003, *Process Control*, Department of automatic control, pages 108-114, 134-153, 169-174, 203-209

[25] Wittenmark B., Åström, K. J., Årzén K-E, 2007,*Computer Control: An Overview*, Department of automatic control, pages 57-74

[26] Ullmann's *Encyclopedia of Industrial Chemistry*, 7th ed., 2007, a_25_569.pdf, pages 41-42

The sample is passed through an aqueous solution of hydrogen peroxide and the amount of sulfuric acid is determined by titration or gravimetric analysis. The fraction of the acid that comes from sulfur dioxide is determined by measuring the SO_2 concentration of a second sample and calculating a sulfuric acid equivalent. This is subtracted from the result of the first determination to give the amount of sulfuric acid from SO_3 alone. One resembling method is to let the gas pass through en isopropyl alcohol solution, which absorbs sulfur trioxide without oxidizing sulfur dioxide. The resulting sulfuric acid is then titrated against a barium chloride solution using Thorin as an indicator[27].

8. Simulation approach

The model is derived from the continuity equation for a tube reactor. The dispersion model was chosen to describe the WSA converter, with the heat exchanger included. A control system will be added to the heat exchanging salt system which will regulate the out coming temperature of the bulk gas. The model will be tuned to fit the three cases in regard to the concentrations out of the converter, the temperature in the converter and the temperature in the salt system.

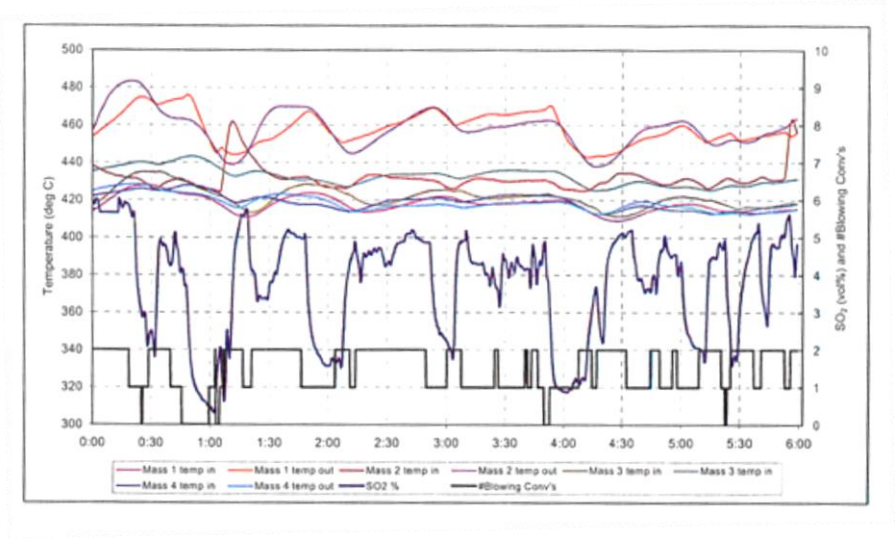

Figure 5. Example of fluctuating feed gas SO_2 concentration.

The next step will be to introduce time-delays and switching between the cases according to figure 5. When doing that it will be possible to see how the transients will propagate through the converter. The next step will be to introduce more unit operations like the condenser and the mist control unit. The last step will be to remove some of the assumptions below and make the model more realistic.

A number of assumptions have been made in order to simplify the model:

1. The system is ideal due to moderate pressures and the physical properties of the gas will therefore be described with equations valid during ideal conditions.
2. The WSA-converter can be described as a tube reactor.
3. There will be dispersion in the axial but none in the radial direction, which results in a one dimensional plug flow reactor model.
4. The external mass transfer will be neglected, which means that the concentration in the gas bulk is uniform all the way into the surface.

[27] Ullmann's *Encyclopedia of Industrial Chemistry*, 7th ed., 2007, a_25_635.pdf, page 64

5. Inner temperature gradients will be neglected as well as the temperature gradient in the stagnant thin layer at the surface.
6. The heat transfer between the gas bulk and salt-system ($k \cdot A$) will be described with a linear polynomial, with data from the data sheets. It will be described as a function of the salt flow.
7. The inner mass transfer is assumed to be included in the intrinsic reaction rate expression, even thou corresponding conditions deviates from experimental conditions.
8. The catalyst beds are adiabatic with no heat-losses.
9. The catalyst will not lose activity due to inactivation or blocking.
10. The heat exchangers in the converter are of counter-current tube type.
11. No heat-losses through the wall or due to fouling in the heat exchangers.
12. The simulation ignores any pressure drops.
13. Uniform porosity throughout the catalyst beds.
14. The catalyst liquid surface does not take under consideration.

9. Derivation of the mathematical model

To follow up the developed approach, a discretization in both time and space is required to give a more accurate model and reflect the time dependent fluctuations. A model is derived that is based on a conservation principle which states:

The rate at which a specified quantity changes in a region is equal to the rate that the quantity leaves and enters the region plus the rate which the quantity is created and destroyed inside the region.

In this report it is assumed that the quantity to be modeled exists in a tube with constant cross section and that the quantity varied in the direction along the tube but not at all within a fixed cross section *A*, according to figure 6. *x* denotes the position along the length of the tube and *t* denotes the time.

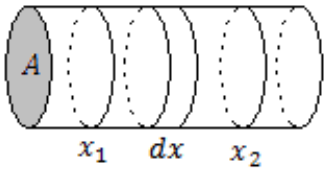

Figure 6. Schematic figure of the discretization of a tube reactor.

The density $\rho(x,t)$, measured in amount of mass per unit volume, varies continuously with the position *x* and time *t*. To be able to express the conservation principle mathematically, a small region of the tube with the width dx and cross section area A is defined. The amount of quantity in this region is $\rho(x,t)Adx$. Let $q(x,t)$ denote the flux at position x and time t and the amount of quantity crossing the section is therefore $Aq(x,t)$. Lastly, let $f(x,t)$ denote the rate that the quantity is created or destroyed within in the small region of width dx per unit time.

The conservation principle for a fixed length of a tube between x_1 and x_2 implies that the rate which flows in at x_1 minus the rate at which it flows out at x_2 plus the rate at which it is created in the differential volume can be written in mathematical terms:

$$\frac{\partial}{\partial t}\int_{x_1}^{x_2}\rho(x,t)Adx = Aq(0,t) - Aq(L,t) + \int_{x_1}^{x_2} f(x,t)Adx. \qquad \text{(eq.4)}$$

The equation 4 above is called the integral formulation of the conservation principle and can be reformulated as following partial differential equation

$$\int_{x_1}^{x_2}\left(\frac{\partial}{\partial t}\rho(x,t)+\frac{\partial}{\partial t}q(x,t)-f(x,t)\right)dx=0. \quad \text{(eq.5)}$$

Since x_1 and x_2 are arbitrary, the integral must be zero at each point, or

$$\frac{\partial}{\partial t}\rho(x,t)+\frac{\partial}{\partial t}q(x,t)=f(x,t). \quad \text{(eq.6)}$$

Many quantities have the property that the quantity flows from regions of high concentration to regions with low concentration, and the rate of flow increases as the difference in concentration increases. As an approximation, the linear relation defines

$$q(x,t)=-a(x,t)\frac{\partial}{\partial x}u(x,t) \quad \text{(eq.7)}$$

where $a(x,t)>0$ is the diffusion coefficient. In general the equation is known as Fick's Law. Substituting 7 into 6 gives the general time-dependent reaction-diffusion equation,

$$\frac{\partial}{\partial t}\rho(x,t)-\frac{\partial}{\partial x}\left(a(x,t)\frac{\partial}{\partial x}\rho(x,t)\right)=f(x,t). \quad \text{(eq.8)}$$

Convection is modeled by assuming a convective relation in which the flux is proportional to the density, i.e.

$$\varphi(x,t)=b(x,t)\rho(x,t), \quad \text{(eq.9)}$$

where the convection coefficient $b(x,t)$ determines the rate and direction of transport of the quantity being modeled. In general, many quantities are modeled by a constitutive relation of the form

$$\varphi(x,t)=-a(x,t)\frac{\partial}{\partial x}\rho(x,t)+b(x,t)\rho(x,t) \quad \text{(eq.10)}$$

which combines both diffusion and convection. Arguing as above, the general reaction-diffusion-convection equation is obtained

$$\frac{\partial}{\partial t}\rho(x,t)-\frac{\partial}{\partial x}\left(a(x,t)\frac{\partial}{\partial x}\rho(x,t)-b(x,t)\rho(x,t)\right)=f(x,t). \quad \text{(eq.11)}$$

A solution is developed for a convection-diffusion equation describing chemical transport with adsorption and production. The problem is formulated in a finite domain where the appropriate law of conservation is valid. In order to specify a unique solution boundary conditions at $x=0$ and $x=L$ must be specified. Also initial data at $t=0$ must be given. The time dependent initial two point boundary value problem reads: find $u(x,t)$ such that

$$\begin{cases}\frac{\partial}{\partial t}\rho-\frac{\partial}{\partial x}\left(a\frac{\partial}{\partial x}\rho-b\rho\right)=f & in\ (0,L)\times(0,T)\\ \rho(0,t)=\rho(L,t)=0 & for\ t\in(0,T)\\ \rho(x,0)=\rho_0(x) & for\ x\in(0,L)\end{cases} \quad \text{(eq.12)}$$

where f and g are given data. The boundary values $\rho(0,t)=\rho(L,t)=0$ are known as homogenous Dirichlet boundary conditions.

Other boundary conditions are homogenous von Neumann[28]:

$$a\frac{\partial}{\partial x}\rho = g. \qquad \text{(eq.13)}$$

9.2 Mathematical model for the converter and the interbed heat exchangers

The mathematical model, which describes the concentration profile in the tubular reactor, derived from the conservation principle is

$$\frac{\partial c_{b_i}}{\partial t} = D_{ax}\frac{\partial^2 c_{b_i}}{\partial x^2} - \frac{v}{\epsilon}\frac{\partial c_{b_i}}{\partial x} - \frac{(1-\varepsilon_c)}{\varepsilon}r_i(T_s) \qquad \text{(eq.14)}$$

where c_{b_i} is the concentration of compound *i* at position *x* and time *t*, ε is the porosity, ε_c is the converter porosity and presented in table VII in appendix B, D_{ax} is the diffusion coefficient in the gas, v is the linear gas velocity and r_i is the rate that the compound *i* is converted within in the small region of width dx per unit time. The reaction rate is dependent of the temperature of the catalytic adiabatic beds, T_s, which is obtained by the energy balance

$$\frac{\partial T_s}{\partial t} = \kappa_s\frac{\partial^2 T_s}{\partial x^2} + \frac{\Delta H r_i}{\rho(T_s)c_p(T_s)}r_i(T_s) - \frac{A_{ht}k}{AL}\frac{1}{\rho(T_s)c_p(T_s)}(T_s - T) \qquad \text{(eq.15)}$$

where κ is the heat conductivity, $\rho(T_s)$ and $c_p(T_s)$ is the density respectively the heat capacity of the catalyst, $\frac{A_{ht}k}{AL}$ represents the heat transfer term which is unknown and tuned in during the solution algorithm.

The bulk temperature T varies according to

$$\frac{\partial T}{\partial t} = \kappa\frac{\partial^2 T}{\partial x^2} - \frac{v}{\epsilon}\frac{\partial T}{\partial x} + \frac{A_{ht}k}{AL}\frac{1}{\rho(T)c_p(T)}(T_s - T) \qquad \text{(eq.16)}$$

where $\rho(T_s)$ and $c_p(T_s)$ is the density respectively the heat capacity of the bulk. Heat is evolved in all reactions, since exothermic reactions take place, which is liberated in the catalytic adiabatic beds. This phenomenon is described according to equation 15. The heat evolved is transferred through the bed, because of the conduction term, as well as exchanged with the bulk because of the current temperature gradient. The heat transferred to the bulk is smeared out because of the diffusion term $\kappa\frac{\partial^2 T_s}{\partial x^2}$, as well as convected according to the corresponding convection term, $\frac{v}{\epsilon}\frac{\partial T}{\partial x}$.

Analogously to the converter, the mathematical model for the heat exchangers was derived from the conservation principle which implies

$$\frac{\partial T}{\partial t} = \frac{G}{A}\frac{\partial T}{\partial x} - kA_{ht}\frac{1}{\rho(T)c_p(T)}(T - T_{ss}) \qquad \text{(eq.17)}$$

where T is the bulk temperature inside the heat exchangers and T_{ss} is the salt temperature which varies according to

$$\frac{\partial T_{ss}}{\partial t} = -\frac{G_{ss}}{A}\frac{\partial T_{ss}}{\partial x} + kA_{ht}\frac{1}{\rho(T_{ss})c_p(T_{ss})}(T - T_{ss}) \qquad \text{(eq.18)}$$

G denotes the volumetric flow, A and kA_{ht} is the cross section area respectively the heat transfer term which both are unknown and tuned in the solution algorithm.

[28] K.Eriksson, D. Estep, C. Johnson, *Applied Mathematics: Body & Soul, Analysis and linear algebra*, pages 757-761, August 2003

The heat exchanger is of the type tube counter-current, according to figure I in appendix D, where the bulk flows in the specified positive direction.

9.3 Reaction thermodynamics

In the contact process, the gas mixture containing sulfur dioxide and oxygen is passed over a catalyst to oxidize the sulfur dioxide to sulfur trioxide according to the reaction 3[29]

$$SO_2 + \frac{1}{2}O_2 \rightleftharpoons SO_3 \qquad \Delta H^o = -99.0\ kJ/mole \qquad \text{(reaction.3)}$$

On account of the negative reaction enthalpy, the SO_2 equilibrium conversion decreases with rising temperature. In the next step, the sulfur trioxide is absorbed where it reacts with present water to form sulfuric acid in the gas phase according to the reaction 4 and 5

$$SO_3(g) + H_2O(g) \rightleftharpoons H_2SO_4(g) \qquad \Delta H^o = -101\ kJ/mole \qquad \text{(reaction.4)}$$

$$H_2SO_4(g) + 0.17\ H_2O(g) \rightleftharpoons H_2SO_4(aq.\ 97\ wt\%) \qquad \Delta H^o = -69\ kJ/mole \qquad \text{(reaction.5)}$$

Notice that heat is produced in the reactions 3, 4 and 5[30]. The position of the equilibrium in the exothermic gas-phase reaction (reaction 3) depends on the prevailing temperature and partial pressures of the reactants.

The thermodynamic equilibrium for reaction 3 can be written as a function of partial pressures and the equilibrium constant, K_p, according to equation 19 below

$$K_p = \frac{p_{SO_3}}{p_{SO_2} \cdot p_{O_2}^{0.5}} \qquad \text{(eq.19)}$$

An increase in pressure will increase the degree of conversion at equilibrium. The maximum possible equilibrium conversion of sulfur dioxide at a given temperature *T* and the total pressure *p* depends upon the SO_2 and O_2 concentrations. However, when air is used as the source of oxygen in the gas phase oxidation, the oxygen and sulfur dioxide concentrations are inversely related. Therefore, the greater the oxygen concentration in the combustion gases the lower the sulfur dioxide content will be. To determine the SO_2 conversion, the volumetric O_2/SO_2 ratio in the feed gas is of great importance. The sulfur dioxide oxidation requires a stoichiometric O_2/SO_2 ratio of 0.5: 1. The presence of excess oxygen raises the SO_2 equilibrium conversion as mentioned before, but it is also an essential prerequisite for maintaining the activity of the vanadium catalyst.

In an industrial plant, sulfur dioxide conversion never reaches the theoretical equilibrium value. The gas-phase oxidation is kinetically inhibited and not feasible at any temperature without a catalyst. Increase in temperature increases the reaction rate, but shifts the position of the equilibrium reaction in an unfavorable way[29].

In the design and construction of any converter intended to assure maximum sulfur dioxide conversion, removal of the considerable reaction heat is of great importance. The reaction is generally carried out during adiabatic conditions, so the temperature of the catalytic bed rises and thereby limiting the level of SO_2 conversion which is consistent with the thermodynamic equilibrium.

[29] Ullmann's *Encyclopedia of Industrial Chemistry*, 7th ed., 2007, a_25_635.pdf, page 10
[30] Rud Bendixen O. Hansen H.K., *Topsoe WSA Technology Provides Efficient Desulfurization of Off-gases from Non-ferrous Roasters, TMS Annual Meeting*, EPD Congress 1996, 1996, page 801

To achieve a high final sulfur dioxide conversion, the total catalyst mass must be divided into several catalyst beds and hot process gas leaving each bed is cooled to the optimal working temperature before it enters the next bed. Figure 7 shows the schematic sulfur dioxide conversion as the function of the temperature for a three bed converter operating under adiabatic conditions.

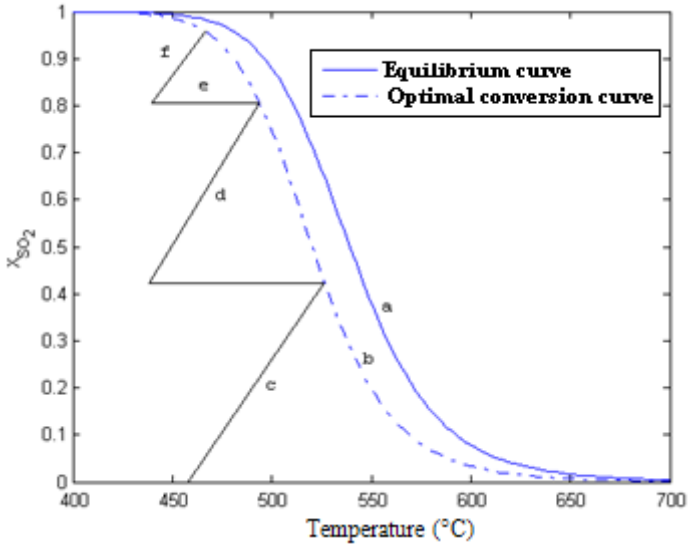

Figure 7. Schematic reaction profiles and SO_2 conversion for 3-bed catalyst a) Equilibrium curve (eq.22); b) Optimal conversion curve (eq.23); c) Adiabatic reaction in bed 1; d) Adiabatic reaction in bed 2; e) Cooling; f) Adiabatic reaction in bed 3.

The solid line represents the equilibrium curve, generated by equation 22 which is valid for a reversible reaction, $SO_2 + \frac{1}{2}O_2 \rightleftharpoons SO_3$, at thermal equilibrium according to

$$k_{SO_2} \cdot c_{SO_2} = k_{SO_3} \cdot c_{SO_3} \qquad \text{(eq.20)}$$

which can be expressed according to

$$\frac{c_{SO_3}}{c_{SO_2}} = \frac{k_{SO_2}}{k_{SO_3}} \exp\left(-\frac{E_{a,SO_2} - E_{a,SO_3}}{RT}\right) = K_{eq} \qquad \text{(eq.21)}$$

and by introducing $c_{SO_2} = c^0_{SO_2}\left(1 - x_{SO_2}\right)$ and $c_{SO_3} = c^0_{SO_3} x_{SO_3}$, the equilibrium conversion can be expressed as

$$x_{SO_2 e} = \frac{K_{eq}}{K_{eq}+1}\,. \qquad \text{(eq.22)}$$

The dashed line represents the curve which gives the optimal conversion, $x_{SO_2 opt}$, of sulfur dioxide at the current temperature, generated by equation 23[31].

$$x_{SO_2 opt} = \frac{\frac{E_{a,SO_2}}{E_{a,SO_3}} \cdot K_{eq}}{\frac{E_{a,SO_2}}{E_{a,SO_3}} \cdot K_{eq} + 1} \qquad \text{(eq.23)}$$

[31] Bjerle I., Lidén G., 2007, *Kemisk reaktionsteknik fk (KET061)*, Institutionen för Kemiteknik LTH, Sep 2007 Lund

9.4 Temperature dependent variables

In the following section, temperature dependent expressions are introduced. The exothermal reactions gave rise to an elevated temperature which effects properties with strong temperature dependencies, e.g. heat capacity and density of the gas bulk.

9.4.1 Reaction rate correlations

In 1984 a correlation of Gio et al[32] on SO_2 oxidation over a vanadium catalyst showed the following kineticsas a function of the partial pressures

$$r_{SO_2} = \frac{k_1 p_{SO_2} p_{O_2}^m (1-a)}{\left(p_{SO_2} + k_2 p_{O_2}^m + k_3 p_{SO_3}\right)} \quad \text{(eq.24)}$$

where a, calculated from equation 25, is an indication of how far the reaction is from equilibrium.

$$a = \frac{p_{SO_3}}{K_p p_{SO_2} p_{O_2}^{0.5}}, \quad \text{(eq.25)}$$

The equilibrium constant depends on the temperature according to the logarithmical expression

$$\log K_p = \frac{4905.5}{T} - 4.6455, \quad \text{(eq.26)}$$

and the reaction rate constants can be expressed according to the Arrhenius equation

$$k_i = k_{i,o} \exp\left(-\frac{E_i}{RT}\right) \quad i = 1,2,3. \quad \text{(eq.27)}$$

The parameters k_i and E_i are presented in table I in appendix B.

When moderate temperatures (room temperature) are at hand, the formation of sulfuric acid, reaction 4, will happen as soon as sulfur trioxide is produced[33]. But as the temperature rise the equilibrium will favor the reactants, as expected since it is an exothermic reaction.

When studying the given cases it is obvious that the equilibrium is favoring the products just slightly. It is very hard finding any kinetic expression describing this reaction, so it has been suggested that it is a second order reaction with regard to the reactants, see equation 28.

$$r_{H_2SO_4} = k_{H_2SO_4} p_{SO_2} p_{H_2O} \quad \text{(eq.28)}$$

9.4.2 Physical properties

Since the pressure is moderate (< 10 bar) throughout the WSA process it is possible to assume that the ideal gas law is valid throughout the process. The ideal gas law is much more sensitive to pressure than temperature enhancement, which implies that the temperature interval will not interfere with the assumption of ideal behaviour.

The specific heat capacity is calculated from equation 29 with constants from table II in appendix B. The interval where the constants are valid can be seen in the same table.

$$C_p = C_1 + C_2 \left(\frac{\frac{C_3}{T}}{\sinh\left(\frac{C_3}{T}\right)}\right)^2 + C_4 \left(\frac{\frac{C_5}{T}}{\cosh\left(\frac{C_5}{T}\right)}\right)^2 \quad \text{(eq.29)}$$

Equation 29 is valid only during ideal conditions and the specific heat capacity will be in $\left(\frac{kJ}{kmol \cdot K}\right)$.

[32] H. X. Gio, Z. H. Han, K. C. Xie, 1984, J. Chem. Ind. Eng. China, vol 37, page 244
[33] Seinfeld J.H. et al, 1998, *Atmospheric Chemistry and Physics*, page 314

Equation 30 is valid during ideal conditions and moderate pressure. The constants are valid throughout the temperature interval. It is only the constants for sulfur trioxide which has been extrapolated above its validity boundary.

$$\eta = \frac{K_1 T^{K_2}}{1+\frac{K_3}{T}+\frac{K_4}{T^2}} \cdot 10^{-3} \quad \text{(eq.30)}$$

The values of the constants K_1, K_2 and K_3 are found in table III in appendix B. The viscosity unit is in $Pa \cdot s$. Equation 31 calculates the density from respective species during ideal behavior. The molecular weights can be found in table IV in appendix B.

$$\rho = \frac{M_W \cdot P_0}{R \cdot T} \quad \text{(eq.31)}$$

The density, in the unit $\mathrm{kg/m^3}$, is derived from the ideal gas law where the pressure, P_o, has to be in Pascal, the molecule weight, M_W, in $\frac{\mathrm{kg}}{\mathrm{mol}}$, the gas constant, R, in $\frac{J}{mol \cdot K}$ and the temperature, T, in K.

9.5 Solution algorithms – schemes for the convection-diffusion equation

To be able to gain a high resolution and accuracy of the simulation of the converter, a spatial discretization of the adiabatic catalytic beds and of the interbed heat exchangers were carried out. This implies that the solution is evaluated at a finite number of points in the physical domain. To be able to implement and analyze the behavior of the partial differential equations, which describe the component concentrations and the temperature in the bulk in the adiabatic catalytic beds, a finite-difference approximation is developed. The method replaces continuous derivatives with finite differences that involve only the discrete values associated with positions on the discretization.

The finite difference approximations developed in the appendix C are now assembled into a discrete approximation to the one dimensional convection-diffusion equation. Space derivatives are replaced by finite differences.

Time derivates are integrated by the implemented MATLAB solver *ode15s* which solves initial value problems for ordinary differential equations. *ode15s* is a variable order solver based on the numerical differentiation formulas. Optionally, it uses the backward differentiation formulas, also known as Gear's method. It is a multistep solver which can handle stiff problems as well as solving a differential-algebraic problem. By specifying the interval of integration, $[t_0, t_f]$, the solver imposes the initial conditions at t_0, and integrates from t_0 to t_f. Further details can be found in MATLAB's Mathematics documentation.

9.6.1 Implementation

In this section the implementation of the one-dimensional convection-diffusion equation is presented. To be able to implement the boundary conditions, false grid points have been introduced[34]. At the inlet Dirichlet conditions are valid and at the outlet von Neumann conditions are applied. This implies that the concentration in the false grid point before the first domain grid point is the same as in the bulk.

A von Neumann condition implies that there is no flux across the boundary, i.e. $c_{N+1} = c_N$.

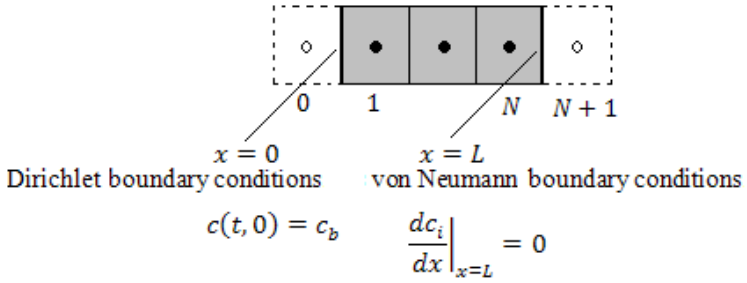

Figure 8. Sampling on a grid.

For equation 14, a backward special difference for the convection part and a centered difference for the diffusion part are sampled on the grid according to figure 8 which gives

$$\underbrace{\frac{d}{dt}\begin{bmatrix} c_1 \\ \vdots \\ c_N \end{bmatrix}}_{\boldsymbol{c}} = D_{ax}\left(\underbrace{\frac{1}{\Delta x^2}\begin{bmatrix} -2 & 1 & 0 & 0 \\ 1 & -2 & \ddots & 0 \\ 0 & \ddots & \ddots & 1 \\ 0 & 0 & 1 & -2 \end{bmatrix}}_{A_2}\underbrace{\begin{bmatrix} c_1 \\ \vdots \\ c_N \end{bmatrix}}_{\boldsymbol{c}} + \underbrace{\frac{1}{\Delta x^2}\begin{bmatrix} 1 & 0 \\ 0 & \vdots \\ \vdots & 0 \\ 0 & 1 \end{bmatrix}}_{A_{f_2}}\underbrace{\begin{bmatrix} c_0 \\ c_{N+1} \end{bmatrix}}_{\boldsymbol{c_f}}\right) -$$

$$\frac{v}{\epsilon}\left(\underbrace{\frac{1}{\Delta x}\begin{bmatrix} 1 & 0 & 0 & 0 \\ -1 & 1 & \ddots & 0 \\ 0 & \ddots & \ddots & 0 \\ 0 & 0 & -1 & 1 \end{bmatrix}}_{A_1}\underbrace{\begin{bmatrix} c_1 \\ \vdots \\ c_N \end{bmatrix}}_{\boldsymbol{c}} + \underbrace{\frac{1}{\Delta x}\begin{bmatrix} -1 & 0 \\ 0 & \vdots \\ \vdots & 0 \\ 0 & 0 \end{bmatrix}}_{A_{f_1}}\underbrace{\begin{bmatrix} c_0 \\ c_{N+1} \end{bmatrix}}_{\boldsymbol{c_f}}\right) - \frac{(1-\varepsilon_c)}{\varepsilon}\underbrace{\begin{bmatrix} r_1 \\ \vdots \\ r_N \end{bmatrix}}_{\boldsymbol{r}} \qquad \text{(eq.32)}$$

where A_2 and A_1 are tridiagonal, nonsymmetrical matrixes with constant coefficients. The equation 32 can be expressed as a matrix multiplication as

$$\frac{d\boldsymbol{c}}{dt} = D_{ax}\left(A_2\boldsymbol{c} + A_{f_2}\boldsymbol{c_f}\right) + \frac{v}{\epsilon}\left(A_1\boldsymbol{c} + A_{f_1}\boldsymbol{c_f}\right) - \frac{(1-\varepsilon_c)}{\varepsilon}\boldsymbol{r}. \qquad \text{(eq.33)}$$

Discretization of the boundary conditions yields

$$\underbrace{\begin{bmatrix} c_o \\ c_{N+1} \end{bmatrix}}_{\boldsymbol{c_f}} = \underbrace{\begin{bmatrix} 0 & \dots & 0 & 0 \\ 0 & \dots & 0 & 1 \end{bmatrix}}_{B_1}\underbrace{\begin{bmatrix} c_1 \\ \vdots \\ c_N \end{bmatrix}}_{\boldsymbol{c}} + \underbrace{\begin{bmatrix} c_b \\ 0 \end{bmatrix}}_{B_0} \qquad \text{(eq.34)}$$

and can analogously be expressed as a matrix multiplication according to

$$\boldsymbol{c_f} = B_1\boldsymbol{c} + B_0 \qquad \text{(eq.35)}$$

[34] B. Nilsson, 2008 Lecture notes, *Space distributed systems*, in the course Process simulation KETN01

Finally the equation 14 can be written as a matrix multiplication as

$$\frac{d}{dt}\boldsymbol{c} = D_{ax}\left(A_2\boldsymbol{c} + A_{f_2}(B_1\boldsymbol{c} + B_0)\right) + \frac{v}{\epsilon}\left(A_1\boldsymbol{c} + A_{f_1}(B_1\boldsymbol{c} + B_0)\right) - \frac{(1-\varepsilon_c)}{\varepsilon}\boldsymbol{r} \quad \text{(eq.36)}$$

which is implemented in the MATLAB code. Three M-files are created for the finite volume method discretization: *FVMdisc2nd* which generated A and A_f for second order derivates, *FVMdisc1st* which generates the same matrixes for first order derivates and finally *FVMdiscBV* which generates B_1 and B_0 for boundary value approximations.

The same procedure was applied on the partial differential equations that describe the temperature in the bulk, in the catalytic adiabatic beds and in the salt system.

10. Implementation of the control system and tuning parameters

10.1 Control of salt system

To be able to maintain a high conversion of sulfur dioxide through all adiabatic catalytic beds, interbed cooling inhibit the temperature raise and gain the exothermal reactions, according to figure 7. The goal for the interbed cooling system was to decrease the outlet gas bulk temperature from every bed to approach the steady state value according to table I and II in appendix D. The tuning described was carried out for the first case, where the maximum temperature elevation occurred. The already established model for the salt system could then be applied on the remaining two cases, where the temperature rises are more moderate, and the steady state temperature were reached with margin.

The salt system model can be considered a gray box model, since volumes, heat transfer areas and heat transfer coefficients have no physical relation. Notable is that its only purpose was to generate the correct gas bulk temperature in the outlet of the catalytic beds. To be able to implement a more accurate model, more date must be supplied.

To be able to control the flow of the molten salt, a basic proportional controller was implemented. The control system equation was defined by a simplified PID-equation (equation 3) and represented in equation 37.

$$q_s = q_{nom} - T_{gain}(T_{ref} - T_g) \quad \text{(eq.37)}$$

The parameter q_{nom} corrects for the stationary error, which come into existence when a proportional control is applied. By subtracting the gain, T_{gain}, multiplied with the difference in temperature, i.e. the stationary value out of the heat exchangers according to table I and II in appendix D, and the current value of the gas bulk, with the nominal flow generates the proper flow of the salt system. The values of the parameters in equation 37 are presented in table V in appendix B. The implemented controller is of the feedback control type with a stationary error correction.

The heat transfer between the salt system and the gas bulk can be described by the general heat transfer equation, according to

$$Q = kA_{ht}(T - T_{ss}), \quad \text{(eq.38)}$$

where k represents the heat transfer coefficient, A_{ht} is the heat transfer area. In the implemented model, the product kA_{ht} was obtained from steady-state calculations within the given values in table I, II and III in appendix D.

The calculated steady state values, i.e. the mean value for all corresponding heat exchangers in all cases, are presented in figure 9 as well as two linear approximations, which represents to the variation of kA_{ht} with the molten salt flow rate. The first linear approximation was insufficient to describe the relation between the flow rate and the heat transfer term because of its inability to reach zero when the flow rate approched zero. A second linear approximation was made by drawing a straight line from origo to the the highest calculated steady state value.

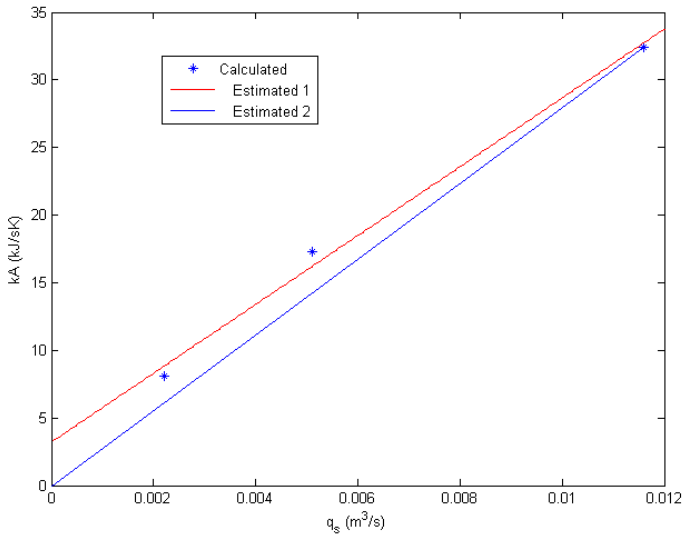

Figure 9. The heat transfer product kA_{ht} as a function of salt flow rate.

10.2 Tuning parameters

To be able to modify the process until the properly steady state values of temperatures and concentrations at the reactor outlet, according to table I and II in appendix D, were reached, an addition of tuning parameters were needed. Those tuning parameters increase respectively decrease a desired phenomenon and provide a value of unknown coefficients and physical parameters. All tuning parameters that have been used in the implantation and the solution algorithm are presented in table 5.

Table 5. Tuning parameters used in the converter model respectively in the interbed heat exchanger model (nomenclature used in the MATLAB code).

Converter		Interbed heat exchangers (1,2,3)	
D_{ax} $\left(\frac{mole}{m^2 s}\right)$	$5 \cdot 10^{-6}$	A_g (m^2)	40, 25, 30
D_S $\left(\frac{W}{mK}\right)$	$2.5 \cdot 10^{-3}$	A_s (m^2)	40, 25, 30
$k_{H_2SO_4}$	55	V_g (m^3)	40, 25, 30
$E - factor$	0.8	V_s (m^3)	40, 25, 30
$k_{reaction}$	1.1		
$k_{heatArea}$	10		

The parameter D_{ax}, which represents the diffusion coefficient in the dispersion model according to equation 14, was denoted with the same value as κ in equation 16 which represents the heat conductivity in the catalytic bed. D_s correspond to the heat transmission between the catalytic bed and the gas bulk and denote by κ_s in equation 15. To be able to correct the intrinsic reaction expression, which describes the conversion of sulfur dioxide, a tuning factor $k_{reaction}$ was introduced in the equation 24. The tuning parameter was multiplied with the equation. Analogously the reaction rate constant, $k_{H_2SO_4}$, of equation 28 denotes the tuning factor for the formation of sulfuric acid.

The heat transfer coefficient, between the surface of the catalyst and the gas bulk, as well as the heat transfer area were unknown and the product $\frac{A_{ht}k}{AL}$ had to be introduced, which represents the heat transfer term, and denoted by $k_{heatarea}$. Finally a tuning parameter, *E-factor*, was introduced to control the reaction heat evolved in equation 15. The parameter was multiplied with the term in equation 15 which corresponds to the generated reaction heat.

11. The course of simulation

The WSA converter has been modeled in MATLAB 7.4.0 (R2007a) and has been divided into 6 files. The course of simulation is visualized in figure 10 (left). The complete MATLAB code can be found in appendix E.

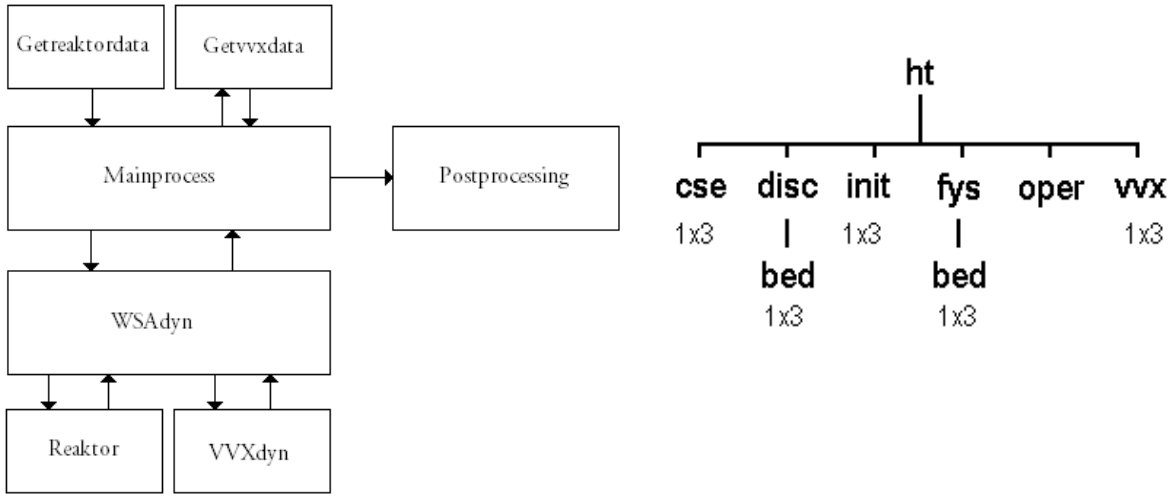

Figure 10. Schematic figure of the simulation of the WSA-converter (left) and the data structure (right).

Getreaktordata and *Getvvxdata* contain physical properties of the gas, converter dimensions, the catalyst, the liquid salt system and initial values to the converter for the three different cases. In these files it is possible to define the desired number of grid points, within the calculation is carried out, to simulate the different catalytic beds and the heat exchangers. Parameters to tune the process and flags that controls how the execution will be carried out can also be found here.

To simplify the information flow, everything is collected in a main data structure, ht, which can be seen in figure 10 (right). It is divided into smaller structures, which holds different data described in appendix D. The structures *init*, *bed*, *vvx* contains data for initial values, discretization and dimensions of every bed and heat exchanger data. The *cse* structure contains data about the different cases. These are 1×3 structures because the same variables are repeated for 3 different beds, heat exchangers and cases. Data of discretization, physical properties and operational conditions are stored in the structures called *disc*, *fys* and *oper*. The physical properties of the bulk, the salt system and the catalyst, converter dimensions and initial values can be found in appendix B.

The *Mainprocess* is the control program and it is from here one executes the simulation. The *Mainprocess* creates an initial vector which is sent into the dynamic solver ODE15s which calls for *WSAdyn*. The *Mainprocess* also arrange the post processing, including temperature and composition plots. The *WSAdyn* keeps track of time and when it is time for a case switch. It is also responsible for the information flow between *Reaktor* and *VVXdyn*. The out coming data from *Reaktor* and *VVXdyn* are transferred to one another in order to give the actual initial value, to the upcoming operation, of the bulk temperature and composition. The *WSAdyn* gathers the information from *Reaktor* and *VVXdyn* and will eventually send it back to *Mainprocess* for post processing.

The *Reaktor* includes 9 partial differential equations, one for each species (CO_2, O_2, H_2O, SO_3, SO_2, H_2SO_4, inert), one for the bulk temperature and one for the catalyst surface temperature. The *VVXdyn* includes 2 partial differential equations, one for the molten salt system and one for the bulk temperature. With the beds divided into *N* grid points and the heat exchanger divided into n_{tanks} grid points, a total of $3(9 \cdot N + 2 \cdot ntanks)$ ordinary differential equation are solved simultaneously.

12. Results

In order to study the converter conditions as well as the outlet concentration, which assure if the guarantees are fulfilled, both steady state and dynamic simulations were carried out. The dynamic study describes how the periodical changes, according to figure 5, in flow rate and sulfur dioxide concentration propagate along the converter. The steady state study indicates if the outlet concentration of sulfur dioxide is below the maximum tolerated value according to table I in appendix D. In the following section, from figure 12 to 20, the heat exchangers are not represented graphically but are of course used during the simulation. The length of respectively bed can be found in table VI in appendix B and the total bed length is 4.9 meters.

12.1 Steady state conditions

Figures of the temperature and the composition profiles are presented below during steady state behavior. The initial values for the three cases respectively are specified in table I, II in appendix D.

The bulk temperature profile through the converter, calculated from equation 16, as a function of real converter length is presented in figure 11. The figure consists of the three catalytic adiabatic beds with inter cooling heat exchangers. An exothermal reaction occurs in all catalytic beds, the temperature elevation corresponds to the amount of sulfur dioxide converted. As expected, the mainly conversion occurred in the first bed since the feed contains the highest sulfur dioxide content there.

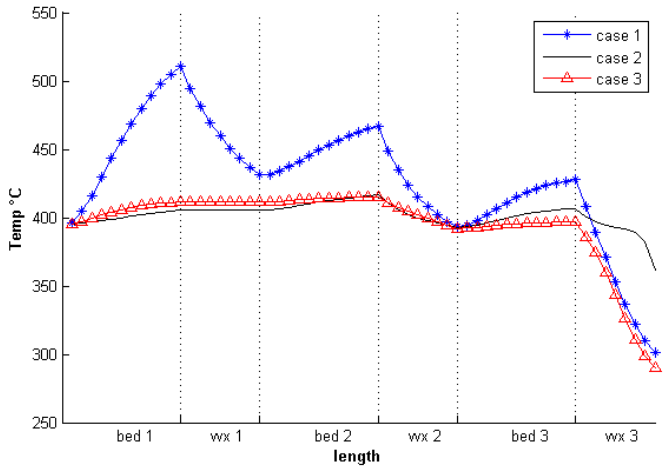

Figure 11. The bulk temperature for each case as a function of space.

The compositions profiles through the total bed length during the first case are presented in figure 12. The decrease in both sulfur dioxide and oxygen content corresponds to the molar relation according to the reversible reaction, $SO_2 + \frac{1}{2}O_2 \rightleftharpoons SO_3$.

The decrease in water content corresponds to the formation of sulfuric acid. The increase in carbon dioxide content depends on an overall molar decrease in the bulk gas.

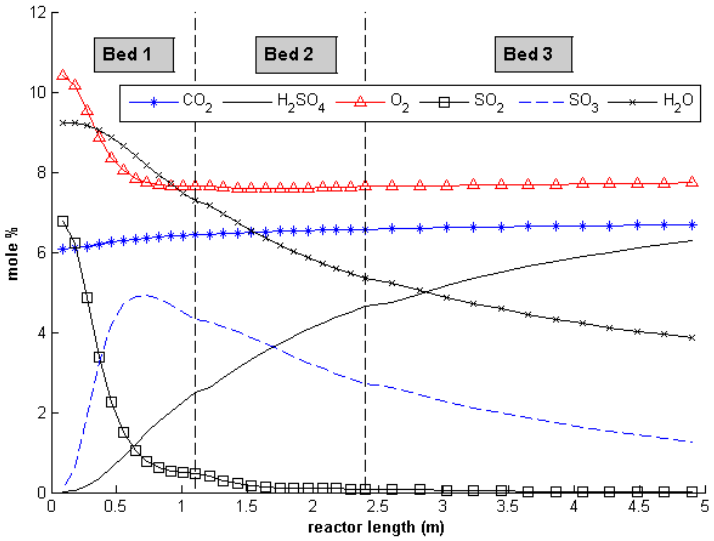

Figure 12. Composition in the bulk gas through the reactor beds during case 1.

The compositions profiles through the total bed length during the second and third case are presented in figure 13. In contrast to the concentration profile according to case 1, the very low conversion in case 2 was expected because of the low sulfur dioxide content in the feed gas. Some conversion can be noticed in case 3 because of the sulfur dioxide content that's twice as high as in case 2. Also notable is that the oxygen content are markedly increased from case 2 to case 3.

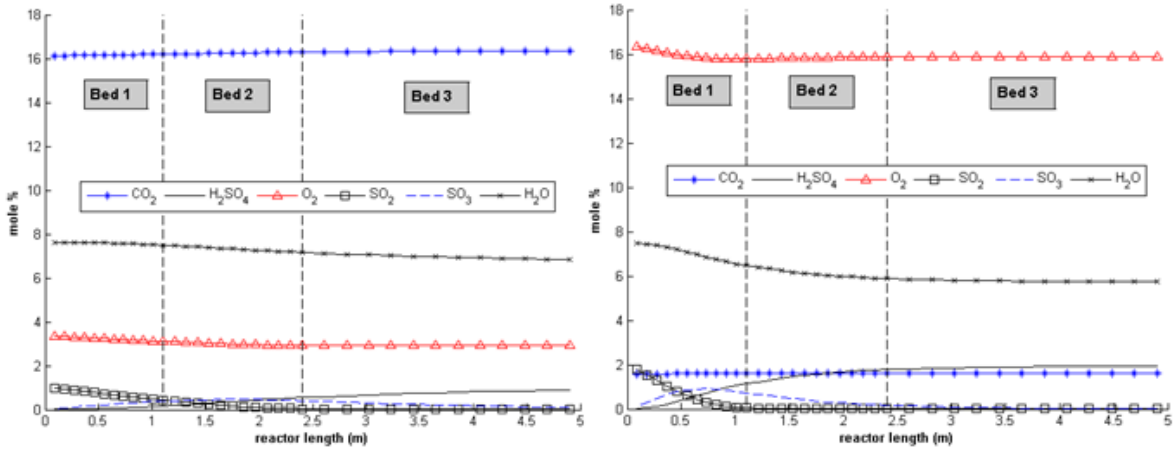

Figure 13. Composition in the bulk gas through the reactor beds during case 2 (left) and case 3 (right).

12.2 Steady state case switch

Another approach was to study how a case switch effects the outlet concentration of sulfur dioxide from bed 3 from one steady state to another steady state condition. The study mainly consists of switching from the case with highest concentration, case 1, to the lowest, case 2, and in the other way. The switching occurs at time zero with the previous case located at the boundary. Notable is that no time delay was implemented and therefore condition switches were carried out instantaneously.

When a condition change was carried out from high concentration to low and vice versa the profiles received the appearance according to figure 14. The time for the new steady state to establish, defined as when the profile change through the converter was uniform, was 0.25 h for the left plot and 0.1 h for the right plot.

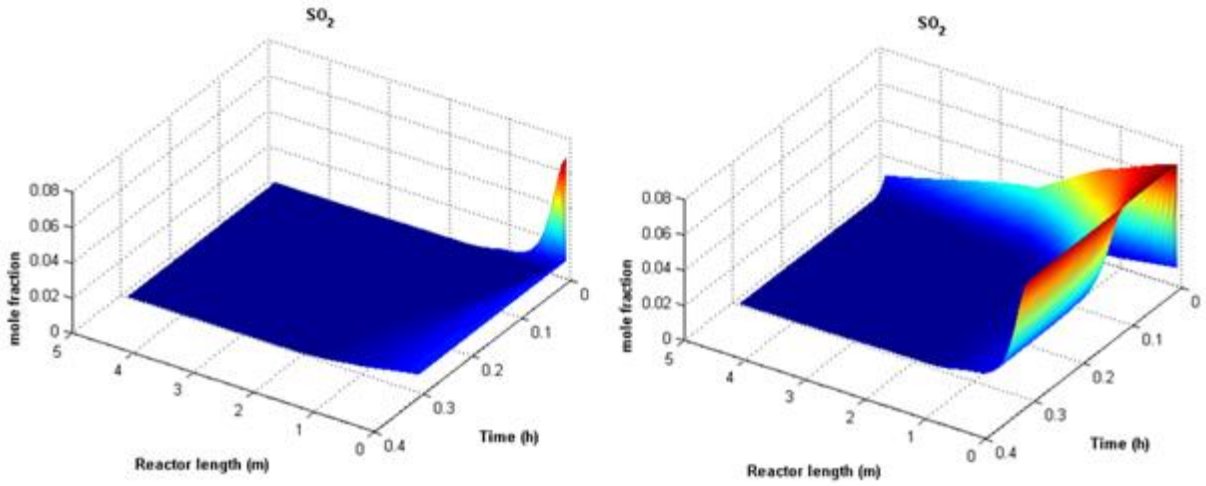

Figure 14. Representation of how the transient reduces and how the steady state approaches, after a switch from case 1 to 2 (left) and vice versa (right).

Another approach was to study the outlet concentration of sulfur dioxide when a case switch was carried out, the result can be seen in figure 15. This figure corresponds to the boundary profile in the third bed according to figure 14. There are small changes in the outlet which indicates that the steady state value has not been reached, but the deviations are in the order of a few ppm and are therefore

neglected. Another observation was that the profile generated from the case switch did not propagate through the converter and was hardly detected in the outlet, according to figure 15. This might be related to the fact that there was no time delay implemented, which would shift the profile further into the converter.

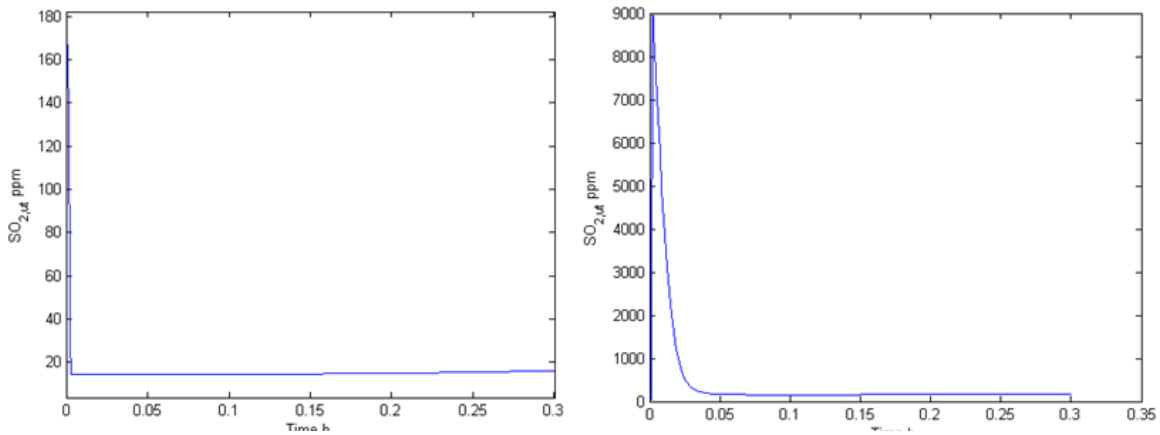

Figure 15. Steady state approach after a switch from case 1 to 2 (left) and vice versa (right).

The steady state values generated from figure 15 can be compared to given values for case 1 and 2, table I appendix D. The comparison showed rough matching, according to table 6. But on the other hand, when comparing the total conversion of sulfur dioxide, the difference between the steady state value and the model generated was small.

Table 6. Comparison between the model generated values and the given values of steady state exit content of sulfuric dioxide according to table I in appendix D.

	Case 1	Case 2
x_{SO_2}(ppm) Steady state	593	106
x_{SO_2}(ppm) Model generated	300	18
Conversion of SO_2 (mole %) Steady state	99.14	98.92
Conversion of SO_2 (mole %) Model generated	99.56	99.82

Analogously with the study where the conversion of sulfur dioxide was investigated, the production of sulfuric acid was studied during a change of both composition and flow rate in the feed. In order to produce sulfuric acid, a conversion of sulfur dioxide must be carried out and therefore a natural time delay will occur. This reasoning holds for the appearance of the concentration profile in figure 16.

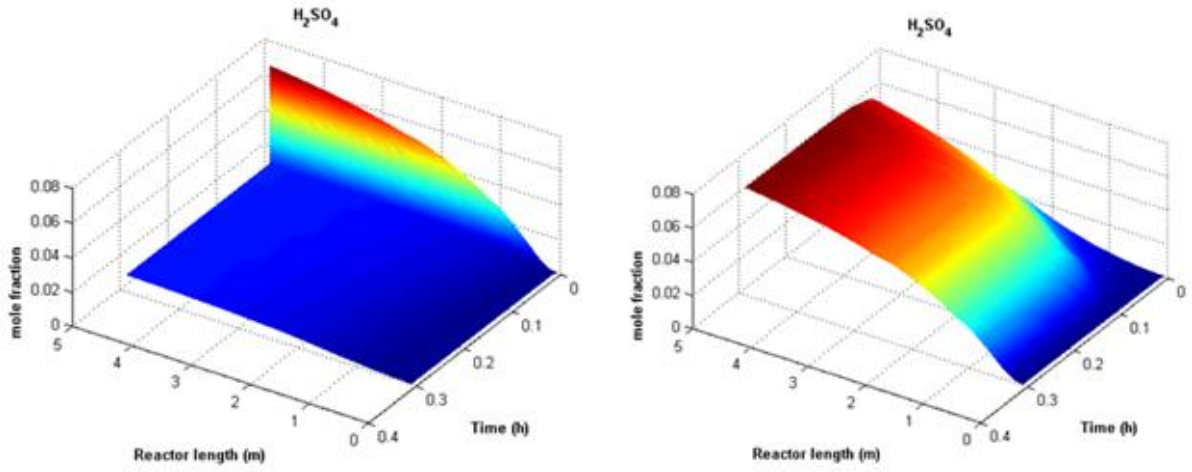

Figure 16. The change in sulfuric acid production after a switch from case 1 to 2 (left) and vice versa (right).

The temperature profiles of the bulk in each bed have different appearances, as can be seen in figure17. In the first bed, the temperature profile had a flat slope initially in contrast to the second bed. This behavior was expected, since there was no sulfur trioxide initially and therefore there was no sulfuric acid produced. There were both sulfur dioxide and sulfur trioxide in the inlet to the second bed, which enabled both reaction 3 and 4 to occur. As a consequence more reaction heat was generated and the temperature was elevated at an earlier stage. The temperature raise in the last bed did not reach the magnitude in the two previously beds. This was also expected because of the low sulfur dioxide content there. The reaction rate will decrease when the sulfur dioxide conversion approaches equilibrium. This phenomenon is shown in figure 17 (right) where the temperature profiles flattens out at longer time.

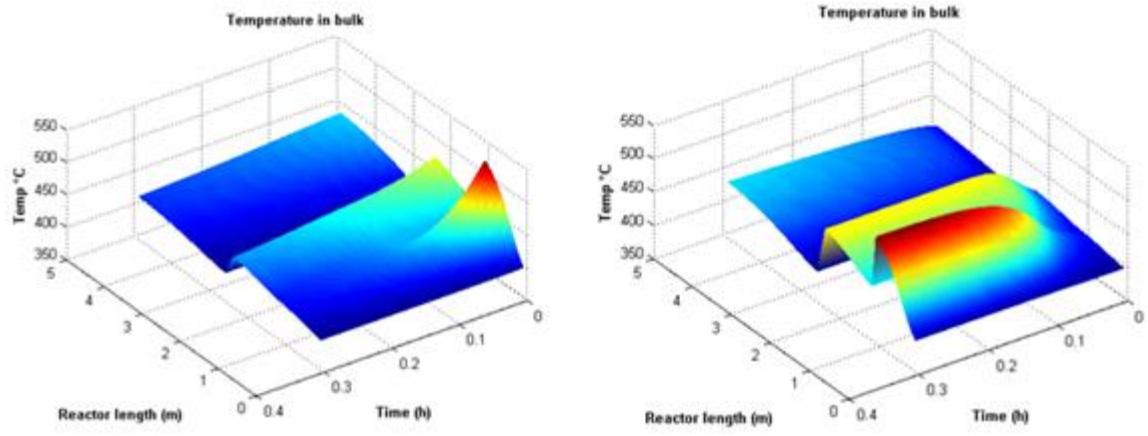

Figure 17. Temperature profile after a switch from case 1 to 2 (left) and 2 to 1 (right).

In order to investigate if the emission legislation is fulfilled during the steady state switching conditions, the amount of sulfur dioxide in the outlet of the converter per ton 100 % sulfuric acid produced was calculated according to equation 39 and presented in figure 18.

$$\frac{kg\ SO_2}{ton\ 100\%\ H_2SO_4} = \frac{x_{SO_2} M_{SO_2}}{(x_{SO_3} + x_{H_2SO_4}) M_{H_2SO_4}} \cdot 1000 \qquad \text{(eq.39)}$$

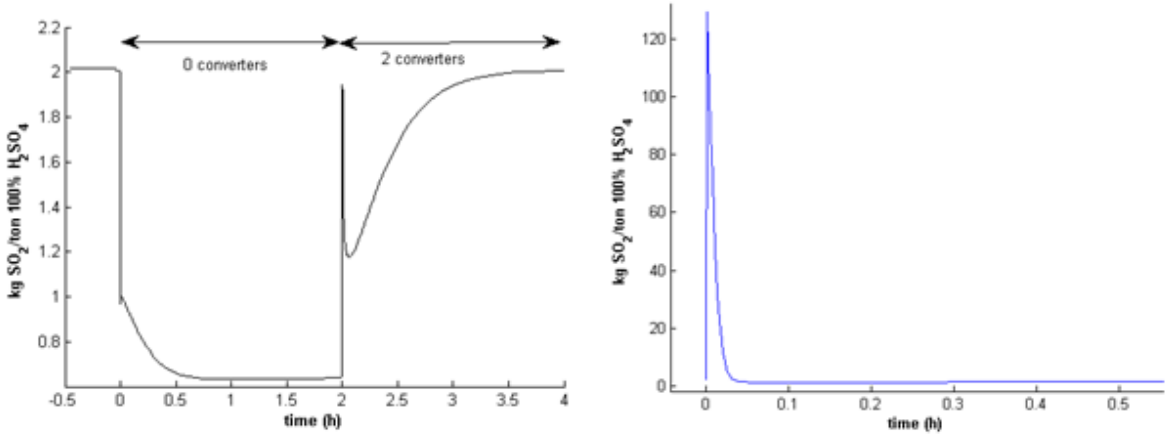

Figure 18. Corresponding outlet concentration of sulfur dioxide as a function of time when switching between case 3 and 1 (zero respectively two Pierce-Smith converters) (left) and between case 2 and 1 (one respectively two Pierce-Smith converters) (right).

To be able to compare the emissions guarantees with the model generated steady state values, calculations according to equation 39 was carried out and the result is shown in table 7. The guarantee was the same for all three cases, 2 kg/ton 100% sulfuric acid after tail-gas treatment.

Table 7. Steady state emissions for the three cases after the WSA converter.

	$\frac{kg\ SO_2}{ton\ 100\%\ H_2SO_4}$ Model generated
case 1	2.01
case 2	2.28
case 3	0.64

12.3 Temperature and composition variations

In order to study the propagations of variations, in both temperature and sulfur dioxide content, the temperature and composition profiles were investigated. The temperature was increased with 20^oC in the first third of the time interval (2 h), in the second third the temperature was returned to its ground state and in the last third a decrease with 20^oC was carried out. This temperature variation is shown in figure 19.

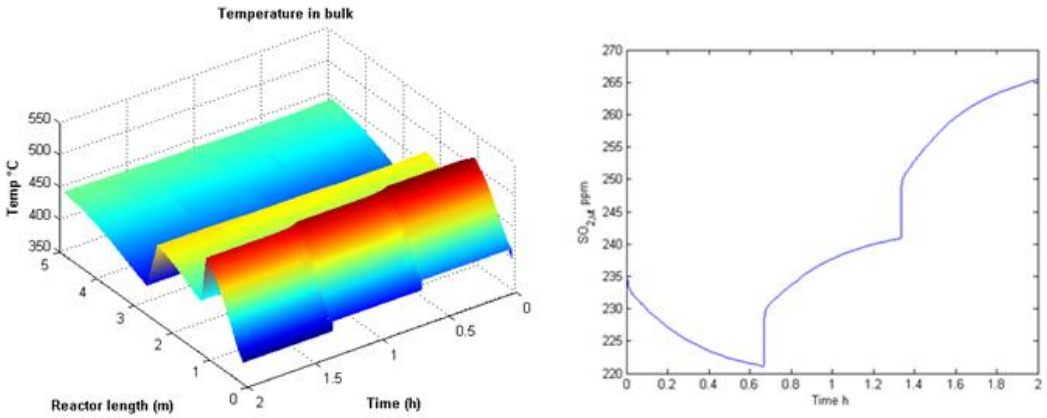

Figure 19. Temperature variations during case one operating conditions (left), consequence of the temperature variation on the sulfur dioxide content in the outlet of the third bed (right).

The temperature variations will affect the conversion rate, according to equation 24, and as a consequence the appearance of the sulfur dioxide profile will change. This was expected since an increase of the temperature will increase the reaction rate as long as the reaction is not at equilibrium.

When the composition was decreased by 20% followed by an increase to the ground state and finally an increase by 20%, the temperature profile and the concentration profile received the appearance according to figure 20.

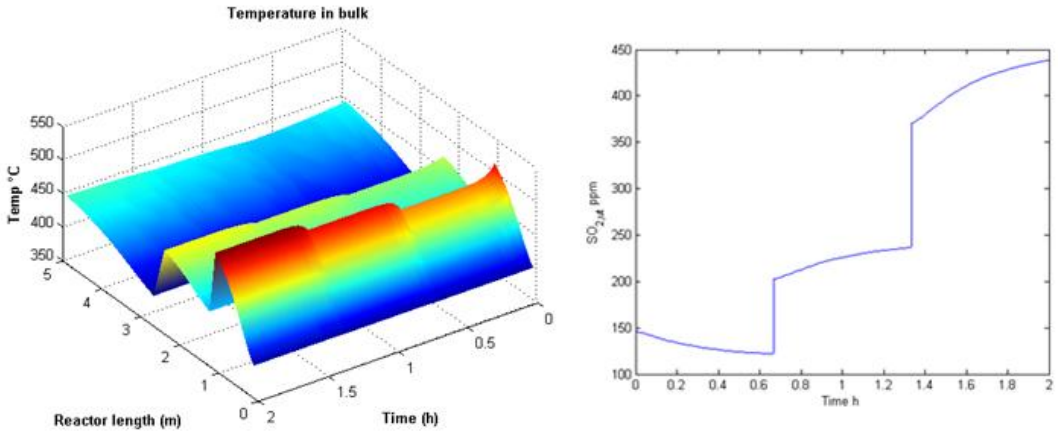

Figure 20. Temperature variations during case one operating conditions with varying concentration (left) and the concentration profile in outlet of the third bed (right).

A decrease in sulfur dioxide content will lower the generated reaction heat, according to figure 20 (left) and the out coming concentration profile in figure 20 (right) is the awaited result of variations of incoming sulfur dioxide content.

12.4 Transient conditions

To be able to validate the mathematical model, it was compared to the dynamic data set scanned from figure 5. The scanned data set matched very well with the concentration profile in figure 5. The concentrations used in the simulation were scanned from figure 5. Figures of the temperature and the composition profiles are presented below in figure 21, 22 and 23. During transient conditions, the exothermal reactions occur in all catalytic beds, where temperature elevation corresponds to the amount of sulfur dioxide converted. As expected, the mainly conversion occurred in the first bed since the feed contains the maximum sulfur dioxide content. This appearance described is clearly presented in figure 21.

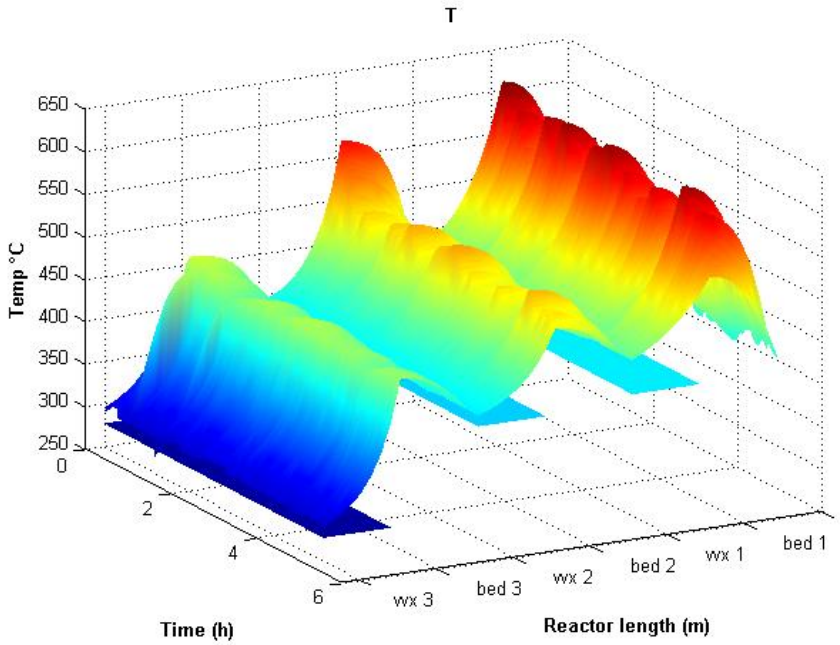

Figure 21. Temperature profile during transient conditions.

The magnitude of the temperature in figure 22 shows a lack of match, because the initial temperature according to the flow sheets, table V in appendix B, and figure 5 are not consistent. Only the behavior of the gradients can be compared.

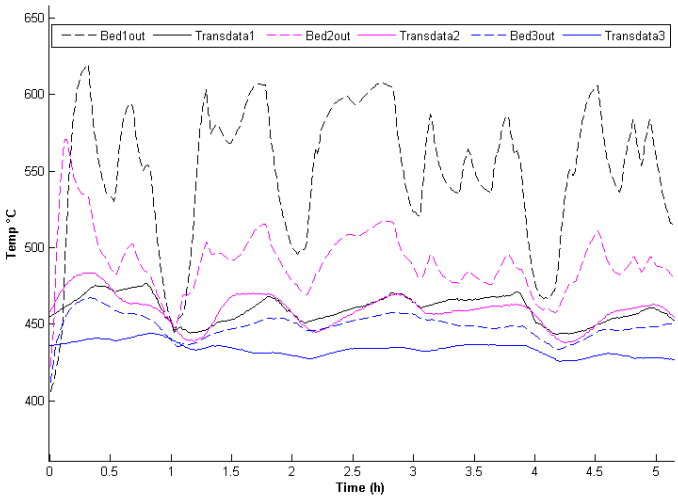

Figure 22. Comparison with temperature profile from the model generated and from figure 5.

Each couple of dashed and solid lines corresponds to the same outlet temperature of every bed. The model generated temperature gradients out of the beds are similar in shape but are much stronger than the original. One general observation is that the higher the concentration of sulfur dioxide, the more the model results deviates from the original ones.

The sulfur dioxide content in the outlet of the converter varies according to figure 23 when the cases are switched periodically.

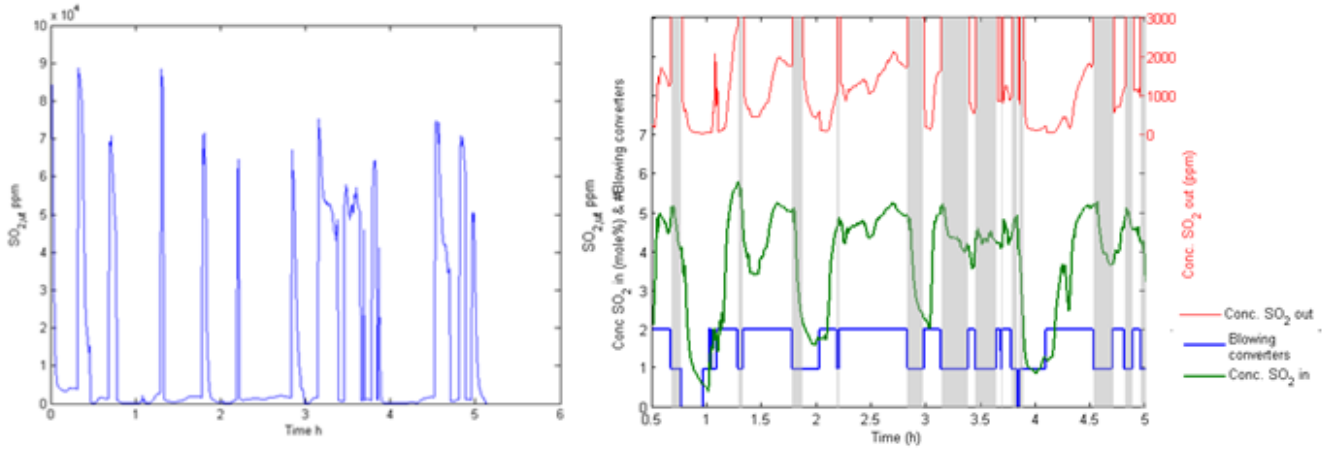

Figure 23. The sulfur dioxide concentration in the outlet of the converter after bed 3 as a function of time (left). An enlargement of the low magnitude concentration with the periodical switches (right).

The high SO_2 concentration can be related to that when a case switch occurs from case 1 to 2, the incoming SO_2 concentration decreases with a delay according to figure 23 (right). The magnitude of the high peaks does not correspond to any incoming concentration and might be explained by a combination of mainly two phenomenon:

1. The oxygen concentration was not modeled to follow a similar pattern as the SO_2 concentration in figure 23 (right). It was instead modeled to change the oxygen concentration instantaneously from one case to another. As a consequence the concentration of oxygen in the converter will change stepwise. Therefore the reaction is inhibited due to the low oxygen content and the SO_2 content will pass through.

2. The conversion of sulfur dioxide decreases with decreased temperature. This is shown in figure 24, except from the interval 0-0.5 h.

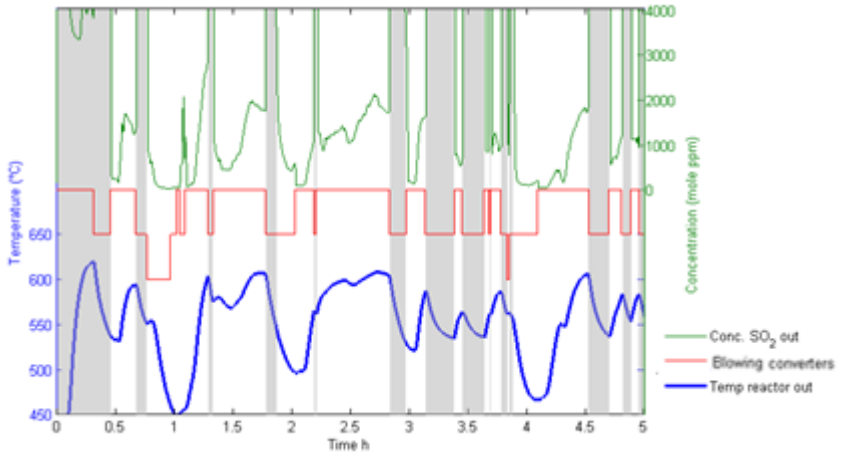

Figure 24. Low magnitude concentration with the periodical switches and the temperature profile (right).

12.5. Correlation between the temperature of the bulk and the catalytic bed surface

According to figure 25, the inlet surface temperature was almost constant during the second and the third case but the high content of sulfur dioxide in the first case gave rise to an elevated temperature. A temperature difference between the two phases arises, which indicates slowness in the transmission of heat. This corresponds to the heat transfer term in equation 15 and 16 and by tuning the heat transfer coefficient, the temperature difference can be changed. A higher value of the heat transfer coefficient will result in a smaller difference between the bulk and the catalysts surface temperature.

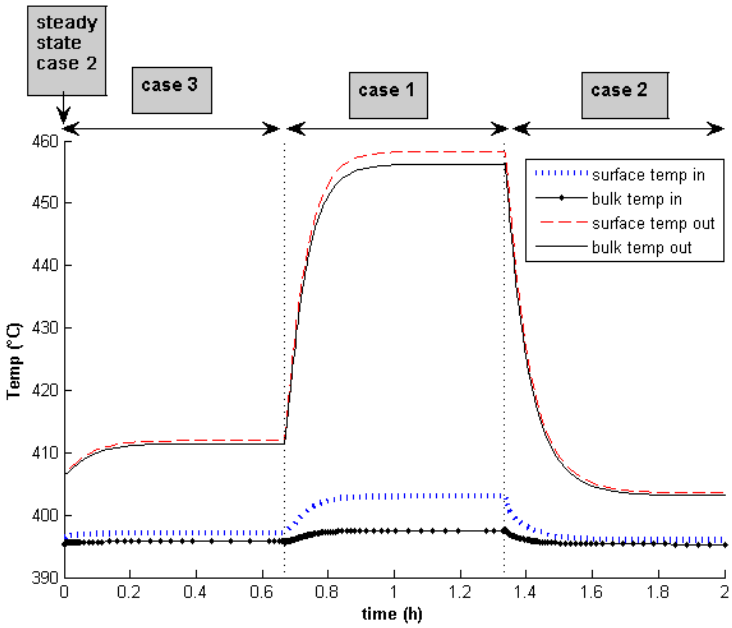

Figure 25. The interaction between the first catalytic bed surface and the bulk during the cases switches, according to: initial case 2 followed by case 3, 1 and finally 2.

By studying the outlet temperature of the catalytic bed for the surface and the bulk, it is obvious that the transfer of heat was almost sufficient to raise the bulk temperature and approach the temperature of the catalytic bed surface for current operating conditions.

13. Model improvements

The mathematical model developed in the previous sections contains the essential process characteristics, non-essential process characteristics and finally incorrect process characteristics, according to figure 26. It is advantageous to develop a new more advanced model which takes more identified essential process characteristics under consideration[35].

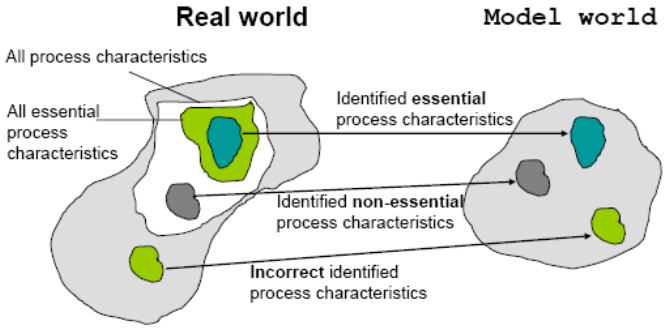

Figure 26. Relation between the ”real world” and the ”model world”.

13.1 Converter

In a fixed-bed reactor the heat transfer between the bulk and the catalyst particle is most important, because the temperature gradient in the film will not be negligible. Also the external mass transport through the stagnant film is of great importance. Introduction of those improvements in the partial differential equations that describes the concentration and the temperature variation in the bulk is described below. The concentration dependence relations can be rewritten as

$$\frac{\partial c_{b_i}}{\partial t} = D_{ax}\frac{\partial^2 c_{b_i}}{\partial w^2} - \frac{v}{\epsilon}\frac{\partial c_{b_i}}{\partial w} - \epsilon A N_{b_i} \qquad \text{(eq.40)}$$

where the term $\epsilon A N_{b_i}$ represents the flux through the stagnant film. The flux can be calculated according to

$$N_{b_i} = k_{g_i}(c_{b_i} - c_{s_i}) \qquad \text{(eq.41)}$$

where k_{g_i} is the bulk-particle mass transfer coefficient and c_s is the concentration at the surface of the particles. The surface concentrations in the adiabatic catalytic beds varies according to

$$\frac{\partial c_{p_i}}{\partial t} = \epsilon_p A N_{b_i} - \frac{(1-\varepsilon_c)}{\varepsilon} r_i(T_s). \qquad \text{(eq.42)}$$

where the components in the flux transported through the film reacts at the surface of the catalytic particles. The converted components are transported in the opposite direction into the bulk according to

$$\frac{\partial c_{prod}}{\partial t} = \frac{(1-\varepsilon_c)}{\varepsilon} r_i(T_s) - \epsilon_p A N_{prod}. \qquad \text{(eq.43)}$$

[35] K.M. Hangos, I.T. Cameron, *Process system engineering Process modeling and model analysis*, vol 4 of PROCESS SYSTEM ENGINEERING, page 21-37

The temperature dependence relations can be written as

$$\frac{\partial T}{\partial t} = \kappa \frac{\partial^2 T}{\partial x^2} - \frac{v}{\epsilon}\frac{\partial T}{\partial x} + \underbrace{\frac{A_{ht}}{AL}}_{constant} k \ \frac{1}{\rho(T)c_p(T)}(T_s - T) + \underbrace{\frac{A_{ht}}{AL}}_{constant} k_w \ \frac{1}{\rho(T)c_p(T)}(T_w - T), \quad \text{(eq.44)}$$

where the term $\underbrace{\frac{A_{ht}}{AL}}_{constant} k_w \ \frac{1}{\rho(T)c_p(T)}(T_w - T)$ represents the energy loss through the wall and k is the heat transfer coefficient in the stagnant film.

To be able to implement the two-film theory, j-factors were introduced to estimate the heat- and mass transfer coefficients. The j-factors are functions of dimensionless numbers and are defined as

$$j_d = \frac{Sh}{ReSc^{1/3}} = \frac{ReScSt_d}{ReSc^{1/3}}, \quad \text{(eq.45)}$$

$$j_h = \frac{Nu}{RePr^{1/3}} = \frac{RePrSt_h}{RePr^{1/3}}. \quad \text{(eq.46)}$$

The dimensionless numbers are defined as

$$St_d = \frac{k_{g_i} M \rho_{f_i}}{v\rho}, \qquad St_h = \frac{h_g}{C_p v \rho} \quad \text{(eq.47, 48)}$$

$$Sc = \frac{\mu}{\rho D_{m_i}}, \qquad Pr = \frac{c_p \mu}{\lambda} \quad \text{(eq.49, 50)}$$

$$Sh = \frac{k_{g_i} D_p M p_{f_i}}{\rho D_{m_i}}, \qquad Nu = \frac{h_g D_p}{\lambda} \quad \text{(eq.51, 52)}$$

$$Re = \frac{\rho \cdot L \cdot v}{\mu}. \quad \text{(eq.53)}$$

There is an analogy between mass and heat transport, for fixed beds Yoshida, Ramaswami and Hougen[36] found the correlations

$$j_d = 0.84Re^{-0.51} \qquad \text{for } 0.01 < Re < 50, \quad \text{(eq.54)}$$

$$j_d = 0.57Re^{-0.41} \qquad \text{for } 50 < Re < 1000, \quad \text{(eq.55)}$$

$$j_h = 1.076 j_d \quad \text{(eq.56)}$$

Another analogy[37] to estimate j-factors is

$$j_d = \frac{0.725}{Re^{41 - 0.15}}, \quad \text{(eq.57)}$$

$$j_h = \frac{j_D}{0.66}. \quad \text{(eq.58)}$$

[36] Yoshida, F. et al, *Temperatures and Partial Pressures at the Surfaces of Catalyst Particles*, AIChE Journal, vol 8, pages 5-11

[37] Nodehi, A., et al., *Simulation and Optimization of an Adiabatic Multi-Bed Catalytic Reactor for the Oxidation of SO_2*, Chem. Eng. Technol., No 1, 2006 pages 84-90

13.2 Interbed heat exchangers

The mathematical model of the interbed heat exchangers, assumed that the heat exchangers were of the counter-current tubular shape type. The stationary heat transfer term, kA_{ht}, was approximated to vary with the molten salt flow rate according to figure 9.

One way to improve the mathematical model would be to calculate the heat transferred from the gas bulk to the salt system by calculating the heat conduction coefficient, *k*, for a tube wall according to

$$k = \left(\frac{d_y}{d_i \cdot \alpha_i} + \frac{1}{\alpha_y} + \sum \frac{ln\frac{d_y}{d_i}}{2\lambda} \right)^{-1} . \qquad \text{(eq.59)}$$

The parameter α represents the heat transfer coefficient for each medium, d_y and d_i denotes the outer respectively the inner diameter of the tube and λ is the heat conductivity in the wall. The heat transfer coefficients, for the medium that flows inside the tube, can be calculated from Nusselt's number according to equation 60.

$$Nu = \frac{\alpha \cdot d}{\lambda} \qquad \text{(eq.60)}$$

With the relation between the dimensionless numbers, Reynold and Prandtl (equation 53 and 50), it is possible to calculate Nusselt's number according to equations 61-65 depending of the magnitude of the Reynold's number. The equations 61-63 holds for Reynold's number less than 2100.

If $Re \cdot Pr \cdot \frac{d}{L} \geq 50$ $\qquad Nu_m = 1.85 \cdot \left(Re \cdot Pr \cdot \frac{d}{L} \right)^{\frac{1}{3}} \cdot \Phi_v$ $\qquad$ (eq.61)

If $1 \leq Re \cdot Pr \cdot \frac{d}{L} \leq 50$ $\qquad Nu_m = 3.66 \cdot \left(Re \cdot Pr \cdot \frac{d}{L} \right)^{0.12} \cdot \Phi_v$ $\qquad$ (eq.62)

If $Re \cdot Pr \cdot \frac{d}{L} \leq 1$ $\qquad Nu_m = 3.66$ $\qquad$ (eq.63)

Once the Nusselt's number is calculated, the heat transfer coefficient for the medium that flows inside the tube can be calculated according to equation 59.

For Reynold's number in the interval $2100 < Re < 10\,000$, the product $Nu \cdot Pr^{-1/3}$ can be read from figure 27.

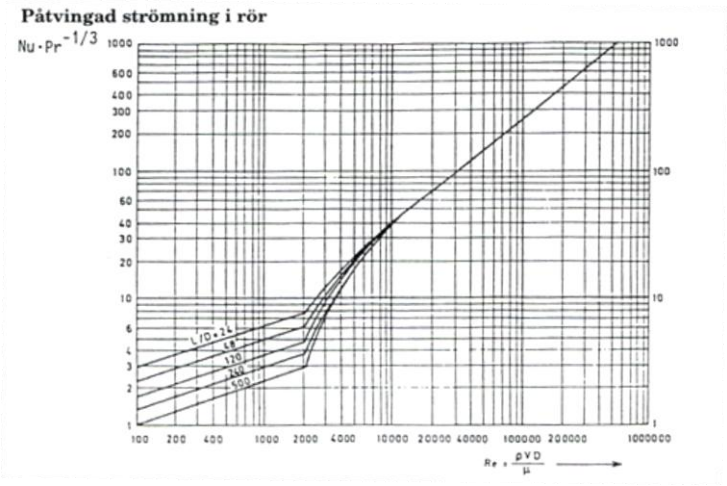

Figure 27. Nu·Pr$^{-1/3}$ as a function of Re in the interval 2100 < Re < 10000.

For Reynold's number exceeded 10000, Nusselt's number are calculated according to

$$Nu_m = 0.023 \cdot Re^{0.8} \cdot Pr^{\frac{1}{3}} \left(1 + \left(\frac{d}{L}\right)^{0.7}\right) . \Phi_v, \quad \text{(eq.64)}$$

where the $\Phi_v$can be calculated by equation (eq.65).

$$\Phi_v = \left(\frac{\mu_{bulk}}{\mu_{wall}}\right)^{0.14} \quad \text{(eq.65)}$$

To calculate the heat transfer coefficient, α, for the medium that flows outside the tube, the following correlation can be used

$$Nu_m = \frac{\alpha \cdot d}{\lambda} = 0.33 \cdot Re^{0.61} \cdot Pr^{0.33} \cdot f_r \cdot f_a, \quad \text{(eq. 66)}$$

where Reynolds number is calculated from equation 67, and the parameters f_r and f_a can be calculated according to equation 68 and 69[38].

$$Re = \frac{\rho \cdot V_e \cdot d}{\mu} \quad \text{(eq.67)}$$

$f_r = 0.8 - 1.0$ (increases with the number of tube rows) (eq.68)

$f_a = 0.8 - 1.2$ (depends on $\frac{s_1}{d}$ and $\frac{s_2}{d}$) (eq.69)

The parameter V_e represents the interstice velocity at the minimum distance between the pipes. A graphic definition of the parameters V_e, s_1 and s_2 is presented in figure 28.

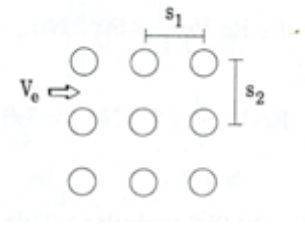

Figure 28. Graphic definition of the parameters V_e, s_1 and s_2.

[38] *Formelsamling, Transportteknik/Energiteknik/Separationsprocesser*, Institutionen för Kemiteknik 2006/2007

13.3 Feed gas processing

According to the model approach, the implemented model only includes the converter. Once the model was established and tuned in according to steady state conditions, an investigation how transients and variations propagate through the converter was carried out. In line with this approach, an improvement of the model would be to describe the feed gas processing, which includes preheating and addition of components to the feed gas before the converter. In order to derive a realistic model of this kind, lots of information is required of pipe dimensions, which describe the flow conditions, and the heat exchangers, which describe the heat transfer conditions. If those entire phenomenon could been taken under account, a time delay could have been described which generates transient conditions in the inlet to the converter. Then an investigation how the transients propagate through the converter could be carried out. These data were not supplied to us though.

One way to overcome the lack of information, which makes a derivation of a mathematical model over the feed gas processing impossible, was to use the shortcut and create a black box model. The foundation of the model was the transient data given in figure 5. The input to the black box model consists of the periodical case switch, presented in figure 29.

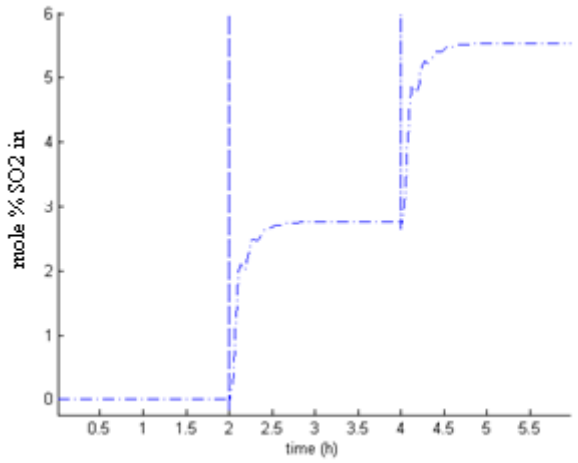

Figure 29. Step responses from case switching of the estimated model. The switches are made in the order 0, 1 and 2 Pierce-Smith converters.

The steady state values are 0, 2.8, 5.5 mole% for 0, 1 and 2 Pierce-Smith converters which can be compared with 1.9, 0.98, 6.87 taken from the steady state values according to table I in appendix D. Notable is that this was not used in the model because of the numerical instability.

The idea was to generate the SO_2 concentration and temperature to the inlet of the converter as the output. It was however only the sulfur dioxide content that was successfully achieved.

A general state space model was developed, according to equation 70 and 71, using MATLAB's *system identification toolbox*.

$$\frac{dx}{dt} = \begin{pmatrix} 0.9628 & -0.1474 & 0.032715 & -0.020054 & -0.01845 \\ 0.13362 & 0.72896 & 0.52405 & 0.26252 & 0.061006 \\ 0.020263 & -0.20022 & 0.27849 & 1.256 & 0.33201 \\ -0.01172 & -0.16723 & 0.63197 & -0.3451 & -0.29843 \\ 0.048884 & 0.15426 & 0.09458 & 0.00068359 & 0.79765 \end{pmatrix} x + \begin{pmatrix} -0.0032435 \\ -0.021217 \\ 0.12855 \\ -0.18581 \\ 0.10128 \end{pmatrix} u \qquad \text{(eq. 70)}$$

$$y = (29.713 \quad -1.6277 \quad 0.054869 \quad -0.15817 \quad 0.33483)x \qquad \text{(eq. 71)}$$

The variable y represents the SO_2 mole fraction to the inlet of the converter and is presented in figure 30 as a function of time.

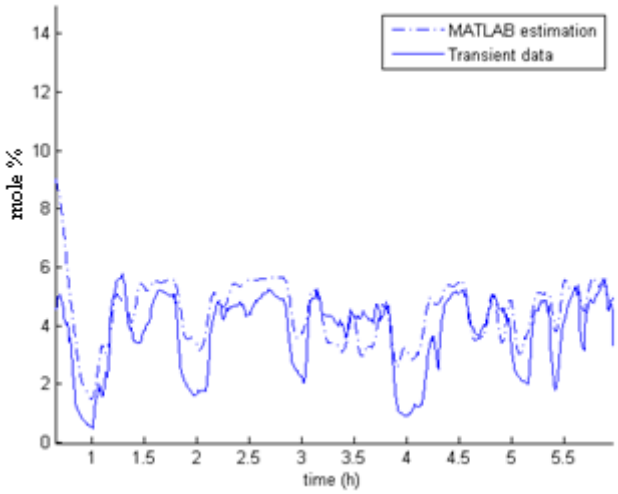

Figure 30. Transient data is approximated with a state space model estimated in MATLAB's system identification toolbox.

The estimation of the sulfur dioxide content contains an error but follows the gradients of the curve approximately. It is obvious that the model needs further improvements in order to represent the transient data since the difference in magnitude is significant.

14. Discussion

The system has been claimed to be ideal, according to the approximations in section 8, since the pressure variation throughout the WSA-system was moderate (less than 2 bar). On the other hand, the sulfuric acid might when formed solve itself with the remaining water and ions will then appear in the water vapor. This would change the ideal system to one that acts as an electrolytic one. An electrolytic system would have changed the equations when calculating the physical properties.

The equation for oxidation of sulfur dioxide to sulfur trioxide (eq.24) was derived from experiments and involves the inner mass transfer limitations. By studying the activation energies, presented in table I appendix B, within the two temperature intervals, a significant decrease of the activation energy, E_1, was noticed. This implies that the inner mass transfer was dominant in temperature region 470-580 °C. According to the literature (ref. 32) the SO_2 oxidation expression is intrinsic. Since the stipulations in the experiments differ to those in the WSA plant, it would probably change the values of the constants in equation 24. In our approach we assumed that the expression (eq. 24) with its constants was still valid. Whether this really means that the reaction is limited by internal diffusion above 470 °C is not clear to us. Since the reaction rate for the formation of sulfuric acid from SO_3 and H_2O was unknown, a second order expression regarding to the reactants with a fix reaction rate constant was suggested, equation 28, see table 5.

In order to gain the probable concentration profile in the converter two tuning parameters, $k_{rection}$ for equation 24 and $k_{H_2SO_4}$ for equation 28, was installed and influenced the reaction rates. A probable composition profile was presented in figure 12 for case 1and figure 13 for case 2 and 3. The exit composition comport reasonably well with the steady state values for all three cases. The compared values for the three cases can be found in table XI in appendix B. As can be seen in table XI in appendix B the molar fractions of sulfur trioxide and sulfuric acid differ giving 2 mole % more acid than expected and 2 mole % less sulfur trioxide. One explanation is that the reaction rate constant, $k_{H_2SO_4}$, was too big and as a consequence the degree of sulfur trioxide conversion was too high. In the same way as the sulfuric acid formation, the composition of the sulfur dioxide was too low in comparison to the steady state value. Since the temperature and the compound composition are strongly related, it is hard to isolate the reason why the composition of sulfur dioxide is less than the given steady state value. Mainly there are two tuning parameters which effect this correlation between the temperature and the composition, *E-factor* and $k_{reaction}$. The *E-factor* was introduced to decrease the reaction heat produced and lowers the temperature elevation and as a consequence decreases the conversion of sulfur dioxide according to equation 24. A decrease in $k_{reaction}$ will decrease the conversion and by combining the contribution of the two parameters, a more accurate composition can be achieved. Actual values for the tuning parameters can be found in table 5.

The temperature profile for the three catalytic beds was seen in figure 11. As can be seen in table X in appendix B there are generally two trends. First, there was too little heat produced in bed 1 and secondly there was too much heat produced in the third bed. The heat produced was reduced with two tuning parameters, *E-factor* for the reaction heat and D_s for the heat conductivity of the catalyst. The first trend can be explained with that the *E-factor* was too small and inhibited the heat development while D_s was too big and the produced heat was therefore conducted and smoothed out in the catalytic bed and decreased the temperature difference between the bed and the bulk. The second trend can be related to a large formation of sulfuric acid, which produced too much heat. A lower value of $k_{H_2SO_4}$ will produce less acid and therefore less heat.

The current salt system was simulated as a grey box model, with the heat transfer described as a linear relation of the flow. To improve the model it is necessary to implement the improvements where the heat transfer coefficient is calculated as a function of both the salt flow rate as well as the gas bulk flow rate, all according to section 13.2. In order to implement these improvements, physical properties like heat exchange areas and heat exchange volumes have to be known.

The used converter model is far from complete since many essential process characteristics are not included. The heat transfer between the gas bulk and catalyst is of most importance along with external mass transfer through the stagnant film. The mass transfer from the gas bulk can be described by a flux, calculated from the concentration gradient and a mass transfer coefficient. The coefficient will be dependent of the dynamic flow conditions as well as physical properties. The same reasoning is valid for the heat transfer coefficient. The reaction term in equation 14, will be replaced by a flux to the surface which results in equation 40 in section 13.1. Further a new partial differential equation will be introduced where the reaction occurs and a transport away from the catalyst surface takes place, according to equation 43 in section 13.1. An implementation of the improvements given above will make the model more physically meaningful and resistances will inhibit the reaction and the heat transfer. This might make the tuning parameters $k_{heatarea}$, $k_{reaction}$ and $E - factor$unecessary.

When switching between the different steady state conditions, there are two things that are notable. First the system showed various time lags for approaching steady state, presented in figure 14. This is explained by the slow temperature decrease when switching from case 1 to 2 in comparison to when switching from case 2 to 1, shown in figure 17. The composition change, from state 1 to 2, corresponds to a drastic decrease in sulfur dioxide content (6.87 to 0.98 mole %) in the inlet of the converter where the temperature was so high that the complete conversion was achieved. Since there was almost no SO_2 to oxidize the temperature slowly declined. When the opposite occurred, i.e. switch from case 2 to 1, the temperature increased more rapidly than it decreased, according to figure 17. This might be explained by the fact that the reaction occurred at the catalyst surface where all the reaction heat was generated and the cooling process was carried out by the bulk gas, which was a poor cooling medium. Last the profile of sulfur dioxide composition propagating through the converter reached steady state before the propagating front reached the exit boundary of the converter. As a consequence the concentration profile at the exit boundary was only effected by the actual condition switch which decreased respectively increased the exit composition, according to figure 18. When switching from case 1 to 2 the exit sulfur dioxide content decreased as expected. But when switching from case 2 to 1, figure 18 (right), there was a high peak of 9000 ppm of SO_2 which indicated that for a short time interval the exit content was higher than desired. The peak in figure 18 (right) correspond with the outlet peak in figure 14.

In order to study the propagations of variations in both temperature and sulfur dioxide content initially introduced, the temperature and composition profiles were investigated and the result is presented in figure 19 and 20. An interpretation of figure 19 (right) indicates that an increase in temperature at the inlet of the converter will give a higher conversion. This is expected since the equilibrium conditions had not been reached and therefore the Le Chatelier's principle, which claims that exothermal reactions will be disfavored with an increase in temperature close to equilibrium, was not valid. In conformity of the equations 24 and 28, an increase in sulfur dioxide content will accelerate the exothermal reaction rates and as a consequence generate more heat.

The approach used to validate the mathematical model consisted of a comparison between the dynamic data set given in figure 5 and the result generated from the mathematical model. The conclusions drawn from figure 22, indicated that the model reflected the transient behavior of the dynamic data set. The implemented model can therefore be considered to be valid during transient conditions. Unfortunately the magnitude of the temperature could not be compared, since the initial temperature according to table I and II in appendix D and figure 5 are not consistent. A more accurate initial temperature would probably force the curves to approach each other. Notable is that the model generated curves are very sensitive to fluctuations, which is clearly shown in figure 22. Since the temperature and the compound composition are strongly related, it is hard to lower the temperature curves by the model generated without effecting the conversion of sulfur dioxide and the formation of sulfuric acid.

The periodical switch of conditions resulted in that the sulfur dioxide content in the outlet of the converter varied according to figure 23. The magnitude of the high peaks was probably caused by the combination of model limitations and a decrease in conversion with a decrease in temperature. There was no dynamic data set available to compare the magnitude of the sulfur dioxide content in the outlet of the converter. But a comparison with the steady state value according to the flow sheet for the first case showed that the transient composition exceeded the steady state value by two magnitudes.

The bulk temperature profile through the converter as a function of time and space during transient conditions was presented in figure 21, showed that the maximum temperature exceeded 600 °C. In the interval 600-650 °C the catalyst activity is lost permanently due to damage to the carrier structure and reduction of its internal surface[18]. Analogously to the reasoning above, in order to obtain a more accurate result it was necessary to tune the model. A decrease in e.g. the tuning parameters, $k_{reaction}$ and *E-factor*, would lower the reaction heat generated and therefore lower the temperature in figure 21 at the expense of the composition accuracy.

To be able to implement a realistic model which includes all events occurring before the converter, lots of information is needed. Many factors have to be modeled including sulfur dioxide evaporation, production of steam, infusion of air and heating from 40 °C to 395°C. A model that fully reflects the real conditions is hard to implement and therefore a simplification is to derive a black box model to relate inputs to outputs. The black box model still requires lots of information. The temperature and composition of the incoming gas from the Pierce-Smith converters varies heavily among the cases. In order to operate the reactor optimally, the temperature, water vapor and oxygen content have to be controlled. This would result in a multiple input multiple output (mimo) system but a simplified single input single output (siso) is preferred. The simplified black box model is described in section 13.3 relating the case switches to the SO_2 concentration. A similar siso black box model can also be applied on the inlet temperature of the reactor. This is important when one wants to reflect the feed gas process dynamics and to obtain more realistic behavior. Therefore this should be one of the next steps in improving the model.

The aim of the WSA plant is primarily to reduce emissions of sulfur dioxide and secondly to produce sulfuric acid. In this case study, Haldor Topsoe A/S gave guarantees of a maximum of 2 kg SO_2 emission per ton 100 % sulfuric acid produced. The emissions from the steady state simulations are found in table 7. As can be seen, not all values fulfill the guarantees. More interesting is to study the behavior of the transients that approximately follows the SO_2 emission curves shown in figure 15. The switches from case 1 to 2 or 3 do not exceed the emission guarantee. The sensitive part is going from case 2 or 3 to 1which results in an overshot.

When going from case 3 to 1, the magnitude of the overshot corresponds to 1.94 kg SO_2 per ton 100 % sulfuric acid produced and does not overstep the guarantees, according to figure 18 (left). When switching from case 2 to 1, as can be seen in figure 18 (right), a large overshot corresponding to 129 kg SO_2 per ton 100 % sulfuric acid produced was obtained. If this magnitude was maintained during a long time period, it would be a violation of the guarantee. The case switch can be interpreted as a step response function which propagates rapidly through the converter due to the high flow rate. When the case switch was carried out, the reaction temperature was not sufficiently high to provide enough conversion. This explains the initially sharp peak which decreased in magnitude as a function of time.

The exit sulfur dioxide amount per ton 100 % sulfuric acid produced was calculated with equation 39. Since the steady stat value in case 1 and 2 presented in table 7, exceeds the guarantee value, the tail gas treatment with hydrogen peroxide is of very high importance. Notable is that the simulated concentration of sulfur dioxide in the outlet was below the steady state values according to table I in appendix D. Therefore will the steady state values be higher than those in table 7.

15. Conclusions

The main conclusions of this study regarding the simulation model of a WSA plant for the metallurgical industry can be summarized as follows:

(i) The resulting composition profile in the converter, with tuning parameter values according to table 5, are presented in figure 12 for case 1and figure 13 for case 2 and 3. The model results compare reasonably with given steady state values, but for the concentrations of sulfur trioxide and sulfuric acid. The molar fractions of sulfur trioxide and sulfuric acid differ by 2 mole % more acid than expected and 2 mol % less for sulfur trioxide. A better accuracy can be achieved by adjusting the value of the tuning parameter $k_{H_2SO_4}$.

(ii) The temperature profile during steady state conditions does not compare very well with the given steady state values. Too little heat was produced in bed 1 in the converter and that can be derived to the *E-factor* which reduced the reaction heat and $k_{reaction}$ which corrects the conversion rate of sulfur dioxide. An implementation of mass and heat transfer limitations would create resistances, replacing the tuning factors. The derived converter model is far from complete since many essential process characteristics are not included.

(iii) When switching between the different steady state conditions, there are two things that are notable:

1. The system showed various time lags for approaching steady state, presented in figure 14. The composition profile of sulfur dioxide propagating through the converter reached steady state before the propagating front reached the boundary of the converter. As a consequence the concentration profile at the boundary was only effected of the actual condition switch which decreased respectively increased the out coming composition, according to figure 15.

2. When switching from case 1 to 2 the out coming sulfur dioxide content decreased as expected. But when switching from case 2 to 1, figure 15 (right), there was a high peak of 9000 ppm which indicated that for a short time interval the exit sulfur dioxide content was higher than desired. The peak in figure 15 (right) correspond with the outlet peak in figure 14.

(iv) The conclusions drawn from figure 22, indicated that the model reflected the transient behavior of the dynamic data set quite well. The implemented model can therefore be considered to be valid during transient conditions. Notable is that the model generated curves are more sensitive to fluctuations than the original data shows and this is clearly shown in figure 22. Since the temperature and the compound composition are strongly related, it is hard to reduce the model generated curves without effecting the conversion of sulfur dioxide and the formation of sulfuric acid.

(v) Since the steady stat value in case 1 and 2, presented in table 7, exceeds the boundary value, the tail gas treatment with hydrogen peroxide is of very high importance. Notable is that the simulated concentration of sulfur dioxide in the outlet was below the given steady state values according to table I in appendix D and the corresponding table 7 values will be higher.

16. Acknowledgements

The authors thank Prof. Ingemar Odenbrand for helpful discussions and valuable advice and many helpful feed back in the preparation of the report. The encouragement and support provided by Associate Prof. Bernt Nilsson and Ph. D. Student Marcus Degerman are also gratefully acknowledged. We are also grateful to Haldor Topsoe A/S for permitting us to carry out this work and especially thanks to Jane Albertus Steenberg and Frank Lindblad Hansen who provided valuable information and great support.

Appendix A. Table of symbols

Symbol	Description	Unit
a	*Reaction coefficient*	$\frac{mole}{m^2 s}$
a	*Diffusion constant*	-
A	*Area*	m^2
A_{1-2}	*Convection and diffusion matrix*	-
$A_{f,1-2}$	*Boundary help matrix*	-
b	*Convection*	m/s
$B_{1\text{-}2}$	*Boundary conditions*	-
c	*Concentration*	$\frac{mole}{m^3}$
C_p	*Specific heat capacity*	$\frac{kJ}{mole \cdot K}$
C_{1-5}	*Heat capacity constants*	-
d	*Diameter*	m
D_{ax}	*Axial diffusion coefficient*	$\frac{mole}{m^2 s}$
D_p	*Particle diameter*	m
D_s	*Heat conductivity, tuning parameter*	W/mK
e	*Error*	-
E-factor	*Tuning parameter*	-
E_a	*Activation energy*	$kJ/mole$
f	*Parameter*	-
F_i	*Shape factor for cylinder*	-
G	*Volumetric gas flow*	Nm^3/h
h	*Converter height*	m
h_{cat}	*Catalyst height*	m
H	*Reaction enthalpy*	$kJ/mole$
$j_{d,h}$	*J factors for mass and heat*	-
k	*Rate constant*	-
$k_{reaction}$	*Tuning parameter*	-
$k_{heatArea}$	*Heat transfer coefficient*	$\frac{kJ}{sK}$
k_g	*Mass transfer coefficient*	m/s
K_{1-4}	*Viscosity constants*	-
K_p	*Equilibrium constant*	atm^{-1}
K_{eq}	*Equilibrium constant*	atm^{-1}
K_d	*Proportional gain*	-
L	*Length*	m
m	*Reaction coefficient*	-
M_1	*Discretisation matrix, 1st order*	$\frac{mole}{m^3 kg}$

M_2	*Discretisation matrix, 2nd order*	$\left(\frac{mole}{m^3 kg}\right)^2$
M_w	*Molar weight*	$\frac{kg}{mole}$
N	*Flux*	$mole/sm^2$
Nu	*Nusselt number*	-
P	*Total pressure*	Pa
Pr	*Prandtl number*	-
p_i	*Partial pressures*	atm
q	*Volumetric gas flow*	$\frac{m^3}{s}$
q	*Flux*	$mole/sm^2$
r	*Reaction rate*	$\frac{mole}{kg\ cat \cdot s}$
r	*Radius*	m
R	*Gas constant*	$\frac{J}{mole \cdot K}$
Re	*Reynold number*	-
s	*Laplace variable*	-
Sc	*Schmidt number*	-
Sh	*Sherwood number*	-
$St_{d,h}$	*Stanton number for mass and heat transfer*	-
t	*Time*	s
T	*Temperature*	K
T_d	*Derivative constant*	-
T_i	*Integration constant*	-
T_{gain}	*Proportional gain*	-
u	*Input signal*	-
v	*Volumetric gas flow*	m^3/s
V	*Volume*	m^3
w	*Catalyst bed length*	m
x_i	*Mole fraction of component i*	-
x	*Discretization length*	m
x	*System state variable*	-
y	*Output signal*	-
α	*Heat transfer coefficient*	W/m^2K
ε	*Porosity*	-
ε_c	*Column porosity*	-
ε_p	*Particle porosity*	-
λ	*Heat conductivity*	W/mK
κ_s	*Heat conductivity*	W/mK
η	*Dynamic viscosity*	$Pa\ s$

$\mathcal{O}$	*Truncation error*	-
Φ	*Viscosity factor*	-
ρ	*Density*	kg/m^3
ν_i	*Stoichiometric coefficient for component i*	-
μ	*Dynamic viscosity*	$Pa\ s$

Appendix B. Physical properties and kinetic data

Table I. Parameter variation in different temperature intervals.

Parameter	For 380-470°C	For 470-580°C
$k_{1,0}$	$3.035 \cdot 10^{7}$	15.63
E_1	169 010.6	78 914.4
$k_{2,0}$	$1.943 \cdot 10^{-7}$	$1.111 \cdot 10^{-5}$
E_2	−72 097.9	−55 714.4
$k_{3,0}$	$3.021 \cdot 10^{4}$	$5.019 \cdot 10^{4}$
E_3	69 118.8	68 969.9
M	0.65	0.55

Table II. Constants for calculation of the specific heat capacity for the different species. The temperature should be in K.

Components	CO_2	H_2SO_4	O_2	SO_2	SO_3	H_2O	N_2
C_1	29.37	40.24	29.103	33.375	33.408	33.363	29.105
C_2	34.54	109.5	10.04	25.864	49.677	26.79	8.6149
C_3	1428	943	2526.5	932.8	873.22	2610.5	1701.6
C_4	26.4	83.7	9.356	10.88	28.563	8.8960	0.10347
C_5	588	393.8	1153.8	423.7	393.74	1169	909.79
Interval (K)	50-5000	100-1500	50-1500	100-1500	100-1500	100-2273.15	50-1500

Table III. Constants for calculation of the viscosity for the different species. The temperature should be in K. The coefficients for sulfur trioxide are valid in the interval 24 – 421 ˚C.

Components	CO_2	H_2SO_4	O_2	SO_2	SO_3	H_2O	N_2
K_1	$2.148 \cdot 10^{-3}$	$2.1097 \cdot 10^{-5}$	$1.101 \cdot 10^{-3}$	$6.863 \cdot 10^{-4}$	$3.9067 \cdot 10^{-3}$	$1.7096 \cdot 10^{-5}$	$6.5592 \cdot 10^{-4}$
K_2	0.46	0.98268	0.5634	0.6112	0.3845	1.1146	0.6081
K_3	290	0	96.3	217	470.1	0	54.714

Table IV. Molecular weights for each species in the bulk gas.

Component	CO_2	H_2SO_4	O_2	SO_2	SO_3	H_2O	N_2
M_w (kg/mole)	0.04401	0.0981	0.0320	0.0641	0.0801	0.0180	0.0280

Table V. Parameters for the control of the salt system.

	T_{ref} (˚C)	T_{gain} (˚C)	q_{nom} $\left[\frac{J}{s \cdot K}\right]$
Case 1	430	0.05	0.012
Case 2	392	0.1	0.0051
Case 3	290	6	0.0022

Table VI. Properties of the catalytic beds.

Bed	V_{bed} (m^3)	h (m)
1	30	1.1
2	37	1.3
3	70	2.5

Table VII. Catalyst data

ε_p	0.90
ε_c	0.60
ρ_{cat} (kg/m^3)	350
Cp_{cat} (J/mol K)	1050

Table VIII. WSA converter dimensions

A (m^2)	28.2743
h (m)	23

Table IX. The composition and properties of the molten salt system

Compound	$NaNO_2$	$NaNO_3$	KNO_3
Molecular weight (kg/mol)	0.0689	0.0849	0.1011
Composition (weight fraction)	0.40	0.07	0.53

Table X. Temperatures for steady state in the converter for the three cases in °C.

	Case 1		Case 2		Case 3	
	Steady state	Model	Steady state	Model	Steady state	Model
T in bed 1	395	-	395	-	395	-
T out bed 1	547	510	419	405	447	411
T in bed 2	430	431	417	405	430	411
T out bed 2	452	467	414	416	428	415
T in bed 3	392	394	392	393	392	392
T out bed 3	392	428	389	406	389	397

Table XI. A comparison between steady state and the model generated values in mole fraction in outlet from the reactor.

	Case 1		Case 2		Case 3	
	Steady state	Model	Steady state	Model	Steady state	Model
x_{CO_2}	0.0655	0.065	0.1631	0.162	0.0161	0.018
$x_{H_2SO_4}$	0.0422	0.060	0.0062	0.01	0.0166	0.020
x_{O_2}	0.076	0.078	0.0292	0.028	0.1571	0.159
x_{SO_2}	$593 \cdot 10^{-6}$	$300 \cdot 10^{-6}$	$106 \cdot 10^{-6}$	$18 \cdot 10^{-6}$	$91 \cdot 10^{-6}$	$7 \cdot 10^{-7}$
x_{SO_3}	0.0313	0.012	0.0037	0.002	0.0077	0.005
x_{H_2O}	0.0572	0.040	0.071	0.069	0.0646	0.058
x_{N_2}	0.7272	0.745	0.7267	0.729	0.7428	0.74

Appendix C. Finite difference method

The finite difference method is one of several techniques for obtaining numerical solutions to equation 11. In all numerical solutions the continuous partial differential equation (PDE) is replaced with a discrete approximation. In this context the word "discrete" means that the numerical solution is known only at a finite number of points in the physical domain. The number of those points can be selected by the user of the numerical method. In general, increasing the number of points not only increases the resolution, but also the accuracy of the numerical solution and the simulation time. The discrete approximation results in a set of algebraic equations that are evaluated for the values of the discrete unknowns. The mesh is the set of locations where the discrete solution is computed. These points are called nodes, and if one were to draw lines between adjacent nodes in the domain the resulting image would resemble a net or mesh. Two key parameters of the mesh are Δx, the local distance between adjacent points in space, and Δt, the local distance between adjacent time steps. The core idea of the finite-difference method is to replace continuous derivatives with so-called difference formulas that involve only the discrete values associated with positions on the mesh.

Applying the finite-difference method to a differential equation involves replacing all derivatives with difference formulas. In the convection-diffusion equation there are derivatives with respect to time, and derivatives with respect to space. Using different combinations of mesh points in the difference formulas results in different schemes. In the limit as the mesh spacing (Δx and Δt) go to zero, the numerical solution obtained with any useful scheme will approach the true solution to the original differential equation. However, the rate at which the numerical solution approaches the true solution varies with the scheme. In addition, there are some practically useful schemes that can fail to yield a solution for bad combinations of Δx and Δt. For example the upwind schemes fails when the CFL[39] (Courant–Friedrichs–Lewy) condition $\frac{\mathrm{a}\Delta \mathrm{x}}{\Delta \mathrm{t}} \leq 1$ is violated, which causes the solution to explode.

Finite difference approximations

The finite difference method obtains an approximate solution for $f(x,t)$ at a finite set of x and t. For the schemes developed in this report the discrete x are uniformly spaced in the interval $0 \leq x \leq L$ such that

$$x_i = (i-1)\Delta x, \quad i = 1,2,\ldots N \qquad \text{(eq.I)}$$

where N is the total number of spatial *nodes*, including those on the boundary. Given L and N, the spacing between the x_i is computed with

$$\Delta x = \frac{L}{N-1}. \qquad \text{(eq.II)}$$

The finite difference method involves using discrete approximations where the quantities are defined on the finite difference mesh. Approximations to the governing differential equation are obtained by replacing all continuous derivatives by discrete formulas. The mesh where the solution is computed is shown in figure I.

[39] Hirsch, C., *Numerical Computation of Internal and External Flows*, ISBN 978-0471924524

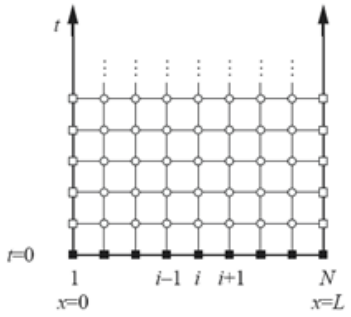

Figure I. Mesh on a semi-infinite strip used for solution to the one-dimensional convection-diffusion equation. The solid squares indicate the location of the initial values. The open squares indicate the location of the boundary values. The open circles indicate the position of the interior points where the finite difference approximation is computed.

Finite difference formulas are first developed with the dependent variable f as a function of only one independent variable *x*. The resulting formulas are then used to approximate derivatives with respect to space[40].

The main advantage of sampling data on a grid is its simplicity; starting from a continuous function $f(x)$ a finite number of values $\{(x_i; f_i)\}$ are calculated on a homogenous mesh x_1 to x_N. If the sampling is dense enough and the function smooth, intermediate values can be interpolated from neighboring data using a Taylor series expansions

$$f(x_i + \Delta x) = f(x_i) + \Delta x \left.\frac{\partial f}{\partial x}\right|_{x_i} + \left.\frac{\Delta x^2}{2}\frac{\partial^2 f}{\partial x^2}\right|_{x_i} + \left.\frac{\Delta x^3}{3!}\frac{\partial^3 f}{\partial x^3}\right|_{x_i} + \cdots \qquad \text{(eq.III)}$$

where Δx is a change in x relative to x_i which consider the value f at the location of the x_{i+1} mesh line.

The first order derivate can be approximated according to

$$\left.\frac{\partial f}{\partial x}\right|_{x_i} = \frac{f(x_i+\Delta x)-f(x_i)}{\Delta x} - \left.\frac{\Delta x^2}{2}\frac{\partial^2 f}{\partial x^2}\right|_{x_i} - \left.\frac{\Delta x^2}{3!}\frac{\partial^3 f}{\partial x^3}\right|_{x_i} + \cdots. \qquad \text{(eq.IV)}$$

Notice that the powers of Δx multiplying the partial derivatives on the right hand side have been reduced by one. Substitute the approximate solution for the exact solution, i.e., use $f_i \approx f(x_i)$ and $f_{i+1} \approx f(x_i + \Delta x)$.

$$\left.\frac{\partial f}{\partial x}\right|_{x_i} \approx \frac{f_{i+1}-f_i}{\Delta x} - \left.\frac{\Delta x}{2}\frac{\partial^2 f}{\partial x^2}\right|_{x_i} - \left.\frac{\Delta x^2}{3!}\frac{\partial^3 f}{\partial x^3}\right|_{x_i} + \cdots. \qquad \text{(eq.V)}$$

The mean value theorem can be used to replace the higher order derivates (exactly)

$$\left.\frac{\Delta x}{2}\frac{\partial^2 f}{\partial x^2}\right|_{x_i} - \left.\frac{\Delta x^2}{3!}\frac{\partial^3 f}{\partial x^3}\right|_{x_i} + \cdots = \left.\frac{\Delta x^2}{2}\frac{\partial^2 f}{\partial x^2}\right|_{\xi} \qquad \text{(eq.VI)}$$

where $x_i \le \xi \le x_{i+1}$. Thus

$$\left.\frac{\partial f}{\partial x}\right|_{x_i} \approx \frac{f_{i+1}-f_i}{\Delta x} + \left.\frac{\Delta x^2}{2}\frac{\partial^2 f}{\partial x^2}\right|_{\xi} \quad \text{or} \quad \left.\frac{\partial f}{\partial x}\right|_{x_i} - \frac{f_{i+1}-f_i}{\Delta x} \approx \left.\frac{\Delta x^2}{2}\frac{\partial^2 f}{\partial x^2}\right|_{\xi}. \qquad \text{(eq.VII)}$$

[40] Recktenwald, G. W., *Finite-Difference Approximations to the Heat Equation*, Jan 21, 2004

The term on the right hand side of equation VII is called the truncation error of the finite difference approximation. It is the error that results from truncating the series in equation VI.

In general, ξ is not known. Furthermore, since the function $f(x,t)$ is also unknown, $\frac{\partial^2 f}{\partial x^2}$ cannot be computed. Although the exact magnitude of the truncation error cannot be known unless the true solution $f(x,t)$ is available in analytical form. The $\mathcal{O}$ notation can be used to express the dependence of the truncation error on the mesh spacing. Note that the right hand side of equation VII contains the mesh parameter Δx, which is chosen by the person using the finite difference simulation. Since this is the only parameter under the user's control that determines the error, the truncation error is simply written

$$\frac{\Delta x^2}{2}\frac{\partial^2 f}{\partial x^2}\Big|_{\xi} = \mathcal{O}(\Delta x^2). \qquad \text{(eq.VIII)}$$

The equals sign in this expression is true in the order of magnitude sense. Rather, the expression means that the left hand side is a product of an unknown constant and Δx^2.
Although the expression does not give us the exact magnitude of $\frac{\Delta x^2}{2}\frac{\partial^2 f}{\partial x^2}\Big|_{\xi}$, it tells us how quickly that term approaches zero as Δx is reduced. Using the $\mathcal{O}$ notation, equation VII can be rewritten as

$$\frac{\partial f}{\partial x}\Big|_{x_i} \approx \frac{f_{i+1}-f_i}{\Delta x} + \mathcal{O}(\Delta x). \qquad \text{(eq.IX)}$$

Equation IX is called the *forward difference* formula for $\frac{\partial f}{\partial x}\Big|_{x_i}$ because it involves nodes x_i and x_{i+1}. The forward difference approximation has a truncation error that is $\mathcal{O}(\Delta x)$. The size of the truncation error can be controlled by choosing a proper mesh size Δx.

First order backward difference

An alternative first order finite difference formula is obtained if the Taylor series like that in equation III is used. When using the discrete mesh variables in place of all the unknowns, one obtains

$$f(x_i - \Delta x) = f(x_i) + \Delta x \frac{\partial f}{\partial x}\Big|_{x_i} + \frac{\Delta x^2}{2}\frac{\partial^2 f}{\partial x^2}\Big|_{x_i} - \frac{\Delta x^3}{3!}\frac{\partial^3 f}{\partial x^3}\Big|_{x_i} + \cdots. \qquad \text{(eq.X)}$$

Solve for $\frac{\partial f}{\partial x}\Big|_{x_i}$ to get

$$\frac{\partial f}{\partial x}\Big|_{x_i} = \frac{f_i - f_{i-1}}{\Delta x} + \Delta x \frac{\partial^2 f}{\partial x^2}\Big|_{x_i} - \frac{\Delta x^2}{2}\frac{\partial^3 f}{\partial x^3}\Big|_{x_i} + \cdots \approx \frac{f_i - f_{i-1}}{\Delta x} + \mathcal{O}(\Delta x). \qquad \text{(eq.XI)}$$

This is called the *backward difference* formula because it involves the values of f at x_i and x_{i-1}. The order of magnitude of the truncation error for the backward difference approximation is the same as that of the forward difference approximation.

First order central difference

Subtracting equation X from equation III yields

$$f(x_i + \Delta x) - f(x_i - \Delta x) = 2\Delta x \frac{\partial f}{\partial x}\Big|_{x_i} + \frac{2\Delta x^3}{3!}\frac{\partial^3 f}{\partial x^3}\Big|_{x_i} + \cdots. \qquad \text{(eq.XII)}$$

Solve for $\frac{\partial f}{\partial x}\Big|_{x_i}$ gives

$$\frac{\partial f}{\partial x}\Big|_{x_i} = \frac{f_{i+1}-f_{i-1}}{2\Delta x} - \frac{\Delta x^3}{3!}\frac{\partial^3 f}{\partial x^3}\Big|_{x_i} + \cdots \approx \frac{f_{i+1}-f_{i-1}}{2\Delta x} + \mathcal{O}(\Delta x^2). \qquad \text{(eq.XIII)}$$

This is the *central difference* approximation to $\left.\frac{\partial f}{\partial x}\right|_{x_i}$. To get good approximations to the continuous problem a small Δx is chosen. When $\Delta x \ll 1$, the truncation error for the central difference approximation goes to zero much faster than the truncation error in the forward and backward difference formulas.

Finite difference approximations to higher order derivatives can be obtained with the additional manipulations of the Taylor Series expansion around $f(x_i)$. Adding equation X and equation III yields

$$f(x_i + \Delta x) + f(x_i - \Delta x) = 2f_i + \Delta x^2 \left.\frac{\partial^2 f}{\partial x^2}\right|_{x_i} + \frac{2\Delta x^4}{4!}\left.\frac{\partial^4 f}{\partial x^4}\right|_{x_i} + \cdots. \quad \text{(eq.XIX)}$$

Solving for $\left.\frac{\partial^2 f}{\partial x^2}\right|_{x_i}$ gives

$$\left.\frac{\partial^2 f}{\partial x^2}\right|_{x_i} = \frac{f_{i+1} - 2f_i + f_{i-1}}{\Delta x^2} + \frac{\Delta x^2}{12}\left.\frac{\partial^4 f}{\partial x^4}\right|_{x_i} + \cdots \approx \frac{f_{i+1} - 2f_i + f_{i-1}}{\Delta x^2} + \mathcal{O}(\Delta x^2). \quad \text{(eq.XX)}$$

This is also called the central difference approximation, but it is the approximation to the second derivative.

Appendix D. Operating conditions for the three cases.

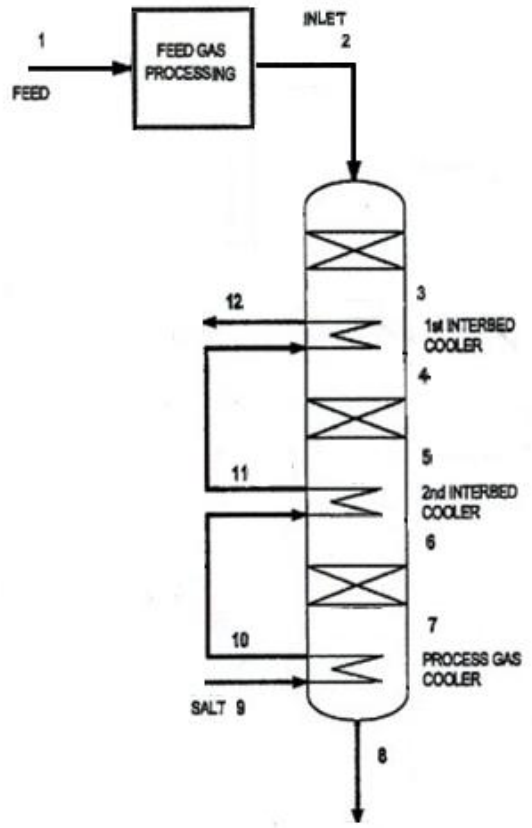

Figure I. Schematic presentation of the WSA converter. The numbering corresponds to those in table I and II.

The data in table I and II are at steady state and given from Haldor Topsoe A/S.

Table I. Composition, pressure, temperature and gas flow in the three cases.

	1			2			8		
	Case 1	Case 2	Case 3	Case 1	Case 2	Case 3	Case 1	Case 2	Case 3
x_{CO_2}	0.1112	0.1894	0.015	0.0607	0.1613	0.0158	0.0655	0.1631	0.0161
$x_{H_2SO_4}$	0	0	0	0	0	0	0.0422	0.0062	0.0116
x_{O_2}	0.0352	0.0114	0.1676	0.1045	0.0337	0.1642	0.076	0.0292	0.1571
x_{SO_2}	0.1261	0.0023	0	0.0687	0.0098	0.019	$593 \cdot 10^{-6}$	$106 \cdot 10^{-6}$	$91 \cdot 10^{-6}$
x_{SO_3}	0	0	0	0	0	0	0.0313	0.0037	0.0077
x_{H_2O}	0.0795	0.079	0.079	0.0922	0.0763	0.0747	0.0572	0.071	0.0646
x_{N_2}	0.648	0.7179	0.7384	0.6739	0.7189	0.7273	0.7272	0.7267	0.7428
P_0 [bar]	1.928	1.934	1.934	2.003	1.984	1.943	1.938	1.941	1.934
T_0 [˚C]	40	40	40	395	395	395	290	290	290
G [Nm³/h]	17832	20797	7601	32728	25175	10548	30332	24899	10329

Table II. All temperatures in ˚C.

	3	4	5	6	7	9	10	11	12
Case 1	547	430	452	392	392	276	380	391	443
Case 2	419	417	414	392	389	276	360	377	378
Case 3	447	430	428	392	389	276	360	385	395

Table III. Heat duty in the three heat exchangers in the converter during three cases, in $\frac{Gcal}{h}$.

	Case 1	Case 2	Case 3
Heat exchanger 1	1.48	0.02	0.06
Heat exchanger 2	0.85	0.21	0.14
Heat exchanger 3	2.31	1.03	0.46

Appendix E. MATLAB program structure translation

All units in SI-units except of cse.P0 that is in bar

Parameters that depends on the running case is stored in the *cse* structures.

ht.cse(caseflag).	x	mole fraction inlet
	T0	temperature inlet
	P0	pressure inlet
	G	bulk flow inlet

Parameters that concerns the discretization is captured in *disc* structures.

ht.disc.	N	grid points of reactor beds
	h	distance between grid points
	ntanks	grid points of heat exchanger
	Ag	backward difference matrix, gas side
	As	forward difference matrix, salt side
	bcg	gas boundary condition
	bcs	salt boundary condition
	tspan	derivation time interval

Discretization matrices for the reactor are stored in *disc.bed* structures.

ht.disc.bed(bedflag).	A1	convection matrix, backward difference matrix
	A1b	boundary convection help matrix
	A2	diffusion matrix, central difference matrix
	A2b	boundary diffusion help matrix

Init is a structure that contains the initial values to each bed.

ht.init(bedflag).	T0	temperature inlet
	Cco2	concentration CO_2 inlet
	Ch2so4	concentration H_2SO_4 inlet
	Co2	concentration O_2 inlet
	Cso2	concentration SO_2 inlet
	Cso3	concentration SO_3 inlet
	Ch2o	concentration water inlet
	Cinert	concentration inert inlet

All the physical properties are stored in *fys* structure. It also contains flags, scale factors and various.

ht.fys.	A	cross section area
	h	WSA reactor height
	epsp	porosity of the particle
	epsc	porosity of the converter
	eps	calculated porosity
	Rhocat	density of catalyst
	Cp_kat	specific heat of catalyst
	R	gas constant
	Hsyra	reaction heat of H_2SO_4 generation
	Hdi2tri	reaction heat of SO_3 generation
	Mw	molar weight
	cflagVect	case flag vector
	cflag	case flag
	Dags	bulk diffusion coefficient
	Ds	thermal conductivity of the catalyst
	kheatArea	heat coefficient, catalyst-bulk interaction
	ksyra	reaction rate coefficient of H_2SO_4 generation
	Efaktor	reaction heat efficiency factor

	k_reakt	reaction rate coefficient of SO_3 generation
	xsalt	mole fraction of salt system
	Mwsalt	molar weight of salt system
	Rhos	density of salt
	Cps	specific heat of salt
	bedflag	bed flag
	transflag	transient flag
	Tscale	temperature scaling factor
	scover	index vector that points out values to scale

Information about the physical dimensions of the beds is stored in *fys.bed*.

ht.fys.bed(bedflag).	V	bed volume
	h	bed height

Help variables that contains operational conditions.

ht.oper.	x	mole fraction
	T	temperature
	P	pressure
	G	bulk flow
	v	flow rate

Physical properties and controller parameters used in the dynamic heat exchanger.

ht.vvx(bedflag).	Tsin	temperature salt system
	Tgain	proportional gain
	qnom	nominal flow of salt
	kA	heat transfer coefficient
	Ag	area gas side
	As	area salt side
	Vg	volume gas side
	Vs	volume salt side
	Tref	reference temperature

All solution data is stored in the following data matrices.

Fout

tout

This solution data is distributed into *bed* and *vvx* cells.

sol.bed{bedflag}	solution matrix of bed. (time x [temp conc])
sol.vvx{bedflag}	solution matrix of vvx. (time x [temp conc])

It is also distributed into concentrations (time x conc) and mole fractions matrices (time x mole fraction) each of them containing all beds and is seen in table I. The temperature column contains solution data for the salt system temperature, the reactor beds temperature and the catalyst surface temperature.

Table I. Solution data matrices in the program

concentrations	mole fractions	Temperatures
Cso2	xso2	Tsalt
Cco2	xco2	T
Ch2o	xh2o	Ts
Ch2so4	xh2so4	
Cinert	xinert	
Co2	xo2	
Cso3	xso3	

Remaining variables that can be seen in the m-file *mainprocess*.

initialvvx	initial values for one heat exchanger
initial3vvx	initial values for three heat exchangers
initialreactor	initial values for one reactor
initial3reactor	initial values for three reactors
initialtot	total initial vector for the heat exchangers and reactors
Tsc	help vector to scale up temperature values

Appendix F. MATLAB code

getreaktordata.m

```
function ht=getreaktordata
%% Physical properties and dimensions
fys.A=        6^2/4*pi;                              %cross section area, m2
fys.h=        23;                                    %height, m
fys.epsp=     0.90;
fys.epsc=     0.60;
fys.eps=fys.epsc+(1-fys.epsc)*fys.epsp;

fys.rhocat=   350;                                   %catalyst density, kg/m3
fys.Cp_kat=   1.050;

fys.R=        8.3145;                                %J/mol/K
fys.Hsyra=   -101;                                   %kJ/mol SO3(g)--->H2SO4(g)
fys.Hdi2tri=  -99;                                   %kJ/mol 2SO2 + o2--->3SO3

fys.Mw=     [(12.01+2*16)        %co2
             (1.008*2+32.07+4*16) %h2so4
             (2*16.00)            %o2
             (32.07+2*16)         %so2
             (32.07+3*16)         %so3
             (1.008*2+16)         %h2o
             (14.01*2)]*1e-3;     %inert   %kg/mol

fys.bed(1).V=  30;                                 %volume, m3
fys.bed(1).h=  1.1;                                %height, m
fys.bed(2).V=  37;
fys.bed(2).h=  1.3;
fys.bed(3).V=  70;
fys.bed(3).h=  2.5;
```

```
%% Operational conditions for different cases
%Steady State values from flow sheet

                %co2        %h2so4  %o2    %so2     %so3    %h2o    %inert
cse(1).x=      [0.0607;    0;      0.1045; 0.0687; 0;      0.0922; 0.6739];
cse(1).T0=     395+273.15;                            %K
cse(1).P0=     (928+75)*1e-3+1;                       %bar
cse(1).G=      32728/3600*(cse(1).T0/273.15);         %inlet volume flow m3/s

                %co2        %h2so4  %o2    %so2     %so3    %h2o    %inert
cse(2).x=      [0.1613;    0;      0.0337; 0.0098; 0;      0.0763; 0.7189];
cse(2).P0=     (934+50)*1e-3+1;                       %bar
cse(2).T0=     395+273.15;                            %K
cse(2).G=      25175/3600*(cse(2).T0/273.15);         %inlet volume flow m3/s

                %co2        %h2so4  %o2    %so2     %so3    %h2o    %inert
cse(3).x=      [0.0158;    0;      0.1642; 0.019 ; 0;      0.0747; 0.7273];
cse(3).P0=     (934+9)*1e-3+1;                        %bar
cse(3).T0=     395+273.15;                            %K
cse(3).G=      10548/3600*(cse(3).T0/273.15);         %inlet volume flow m3/s

%% Flags
fys.transflag=0;            %binary transient flag
fys.cflagVect=[2 2 2];      %case determining flag
fys.cflag=fys.cflagVect(1); %starting case
```

```
%% Tuning parameters, Reaktor
fys.Dax=5e-6;           %Diffusion
fys.Ds=1.8e-3;          %catalyst heat conductivity
fys.kheatArea=1e1;      %heat transfer catalyst surface-bulk
fys.ksyra=5.5e1;        %reaction rate constant for acid formation
fys.Efaktor=0.9;        %Reactions heat
fys.k_reaktion=1;       %Reaction rate tuning for so2-so3
```

```
%% Discretization
disc.N=14;                          %Number of grid points
disc.h(1)=fys.bed(1).h/disc.N;
disc.h(2)=fys.bed(2).h/disc.N;
```

```
disc.h(3)=fys.bed(3).h/disc.N;

% Matrices för pde
[disc.bed(1).A1,disc.bed(1).A1b]=FVMdisc1st(disc.N,disc.h(1),   '2pb', 'sparse');
[disc.bed(1).A2,disc.bed(1).A2b]=FVMdisc2nd(disc.N,disc.h(1),   '3pc', 'sparse');
[disc.bed(2).A1,disc.bed(2).A1b]=FVMdisc1st(disc.N,disc.h(2),   '2pb', 'sparse');
[disc.bed(2).A2,disc.bed(2).A2b]=FVMdisc2nd(disc.N,disc.h(2),   '3pc', 'sparse');
[disc.bed(3).A1,disc.bed(3).A1b]=FVMdisc1st(disc.N,disc.h(3),   '2pb', 'sparse');
[disc.bed(3).A2,disc.bed(3).A2b]=FVMdisc2nd(disc.N,disc.h(3),   '3pc', 'sparse');
```

```
%% packing
ht.fys=fys;
ht.cse=cse;
ht.disc=disc;
```

```
%% FVMdisc1st
function [A,Af]=FVMdisc1st(N,h,Atype,varargin)
% [A,Af]=FVMdisc1st(N,h,Atype)
% [A,Af]=FVMdisc1st(N,h,Atype,spflag)
% FVMdisc1st is a Finite Volume Method domain discritisation
%   of 1st order derivative
% input:
%   N: number of grid points
%   h: grid size
%   Atype: type of 1st order derivative discritisation
%    Atype='2pb'  => 2-point backward approximation
% optional input:
%   spflag: 'sparse' generate sparse discritisation matrices

switch Atype
    case '2pb'
        A=1/h*(eye(N)-diag(ones(N-1,1),-1));
        Af=1/h*[[-1;zeros(N-1,1)],[zeros(N,1)]];
end

if length(varargin)==0
    spflag='full';
else
    spflag=varargin{1};
end
switch spflag
    case 'sparse'
        A=sparse(A);
        Af=sparse(Af);
end
```

```
%% FVMdisc2nd
function [A,Af]=FVMdisc2nd(N,h,Atype,varargin)
% [A,Af]=FVMdisc2nd(N,h,Atype)
% [A,Af]=FVMdisc2nd(N,h,Atype,spflag)
% FVMdisc2nd is a Finite Volume Method domain discritisation
%   of 2nd order derivative
% input:
%   N: number of grid points (in domain)
%   h: grid size
%   Atype: type of 2nd order derivative discritisation
%     Atype='3pc'  => 3-point central approximation
% optional input:
%   spflag: 'sparse' generate sparse discritisation matrices

if length(varargin)==0
    spflag='full';
else
    spflag=varargin{1};
end
switch spflag
    case 'sparse'
        switch Atype
            case '3pc'
                e=ones(N,1);
                A=1/h^2*spdiags([e -2*e e], -1:1, N, N);
                Af=spalloc(N,2,2);
                Af(1,1)=1/h^2;
                Af(N,2)=1/h^2;
        end
```

```
    otherwise
        switch Atype
            case '3pc'
                A=1/h^2*(diag(ones(N-1,1),1)-2*eye(N)+diag(ones(N-1,1),-1));
                Af=1/h^2*[[1;zeros(N-1,1)],[zeros(N-1,1);1]];
        end
end
```

getVVXdata.m

```
function ht=getVVXdata(ht)
%% Unpacking
fys=ht.fys;
cse=ht.cse;
disc=ht.disc;
```

```
%% Physical data,  and compositions

%        NaNO2  NaNO3  KNO3
fys.xsalt=[ .40     0.07    0.53];
fys.Mwsalt=[22.949+14+2*16;         %NaNO2
            22.949+14+3*16;         %NaNO3
            39.098+14+3*16]*1e-3;   %KNO3

% salt temperatures in from flow sheet
vvx(1).Tsin=391+273.15;
vvx(2).Tsin=380+273.15;
vvx(3).Tsin=276+273.15;

fys.rhos=1816.29;
fys.Cps=1521.69;  %J/(K,kg)
```

```
%% Controller parameters'

% proportional gains
vvx(1).Tgain=0.05;
vvx(2).Tgain=0.1;
vvx(3).Tgain=6;

% nominal salt flows
vvx(1).qnom=75313/3600/fys.rhos;    %m3/s
vvx(2).qnom=33035/3600/fys.rhos;
vvx(3).qnom=14013/3600/fys.rhos;
```

```
%% Tuning parameters VVX
% heat transfer coeffecient, calculated from case 1 flow sheet (J/s°C)
vvx(1).kA=33.05e3;
vvx(2).kA=32.21e3;
vvx(3).kA=31.93e3;

% Gas vvx areas, tuned for best performance
vvx(1).Ag=40;
vvx(2).Ag=25;
vvx(3).Ag=30;

% salt vvx areas, approximately the same as gas vvx areas
vvx(1).As=vvx(1).Ag;
vvx(2).As=vvx(2).Ag;
vvx(3).As=vvx(3).Ag;

% Gas vvx volumes, same as areas due to lack of information
vvx(1).Vg=vvx(1).Ag;
vvx(2).Vg=vvx(2).Ag;
vvx(3).Vg=vvx(3).Ag;

% Salt vvx volumes, same as areas due to lack of information
vvx(1).Vs=vvx(1).As;
vvx(2).Vs=vvx(2).As;
vvx(3).Vs=vvx(3).As;

% set points
vvx(1).Tref=430+273.15;
vvx(2).Tref=392+273.15;
```

```
vvx(3).Tref=290+273.15;

fys.bedflag=1;
```

```
%% Discretization
disc.ntanks=6;

disc.Ag = diag(-ones(disc.ntanks,1))+diag(ones(disc.ntanks-1,1),-1);
disc.As = diag(-ones(disc.ntanks,1))+diag(ones(disc.ntanks-1,1),1);

disc.bcg   = [1; zeros(disc.ntanks-1,1)];
disc.bcs  = [zeros(disc.ntanks-1,1); 1];
```

```
%% packing
ht.vvx=vvx;
ht.fys=fys;
ht.cse=cse;
ht.disc=disc;
```

mainprocess.m

```
function mainprocess()
%% Get data from unit operations
ht=getreaktordata;
ht=getVVXdata(ht);

% unpacking
fys=ht.fys;
cse=ht.cse;
disc=ht.disc;
vvx=ht.vvx;
```

```
%% loading and packing of transient data set
if fys.transflag
    load fluctdata4.mat  %Contains transient data set

    fys.bed1so2in=bed1norm;
    fys.bed1out=bed1normout;
    fys.bed2out=bed2normout;
    fys.bed3out=bed3normout;
    fys.bed4out=bed4normout;
    fys.bed1in=bed1normin;
    fys.bed2in=bed2normin;
    fys.bed3in=bed3normin;
    fys.bed4in=bed4normin;
    fys.casenorm=round(casenorm);
    fys.tid=0:.001:6;
end
```

```
%% Calculations of initial data

% The operational values are dependent of which case that is running
oper.x  = cse(fys.cflag).x;
oper.T0 = cse(fys.cflag).T0;
oper.P0 = cse(fys.cflag).P0*1e5;     %OBS! i Pa
oper.G  = cse(fys.cflag).G;
oper.v  = cse(fys.cflag).G/fys.A;

% initial values to reactor bed 1
init(1).T0=        oper.T0;
init(1).Cco2=      oper.P0*oper.x(1)/(fys.R*oper.T0);
init(1).Ch2so4=    oper.P0*0        /(fys.R*oper.T0);
init(1).Co2 =      oper.P0*oper.x(3)/(fys.R*oper.T0);
init(1).Cso2 =     oper.P0*oper.x(4)/(fys.R*oper.T0);
init(1).Cso3 =     oper.P0*0        /(fys.R*oper.T0);
init(1).Ch2o=      oper.P0*oper.x(6)/(fys.R*oper.T0);
init(1).Cinert=    oper.P0*oper.x(7)/(fys.R*oper.T0);

% Making of initial vector for every grid point in one bed
initialbed=[ oper.T0   * ones(disc.N,1);
       (oper.T0+15) * ones(disc.N,1);
```

```
       init(1).Cco2    * ones(disc.N,1);
       init(1).Ch2so4 * ones(disc.N,1);
       init(1).Co2  * ones(disc.N,1);
       init(1).Cso2  *0.1  * ones(disc.N,1);
       init(1).Cso3  * ones(disc.N,1);
       init(1).Ch2o  * ones(disc.N,1);
       init(1).Cinert * ones(disc.N,1)];

% Making of initial vector for every grid point in one vvx
initialvvx=[ (400+273.15)   * ones(disc.ntanks,1);                  %salt  i Kelvin
            (vvx(fys.bedflag).Tsin) * ones(disc.ntanks,1)];

% Repetition of initial vectors for 3 beds/vvx
initial3reaktor=    repmat(initialbed,3,1);
initial3vvx=        repmat(initialvvx,3,1);
initialtot=         [initial3reaktor;initial3vvx];

% loading initial data from last run
try
    load initdata.mat      %Contains initialdata from last run
    initialtot=initdata;
catch
    disp('initialdata could not load')
end

% scaling factors
fys.Tscale=600;
fys.scover=find(initialtot>350);    %Only temperatures have values above 350K, no scale of
conc.
initialtot(fys.scover)=initialtot(fys.scover)/fys.Tscale;
```

```
%% ODE-solver mm

% Time interval
if fys.transflag
    disc.tspan=fys.tid*3600;
else
    disc.tspan=[0 1]*3600*6;
end

disc.hbar = waitbar(0,'Stopp i galoppen');

% packing
ht.init=init;
ht.fys= fys;
ht.disc=disc;
ht.cse= cse;
ht.oper=oper;
ht.vvx=vvx;

tic
[tout,Fout]=ode15s(@(t,F) WSAdyn(t,F,ht),disc.tspan,initialtot);
toc

close(disc.hbar)  %waitbar

% scaling up
Tsc=ones(1,size(Fout,2));
Tsc(fys.scover)=fys.Tscale;
Tsc=repmat(Tsc,numel(tout),1);
Fout=Tsc.*Fout;
```

```
%% Postprocessing

% sorting of solution matrix into beds and vvx (time x space)
for j=1:3
    sol.bed{j}=Fout(:,(j-1)*9*disc.N   +(1:9*disc.N));
    sol.vvx{j}=Fout(:,3*9*disc.N +   (j-1)*2*disc.ntanks  +  (1:2*disc.ntanks));
end

% Making of matrix of temperatures through reactor and vvx (time x space)
Tvvx=      [sol.bed{1}(:,(1:disc.N)) ...
            sol.vvx{1}(:,(1:disc.ntanks)) ...
```

```
            sol.bed{2}(:,(1:disc.N)) ...
            sol.vvx{2}(:,(1:disc.ntanks)) ...
            sol.bed{3}(:,(1:disc.N)) ...
            sol.vvx{3}(:,(1:disc.ntanks))];

% Taking of temperatures and compositions through... (time x space)
T=[];Ts=[];Cco2=[];Ch2so4=[];Co2=[];Cso2=[];Cso3=[];Ch2o=[];Cinert=[];Tsalt=[];

    for j=1:3
        Tsalt=     [Tsalt sol.vvx{j}(:,disc.ntanks +(1:disc.ntanks))]; %...vvx
        T=         [T  sol.bed{j}(:,                (1:disc.N))];      %...bed
        Ts=        [Ts sol.bed{j}(:,   1*disc.N    +(1:disc.N))];      %...bed

        Cco2=      [Cco2 sol.bed{j}(:, 2*disc.N    +(1:disc.N))];      %...bed
        Ch2so4=    [Ch2so4 sol.bed{j}(:,3*disc.N   +(1:disc.N))];      %...bed
        Co2=       [Co2 sol.bed{j}(:,  4*disc.N    +(1:disc.N))];      %...bed
        Cso2=      [Cso2 sol.bed{j}(:, 5*disc.N    +(1:disc.N))];      %...bed
        Cso3=      [Cso3 sol.bed{j}(:, 6*disc.N    +(1:disc.N))];      %...bed
        Ch2o=      [Ch2o sol.bed{j}(:, 7*disc.N    +(1:disc.N))];      %...bed
        Cinert=    [Cinert sol.bed{j}(:,8*disc.N   +(1:disc.N))];      %...bed
    end

     % reactor length translation from grid points
Ltub=[                          disc.h(1):disc.h(1):fys.bed(1).h...
       fys.bed(1).h+                    (disc.h(2):disc.h(2):fys.bed(2).h)...
       fys.bed(1).h+fys.bed(2).h +      (disc.h(3):disc.h(3):fys.bed(3).h)];

    % Matrix that shows gas [In, Ref, Out] temperatures at end of time
    TgasIn_ref_Ut=[sol.vvx{1}(end,1) vvx(1).Tref   sol.vvx{1}(end,disc.ntanks)
                sol.vvx{2}(end,1)   vvx(2).Tref    sol.vvx{2}(end,disc.ntanks)
                sol.vvx{3}(end,1)    vvx(3).Tref   sol.vvx{3}(end,disc.ntanks)]-273.15
```

```
%% Calculations of molar fractions
Cout=[Cco2, Ch2so4, Co2, Cso2, Cso3, Ch2o, Cinert];
x=c2xv2(Cout,disc.N);

xco2=      [x(:, 0*3*disc.N     +(1:3*disc.N))];
xh2so4=    [x(:, 1*3*disc.N     +(1:3*disc.N))];
xo2=       [x(:, 2*3*disc.N     +(1:3*disc.N))];
xso2=      [x(:, 3*3*disc.N     +(1:3*disc.N))];
xso3=      [x(:, 4*3*disc.N     +(1:3*disc.N))];
xh2o=      [x(:, 5*3*disc.N     +(1:3*disc.N))];
xinert=    [x(:, 6*3*disc.N     +(1:3*disc.N))];

disp('steady-state concentrations at the end time in mole%:')
ssxx=[xco2(end,end) xh2so4(end,end) xo2(end,end) xso2(end,end)  xso3(end,end) xh2o(end,end)...
xinert(end,end)]*100

% saves initialdata to be used next run
initdata=Fout(end,:);
save initdata.mat initdata
load tempplotdata.mat
```

```
%% Figur 1 temperatures in reactor
close all
figure(1)

surf(Ltub,tout/3600,T-273.15)
shading interp
view(-125,52)
title('Temperature in bulk','FontWeight','bold')
ylabel('Time (h)','FontWeight','bold')
xlabel('Reactor length (m)','FontWeight','bold')
zlabel('Temp °C','FontWeight','bold')
```

```
%% Figur 2 molar fractions of so2, h2so4
figure(2)

surf(Ltub,tout/3600,xso2)
surf(Ltub,tout/3600,xh2so4)
shading interp
view(-147,52)
title('SO 2','FontWeight','bold')
ylabel('Time (h)','FontWeight','bold')
```

```
xlabel('Reactor length (m)','FontWeight','bold')
zlabel('mole fraction (mole %)','FontWeight','bold')
```

```
%% Figur 3 Temperatures in reactor, heat exchanger
figure(3)
hold on

surf(1:3*(disc.N+disc.ntanks),tout/3600,Tvvx-273.15)
surf(disc.N                    +(1:disc.ntanks),tout/3600,Tsalt(:,
1:disc.ntanks)-273.15)
surf(2*disc.N   +disc.ntanks    +(1:disc.ntanks),tout/3600,Tsalt(:,disc.ntanks +
(1:disc.ntanks))-273.15)
surf(3*disc.N   +2*disc.ntanks  +(1:disc.ntanks),tout/3600,Tsalt(:,2*disc.ntanks +
(1:disc.ntanks))-273.15)
shading interp
view(-147,52)
title('T','FontWeight','bold')
ylabel('Time (h)','FontWeight','bold')
xlabel('Reactor length (m)','FontWeight','bold')
zlabel('Temp °C','FontWeight','bold')
```

```
%% Figur 6 Transient runnings, temperatures from data set comparing the model
if fys.transflag
figure(6)
hold on

% Out from bed 1
plot(tout/3600,T(:,disc.N)-273.15,'k--')
plot(fys.tid,fys.bed1out,'k')

% Out from bed 2
plot(tout/3600,T(:,2*disc.N)-273.15,'m--')
plot(fys.tid,fys.bed2out,'m')

% Out from bed 3
plot(tout/3600,T(:,end)-273.15,'--')
plot(fys.tid,fys.bed3out)

xlabel('Time (h)','FontWeight','bold')
ylabel('Temp °C','FontWeight','bold')
legend({'Bed1out' 'Transdata1' 'Bed2out' 'Transdata2' 'Bed3out'
'Transdata3'},'Location','North')
```

```
%% figur 7 molar fraction of SO2 out from the reactor as a function of time
figure(7)
plot(tout/3600,xso2(:,end)*1e6)
xlabel('Time h')
ylabel('SO_{2,ut} ppm')
```

```
%% Figur 8 Steady state molar fraction as a function of reactor length
figure(8)
hold on
plot(Ltub,xco2(end,:)*100,'-*')
plot(Ltub,xh2so4(end,:)*100,'k-')
plot(Ltub,xo2(end,:)*100,'r-^')
plot(Ltub,xso2(end,:)*100,'k-s')
plot(Ltub,xso3(end,:)*100,'--')
plot(Ltub,xh2o(end,:)*100,'k-x')
% plot(Ltub,xinert(end,:),'k*')

xlabel('reactor length (m)','FontWeight','bold')
ylabel('mole fraction (mole %)','FontWeight','bold')
legend({'CO_2', 'H_2SO_4', 'O_2', 'SO_2', 'SO_3', 'H_2O'}) %,'Inert'
```

```
%% concentrations to molar fractions
function x=c2x(c)

Ctot=sum(c,2);
x=c./repmat(Ctot,1,size(c,2));
```

```
%% modified concentrations to molar fractions
function x=c2xv2(c,N)
```

```
Ctot=c(:,1:3*N)+...
    c(:,3*N+ (1:3*N))+...
    c(:,2*3*N+ (1:3*N))+...
    c(:,3*3*N+ (1:3*N))+...
    c(:,4*3*N+ (1:3*N))+...
    c(:,5*3*N+ (1:3*N))+...
    c(:,6*3*N+ (1:3*N));

x=c./repmat(Ctot,1,7);
```

WSAdyn.m

```
function der=WSAdyn(t,in,ht)
%% Unpacking
disc=ht.disc;
fys=ht.fys;
init=ht.init;
cse=ht.cse;
vvx=ht.vvx;
in(fys.scover)=in(fys.scover)*fys.Tscale;           %scaling up

inr1=   in(                                  (1:9*disc.N));
inr2=   in(  9*disc.N                       +(1:9*disc.N));
inr3=   in(2*9*disc.N                       +(1:9*disc.N));
invvx1= in(3*9*disc.N                      +(1:2*disc.ntanks));
invvx2= in(3*9*disc.N + 1*2*disc.ntanks    +(1:2*disc.ntanks));
invvx3= in(3*9*disc.N + 2*2*disc.ntanks    +(1:2*disc.ntanks));
```

```
%% case switching
if ~fys.transflag
    waitbar(t/diff(disc.tspan),disc.hbar);
    if t<disc.tspan(end)/3
        %initial case is set in reaktordata.m
    elseif t<2*disc.tspan(end)/3
         fys.cflag=fys.cflagVect(2);
    elseif t<=3*disc.tspan(end)/3
         fys.cflag=fys.cflagVect(3);
    end
else    % Transientdata
    waitbar(t/(6*3600),disc.hbar); % Vid transientkörning
    Tidx=find(t/3600>=fys.tid,1,'last');
    tempflag=fys.casenorm(Tidx);
    switch tempflag
        case 0
            fys.cflag=3;
        case 1
            fys.cflag=2;
        case 2
            fys.cflag=1;
    end
end


% The operational values are dependent of which case that is running
oper.x = cse(fys.cflag).x;
oper.T0 = cse(fys.cflag).T0;
oper.P0 = cse(fys.cflag).P0*1e5;     %OBS! i Pa
oper.G = cse(fys.cflag).G;
oper.v=cse(fys.cflag).G/fys.A;
```

```
%% Setting boundary values into the first reactor bed
init(1).T0=        oper.T0;
init(1).Ts=        oper.T0;
init(1).Cco2=      oper.P0*oper.x(1)/(fys.R*oper.T0);
init(1).Ch2so4=    oper.P0*oper.x(2)/(fys.R*oper.T0);
init(1).Co2 =      oper.P0*oper.x(3)/(fys.R*oper.T0);
init(1).Cso2 =     oper.P0*oper.x(4)/(fys.R*oper.T0);
init(1).Cso3 =     oper.P0*oper.x(5)/(fys.R*oper.T0);
init(1).Ch2o=      oper.P0*oper.x(6)/(fys.R*oper.T0);
init(1).Cinert=    oper.P0*oper.x(7)/(fys.R*oper.T0);

% Boundary values of SO2 in transient runnings
if fys.transflag
```

```
    Csum=init(1).Cco2+ init(1).Ch2so4+ init(1).Co2+ init(1).Cso3+ init(1).Ch2o+
init(1).Cinert;
    xso2in=fys.bed1so2in(Tidx);
    init(1).Cso2=xso2in*Csum/(100-xso2in);
%     init(1).Cso2=xso2in;
end
```

```
%% Setting boundary values into remaining reactor beds  (last value from previous unit oper.)
init(2).T0=         invvx1(disc.ntanks);
init(2).Ts=         invvx1(disc.ntanks);
init(2).Cco2=       inr1(3*disc.N);
init(2).Ch2so4=     inr1(4*disc.N);
init(2).Co2 =       inr1(5*disc.N);
init(2).Cso2 =      inr1(6*disc.N);
init(2).Cso3 =      inr1(7*disc.N);
init(2).Ch2o=       inr1(8*disc.N);
init(2).Cinert=     inr1(9*disc.N);

init(3).T0=         invvx2(disc.ntanks);
init(3).Ts=         invvx2(disc.ntanks);
init(3).Cco2=       inr2(3*disc.N);
init(3).Ch2so4=     inr2(4*disc.N);
init(3).Co2 =       inr2(5*disc.N);
init(3).Cso2 =      inr2(6*disc.N);
init(3).Cso3 =      inr2(7*disc.N);
init(3).Ch2o=       inr2(8*disc.N);
init(3).Cinert=     inr2(9*disc.N);
```

```
%% Setting boundary values into the heat exchangers
vvx(1).Tgin=inr1(disc.N);
vvx(2).Tgin=inr2(disc.N);
vvx(3).Tgin=inr3(disc.N);
vvx(1).C=inr1([3:9]*disc.N);
vvx(2).C=inr2([3:9]*disc.N);
vvx(3).C=inr3([3:9]*disc.N);
vvx(1).x=c2x(vvx(1).C');
vvx(2).x=c2x(vvx(2).C');
vvx(3).x=c2x(vvx(3).C');
```

```
%% Generation of derivatives

% packing
ht.fys=fys;
ht.vvx=vvx;
ht.init=init;
ht.disc=disc;

% bed and vvx 1
ht.fys.bedflag=1;
der_r1=reaktor(t,inr1,ht);
der_vvx1=VVXdyn(t,invvx1,ht);

% bed and vvx 2
ht.fys.bedflag=2;
der_r2=reaktor(t,inr2,ht);
der_vvx2=VVXdyn(t,invvx2,ht);

% bed and vvx 3
ht.fys.bedflag=3;
der_r3=reaktor(t,inr3,ht);
der_vvx3=VVXdyn(t,invvx3,ht);



der=[der_r1
    der_r2
    der_r3
    der_vvx1
    der_vvx2
    der_vvx3];
der(fys.scover)=der(fys.scover)/fys.Tscale;    %scaling down
```

```
%%
function x=c2x(c)
%ämnen som kolumner
```

```
%spottar ut kolonnvektor

Ctot=sum(c,2);
x=c./repmat(Ctot,1,size(c,2));
x=x';
```

reaktor.m

```
function der=reaktor(t,in,ht)
%% Unpacking
disc=   ht.disc;
fys=    ht.fys;
init=   ht.init;
oper=   ht.oper;

T=      in(             (1:disc.N));
Ts=     in(disc.N   +   (1:disc.N));
Cco2=   in(2*disc.N +   (1:disc.N));
Ch2so4= in(3*disc.N +   (1:disc.N));
Co2=    in(4*disc.N +   (1:disc.N));
Cso2=   in(5*disc.N +   (1:disc.N));
Cso3=   in(6*disc.N +   (1:disc.N));
Ch2o=   in(7*disc.N +   (1:disc.N));
Cinert= in(8*disc.N +   (1:disc.N));
```

```
%% molar fraction calculations

C=[Cco2, Ch2so4, Co2, Cso2, Cso3, Ch2o, Cinert]; % Nx7 - Matrix    (7 ämnen)
Ctot=sum(C,2);          % Nx1 - Column vectors with sum of concentrations of every grid point
x=C./repmat(Ctot,1,7);  % Nx7 - Matrix
```

```
%% Calculation of physical properties
for i=1:disc.N
    xi = x(i,:)';
    rho         = density(T(i),xi,ht);
    Cp          = heatcapacity(T(i),xi)*1e-3; %kJ/(mol K)
end

xo2=(x(:,3));
xso2=x(:,4);
xso3=x(:,5);
xh2o=x(:,6);
```

```
%% Reaction parameters
% Reaction model only valied for temperatures between 380 and 580

% Index matrices determing if grid point temp is <> 470 °C
Tunder=(Ts-273.15<470);
Tover=(Ts-273.15>=470);

k10= 3.035e7 *Tunder + 15.63    *Tover;
E1=  169010.6*Tunder + 78914.4  *Tover;
k20= 1.943e-7*Tunder + 1.111e-5 *Tover;
E2=  -72097.9*Tunder + -55714.1 *Tover;
k30= 3.021e4 *Tunder + 5.019e4  *Tover;
E3=  69118.8 *Tunder + 68969.9  *Tover;
m=   0.65    *Tunder + 0.55     *Tover;

k1=k10.*exp(-E1./(fys.R*Ts));
k2=k20.*exp(-E2./(fys.R*Ts));
k3=k30.*exp(-E3./(fys.R*Ts));

Kp=10.^(4905.5./Ts-4.6455);
P=oper.P0/101325;               % tryck i atm
a=(xso3*P)./(Kp.*(xso2.*P).*(xo2.*P).^0.5);
```

```
%% Reaction
% Unit of P is given in bar

% Reaction rate for 2so2 + o2 --> 2so3
rso2=(k1.*(xso2.*P).*(xo2.*P).^m.*(1-
a))./((xso2.*P)+k2.*(xo2.*P).^m+k3.*(xso3.*P))*1e3*fys.k_reaktion;
```

```
% Reaction rate for so3 + h2o --> h2so4
rsyra=fys.ksyra*(xso3*P).*(xh2o*P);
```

```
%% Diskretisering

% Boundary conditions, left dirichlet and right neumann
disc.B1=[-1 0;zeros(disc.N-2,2);0 1]';
disc.B0so2=[2*init(fys.bedflag).Cso2;0];
disc.B0so3=[2*init(fys.bedflag).Cso3;0];
disc.B0o2=[2*init(fys.bedflag).Co2;0];
disc.B0co2=[2*init(fys.bedflag).Cco2;0];
disc.B0h2so4=[2*init(fys.bedflag).Ch2so4;0];
disc.B0inert=[2*init(fys.bedflag).Cinert;0];
disc.B0h2o=[2*init(fys.bedflag).Ch2o;0];
disc.B0T=[2*init(fys.bedflag).T0;0];
disc.B0Ts=[2*init(fys.bedflag).Ts;0];

b=fys.bedflag;

M2so2=      disc.bed(b).A2*Cso2 + disc.bed(b).A2b * (disc.B1*Cso2 + disc.B0so2);
M2so3=      disc.bed(b).A2*Cso3 + disc.bed(b).A2b * (disc.B1*Cso3 + disc.B0so3);
M2o2=       disc.bed(b).A2*Co2 + disc.bed(b).A2b * (disc.B1*Co2 + disc.B0o2);
M2co2=      disc.bed(b).A2*Cco2 + disc.bed(b).A2b * (disc.B1*Cco2 + disc.B0co2);
M2h2so4=    disc.bed(b).A2*Ch2so4 + disc.bed(b).A2b * (disc.B1*Ch2so4 + disc.B0h2so4);
M2inert=    disc.bed(b).A2*Cinert + disc.bed(b).A2b * (disc.B1*Cinert + disc.B0inert);
M2h2o=      disc.bed(b).A2*Ch2o + disc.bed(b).A2b * (disc.B1*Ch2o + disc.B0h2o);
M2T=        disc.bed(b).A2*T + disc.bed(b).A2b *      (disc.B1*T + disc.B0T);
M2Ts=       disc.bed(b).A2*Ts + disc.bed(b).A2b *      (disc.B1*Ts + disc.B0Ts);

M1so2=      disc.bed(b).A1*Cso2 + disc.bed(b).A1b * (disc.B1*Cso2 + disc.B0so2);
M1so3=      disc.bed(b).A1*Cso3 + disc.bed(b).A1b * (disc.B1*Cso3 + disc.B0so3);
M1o2=       disc.bed(b).A1*Co2 + disc.bed(b).A1b * (disc.B1*Co2 + disc.B0o2);
M1co2=      disc.bed(b).A1*Cco2 + disc.bed(b).A1b * (disc.B1*Cco2 + disc.B0co2);
M1h2so4=    disc.bed(b).A1*Ch2so4 + disc.bed(b).A1b * (disc.B1*Ch2so4 + disc.B0h2so4);
M1inert=    disc.bed(b).A1*Cinert + disc.bed(b).A1b * (disc.B1*Cinert + disc.B0inert);
M1h2o=      disc.bed(b).A1*Ch2o + disc.bed(b).A1b * (disc.B1*Ch2o + disc.B0h2o);
M1T=        disc.bed(b).A1*T + disc.bed(b).A1b * (disc.B1*T + disc.B0T);
```

```
%% Partial diffential equations

% Temperatures
Q   =  fys.kheatArea*(Ts-T);
dT=  fys.Dax*M2T - oper.v/fys.eps*M1T                          + Q/(rho*Cp);
dTs= fys.Ds*M2Ts+(- fys.Efaktor*(fys.Hdi2tri*rso2*fys.rhocat +fys.Hsyra*rsyra)-
Q)/(fys.rhocat*fys.Cp kat);   %rhocat approx medel av bulk plus cat

%Compositions
dc_co2= fys.Dax*M2co2       - oper.v*M1co2/fys.eps    + 0;
dc h2so4= fys.Dax*M2h2so4   - oper.v*M1h2so4/fys.eps                        + rsyra;
dc o2= fys.Dax*M2o2         - oper.v*M1o2/fys.eps     - (rso2/2)*fys.rhocat;
dc so2=fys.Dax*M2so2        - oper.v*M1so2/fys.eps    - rso2*fys.rhocat ;
dc so3=fys.Dax*M2so3        - oper.v*M1so3/fys.eps    + rso2*fys.rhocat      -rsyra;
dc_h2o= fys.Dax*M2h2o       - oper.v*M1h2o/fys.eps                          - rsyra;
dc_inert= fys.Dax*M2inert   - oper.v*M1inert/fys.eps  + 0;

der=[dT; dTs; dc_co2; dc_h2so4; dc_o2; dc_so2; dc_so3; dc_h2o; dc_inert];
```

VVXdyn.m

```
function der = VVXdyn(t,in,ht)
%% Unpacking
vvx=ht.vvx;
fys=ht.fys;
disc=ht.disc;
cse=ht.cse;

Tg=   in(1:disc.ntanks);
Ts=  in(disc.ntanks + (1:disc.ntanks));
TsC=Ts-273.15;
```

```
%% Physical properties calculations for gas
Cpg=zeros(disc.ntanks,1);
```

```
Cps=zeros(disc.ntanks,1);
rhog=zeros(disc.ntanks,1);
rhos=zeros(disc.ntanks,1);
for i=1:disc.ntanks
    Cpg(i)=    heatcapacity(Tg(i),vvx(fys.bedflag).x);
    rhog(i)=   density(Tg(i),vvx(fys.bedflag).x,ht);
%     rhos(i)=   1972-0.745*(TsC(i)-150);              %kg/m3
%     Cps(i)=    (1303.9+0.60666*TsC(i));         %J/kgC
end
```

```
%% heat exchanger control
b=fys.bedflag;
fys.qs= vvx(b).qnom-vvx(b).Tgain*(vvx(b).Tref-Tg(end));  %Tg(end)=inlet temp of gas
if fys.qs<0
   fys.qs=0;
elseif fys.qs>100*vvx(b).qnom;
    fys.qs=100*vvx(b).qnom;
end
fys.kA=fys.qs*3.6621e3;
```

```
%% Derivator
MTg=(disc.Ag*Tg + disc.bcg.*vvx(b).Tgin);
MTs=(disc.As*Ts + disc.bcs.*vvx(b).Tsin);
vvx(b).As=10*vvx(b).As;

Qc=fys.kA*(Tg-Ts);
dTg=cse(fys.cflag).G/vvx(b).Ag *MTg  -   Qc./(Cpg   .*rhog    *vvx(b).Vg);
dTs=fys(1).qs       /vvx(b).As *MTs  +   Qc /(fys.Cps*fys.rhos*vvx(b).Vs);

der=[dTg;dTs];
```

blackboxmodel.m

```
function blackboxmodel
%% Preprocessing
load case-so2.mat   %Contains the black box of the system in n4s5
load fluctdata4.mat %Contains transient data set
ts.tflag=0;         %A binary transient flag

% packing transient data and making corresponding time
ts.casenorm=casenorm;
ts.casekoff=casekoff;
ts.tid=[0:0.01:6];

% converting the system to state space matrices
[ts.a,ts.b,ts.c,ts.d,init]=makeTF(n4s5);
```

```
%% ODE-solver and settings
tspan=[0 6];
init=zeros(size(ts.a,1),1);
[t,x]=ode15s(@(t,in) so2flukt(t,in,ts),tspan,init);
```

```
%% Postprocessing

% Getting input signal
u=zeros(size(t));
if ts.tflag
    u=ppval(casekoff,t);
else
    for i=1:numel(t)
        u(i)=inp(t(i));
    end
end

% calculation of output signal
y=ts.c*x' + ts.d*u';
```

```
%% figure 1, SO2 fluctuation as a function of time
figure(1)
hold on

plot(t,y,'-.')
if ts.tflag
```

```
    plot(ts.tid,bed1norm);
end

xlabel({'time (h)'});
ylabel({'mole fraction SO_2 in'});


function der=so2flukt(t,x,ts)
%% derivatives from state space system

% Input is depending of transient data set runs or not
if ts.tflag
    u=ppval(ts.casekoff,t);
else
    u=inp(t);
end

der=ts.a*x +  ts.b* u;


function u=inp(t)
%% getting input values of case
if t<2;             u=0;
elseif t<4          u=1;
elseif t<=6         u=2;
else                u=2;
end


function [a,b,c,d,init]=makeTF(n4s5)
%% converting the system to state space matrices
[a,b,c,d] = ssdata(n4s5);
H=ss(a,b,c,d,0.01);
G = d2c(H,'tustin');
[a,b,c,d] = ssdata(G);


init=[  0.062403
 -0.040133
 -0.0032934
 -0.022707
    0.02556];
```

heatcapacity.m

```
function cp=heatcapacity(T,x)
%skicka in temperaturen i K, alt ändra i programmet. Får ut Cp i J/mol K

%           k1             k2           k3              k4       k5
konst=  [0.02937000   0.03454000   1.42800000   0.02640000   0.58800000 %co2
         0.04024000   0.10950000   0.94300000   0.08370000   0.39380000 %h2so4
         0.02910300   0.01004000   2.52650000   0.00935600   1.15380000 %o2
         0.03337500   0.02586400   0.93280000   0.01088000   0.42370000 %so2
         0.03340800   0.04967700   0.87322000   0.02856300   0.39374000 %so3
         0.03336300   0.02679000   2.61050000   0.00889600   1.16900000 %h2o
         0.02910500   0.00861490   1.70160000   0.00010347   0.90979000]*1e3; %n2

Cpi=konst(:,1)+konst(:,2).*((konst(:,3)./T)./sinh(konst(:,3)./T)).^2+konst(:,4).*((konst(:,5).
/T)./cosh(konst(:,5)./T)).^2;
cp=Cpi'*x;
```

density.m

```
function rho=density(T,x,ht)

rho=x'*ht.fys.Mw  *ht.oper.P0./(ht.fys.R*T);
```